Energy Release Rate in Fracture Mechanics

By Leyu Wang

B.S. in Aerospace Engineering, May 2006, Beihang University
M.S. in Mechanical Engineering, June 2008, The George Washington University

A dissertation submitted to

The Faculty of
School of Engineering and Applied Science
of The George Washington University
in partial fulfillment of the requirements
for the degree of Doctor of Philosophy

May 17th, 2015

Dissertation directed by

James D. Lee
Professor of Engineering and Applied Science

The School of Engineering and Applied Science Engineering of The George Washington University certifies that Leyu Wang has passed the Final Examination for the degree of Doctor of Philosophy as of Mar 30th 2015. This is the final and approval form of the dissertation.

Energy Release Rate in Fracture Mechanics

Leyu Wang

Dissertation Committee:

James D. Lee, Professor of Engineering and Applied Science
Dissertation Director

Michael W. Plesniak, Professor of Engineering and Applied Science,
Committee Member

Azim Eskandarian, Professor of Engineering and Applied Science
Committee Member

Yongsheng Leng, Associate Professor of Engineering and Applied Science,
Committee Member

Tianshu Li, Assistant Professor of Engineering and Applied Science,
Committee Member

Xianqiao Wang, Assistant Professor of Mechanical Engineering, University of Georgia, Committee Member

© Copyright 2015 by Leyu Wang
All rights reserved

Dedication

The author wishes to dedicate this dissertation to his wife Hongying Chen, his son Dazhuang Wang, his parents Jian Wang, Xiaojian Liu and his parents in law Guanming Chen, Zuofeng Shen

Acknowledgments

I would like to thanks my advisor, Professor James D. Lee, whose expertise, understanding and mentorship added considerably to my graduate experience.

I would like to thanks Professor Michael Plesniak for his encouragement understanding, whose expertise, understanding and mentorship added considerably to my graduate experience.

I would like to thanks the department of mechanical engineering, the department of civil and environmental engineering, national crash analysis center and the school of applied engineering and applied science for the financial support.

I would also like to thanks my collogue Zidong Yang, Jiaoyan Li, Deryou Gao and Zheng Zhang for their collaboration work and discussion.

Finally I would like to thanks my family, Hongying Chen, Dazhuang Wang, Jian Wang, Xiaojian Liu, Zuofeng Shen, Guanming Chen, Xinting Cai, Guiwen Zheng, William Clay Parrish and Marianna Howard Parrish.

Abstract

Energy Release Rate Based Fracture Mechanics

This dissertation aims at developing theories and methods to simulate dynamic crack propagation in large deformation. The analytical solution of linear elastic fracture mechanics is utilized to find the shape of the crack surface after deformation. It is discovered that the deformed shape of a line crack is an ellipse and the deformed shape of an elliptical void is also an ellipse under mode I tensile loading. A numerical example shows that the small strain formulation in linear elastic fracture mechanics overestimates the crack tip stress compared to large strain formulation. Therefore stress intensity factor, as a conclusion from linear elastic fracture mechanics, is not accurate in large deformation or at the close neighborhood of crack tip. Energy release rate fracture criterion is revisited by taking molecular dynamics point of view. It is proved by theory and numerical example that the critical energy release rate is not related to surface energy. The energy release rate is the decrease of potential energy per unit crack advance. The surface energy is the increase of potential energy per unit crack advance. The two quantities always have an opposite signs therefore they cannot be equal. It is suggested that the energy release rate is also the kinetic and/or thermo energy generation rate according to conservation of energy. It is noticed that the plasticity exists even in perfect brittle fracture due to the lattice reorientation occurring at the edge of the material. Fracture is a dynamic and irreversible process in nature. It is emphasized that proper region should be chosen to calculate the energy release rate. A proper region should include all plastic zone caused by fracture but

exclude the plastic zone unrelated to fracture. The same principle also applies to J-integral. Therefore such integral is path dependent. A general method is proposed to calculate energy release rate in molecular dynamics for dynamic or static, brittle or ductile fracture. The equivalency between interatomic potential energy and strain energy is established with new definitions for stress and strain in molecular dynamics. Here, in molecular dynamics, strain energy is defined as the area under the stress-strain curve. The stress and the strain are defined on each atom by taking the summation and the average, respectively, of the influence from all other atoms. Such stress and strain satisfy conjugacy in multi-atom cases with arbitrary configuration under zero temperature. Due to the equivalency of strain energy and interatomic potential energy, the potential energy release rate calculated in molecular dynamics is the same as the strain energy release rate in continuum mechanics. The node release method in finite element analysis is rigorously formulated and verified. The formula to calculate energy release rate in node release method is proposed and validated. The methods to control the crack speed, energy release rate, crack initiation, crack propagation and crack direction are proposed. With such methods, the following conclusions are made: (1) Node release method does not influence material behavior prior to crack extension. (2) Node release method is independent of the steps chosen to release the force. (3) The force-displacement relationship of the releasing nodes, often referred as the cohesive law, depends on the crack speed. The linear relationship is only valid with slow crack speed. (4) Node release method is able to calculate static energy release rate with great accuracy. The static energy release rate is dynamic energy release rate with a slow crack speed. (5) Node release method can be applied to specimen with no initial crack. Therefore the fracture toughness can be obtained from simple tension test. (6)

Node release method can simulate dynamics crack propagation. The linear relationship between static and dynamics energy release rates, $G = G_0(1 - v/v_R)$, is in good agreement with simulation result. In the simulation, the crack speed asymptotically reaches Rayleigh wave speed in elastic material with fixed grip boundary condition. (7) It is discovered that plasticity is one of the mechanisms that reduces the crack speed. The crack in elasto-plastic material will asymmetrically reach 60% of Rayleigh wave speed. (8) The plasticity influences the crack path in mixed mode fracture.

For convenience, all units are normalized Unless otherwise specified.

Table of Contents

Dedication iv

Acknowledgments v

Abstract vi

Energy Release Rate Based Fracture Mechanics vi

Table of Contents ix

List of Figures xii

List of Tables xvii

Chapter 1 Introduction: Limitation of linear elastic fracture mechanics. 1

1.1 Introduction 1

1.2 LEFM Analytical Solution of Line Crack 2

1.3 LEFM Analytical Solution of Elliptical Crack 15

1.4 Discussion 18

1.5 Small Strain and Large Strain Finite Element Formulation 19

1.6 Conclusion 28

Chapter 2 Energy Release Rate Interpreted by Molecular Dynamics 29

2.1 Introduction 29

2.2 Surface Energy Calculation 31

2.2.1. Surface energy Calculation from Bond Energy 33

2.2.2. Surface Energy Calculation from Molecular Dynamics 34

2.2.3 ratio between surface energy of different directions 37

2.3 Revisit Griffith's Energy Release Rate 40

2.3.1 Magnitude of Energy Release Rate and Surface Energy 43

2.4 Modified Energy Release Rate Fracture Criterion....45
2.5 Energy Release Rate Calculation for Brittle and Non-Brittle Material....47
Chapter 3 Work Conjugacy between Stresses and Strains in Molecular Dynamics....58
3.1. Introduction....58
3.2 . Work Conjugacy between Stress and Strain....60
3.3 Hencky Strain....63
3.4 . Stress and strain in simple tension case....65
3.5 Interatomic potential and atomistic strain energy....71
3.6 Atomistic Kirchhoff stress/atomistic Hencky strain conjugate pair in general 3D case for 2-atom system....76
3.7 The conjugate pair of Atomistic second order Piola-Kirchhoff stress and atomistic Lagrangian strain in general 3D case for 2-Atom....85
3.8 Generalization of stress and strain to multi-atom system....93
3.9 Summary....100
3.10 Discussion....105
Chapter 4 Finite Element Study of Energy Release Rate Based Fracture Mechanics....107
4.1 Introduction....107
4.2. Methodology of crack opening method....109
4.3 Energy Release Rate Calculated by Virtual Crack Opening Method....113
4.4 Crack Speed Control....115
4.5 Energy Release Rate Fracture Criterion....117
4.6 Iterative meshing to determine the crack propagation direction....122
Summary....143

Chapter 5 Contribution and Future Work 146

Bibliography of Reference 149

List of Figures

Figure 1-1 Mode I Crack Configuration 3

Figure 1-2 Elliptical Coordinate Definitions 5

Figure 1-3 Mode II Crack 7

Figure 1-4 Parameter definitions in Westgaard functional theory for a mixed mode crack 10

Figure 1-5 Deformed Crack Surface Shape of Mixed Mode Line Crack 14

Figure 1-6 Elliptical Coordinate Definitions 15

Figure 1-7 Comparison between original shape and deformed shape of ellipsoid void in mode I tension. 17

Figure 1-8 Crack Tip Von Misses Stress Contour with three different meshes 25

Figure 1-9 LEFM Analytical Solution Overestimates Crack Tip Stress 27

Figure 2-1 (a) original specimen of graphene at stress free stage. (b) cracked specimen of graphene at stress free stage. 35

Figure 2-2 (a) Graphene with a pre manufactured crack (b) The stress free graphene specimen after natural crack propagation through the length. 37

Figure 2-3 Zigzag and Armchair crack direction of grapheme 38

Figure 2-4 The logical diagram of surface energy, potential energy and kinetic energy 42

Figure 2-5 Graphene specimen before and after crack extension 44

Figure 2-6 Potential Energy and Total Energy of Graphene Fracture 49

Figure 2-7 (a) Graphene at initial state. (b) Graphene right before bonds broken. (c) Graphene right after bond broken. (d) Lattice reorientation after bond broken(..... 53

Figure 2-8 (a) Tensile and Fracture Combined Specimen. (b) Specimen undergo plastic deformation in area C and crack extends in area B (c) specimen after loading is removed. 54

Figure 2-9 Force Displacement Curve of Tension Crack Combined Specimen 55

Figure 2-10 Region Selection in Energy Release Rate Calculation. (a) Inappropriate selection: Contain plastic zone not associate with crack. (b) Inappropriate selection: Does not contain the whole plastic zone associates with crack. (c) Appropriate selection: Contains the whole plastic zone caused by crack and part of the elastic zone involves the lattice relaxation after bond breaking but excludes the plastic zone not caused by crack. The shaded area represents the plastic zone and the elastic zone that involves lattice relaxation after bond breaking 56

Figure 2-11 Integral Path Selection for J-Integral. Shaded area represents the plastic zone. (a) Inappropriate selection: Integral path enclose the plastic zone not caused by crack. (b) Inappropriate selection: Integral path does not enclose entire plastic zone caused by the crack. (c) Appropriate selection: Integral path remains in elastic region and contains the whole plastic zone caused by crack but excludes the plastic zone not caused by crack 57

Figure 3-1 Three Dimensional Simple Tension Case 65

Figure 3-2 Atomistic Simple Tension Case 74

Figure 3-3 Deformation of two atoms: Atomistic Hencky Strain 77

Figure 3-4 Deformation of two atoms: Atomistic Lagrangian strain 85

Figure 3-5 (a): Atomistic point of view and defined original volume. (b): Continuum point of view with the region seen as solid material with all quantities uniform within its boundary. 93

Figure 4-1 Nodal Force Releasing Method. (a) Ordinary Finite Element Mesh. (b) Rigid Body Connection with Double Nodes. (c) Releasing Connection Force 111

Figure 4-2 Force-displacement curve of a nodal point during releasing process. 112

Figure 4-3 Node releasing procedure ensures the constraint force between the node pair is always point towards each other 113

Figure 4-4 Conventional Energy Release Rate Calculation (a) Initial Fracture Specimen (b) Final Fracture Specimen (c) The Shaded Area of Force Displacement Curve is the Energy Reduced Due to Fracture. 114

Figure 4-5 Finite Element Model for nodal releasing method 116

Figure 4-6 Flow Chart of Crack Initiation Judgment 119

Figure 4-7 Flow Chart of Energy Release Rate Control 121

Figure 4-8 Iterative process to adjusts time step such that energy release rate reaches critical energy release rate. 122

Figure 4-9 Left: Line crack specimen modeled with ordinary FEM Right: Line Crack Specimen modeled with Rigid Spot-weld Connection 124

Figure 4-10 Displacement vs. Stress Comparisons with and without Spot-weld Connected 124

Figure 4-11 Force displacement curve of different time step of the same crack speed. 125

Figure 4-12 Force displacement relation of releasing nodes with respect to different crack speed. The relationship is linear only when crack speed is very low 126

Figure 4-13 Specimen Configuration for verify the energy release rate defined by the virtual opening method.....127

Figure 4-14 FEM Simulation with Node Releasing Method. (a) Initial Stress Free Stage (b) Tensile Loading Applied (c) Grip Fixed (d) Damping is applied until kinetic energy damped out then damping is removed (e) Crack advance one element forward with a very low crack speed.....130

Figure 4-15 Force Displacement Curve of Connection Force Releasing History.....130

Figure 4-16 Force-Displacement curve of node releasing process at constant crack speed of 41.3% Rayleigh Wave Speed.....131

Figure 4-17 Cast Iron Simple Tension Specimen(Unknown).....132

Figure 4-18 (a) Class 40 Cast Iron Tensile Test Data. (b) Class 40 Cast Iron Fracture Toughness Test Data (Davis 1996).....133

Figure 4-19 (a) Von-Mises Stress Contour of Crack Extension at Different Time (b)Energy Release Rate Time History. (c) Crack Speed Time history.....135

Figure 4-20 Connection Force and Relative Displacement between Paired Nodes During Node Releasing Process.....135

Figure 4-21 Crack tip displacement, velocity and acceleration according to $G = G_o(1 - v / v_R)$ and $G = const.$.....137

Figure 4-22 Top: Von-Mises Stress Contour and Crack Speed at Different Stage of Crack Extension Left: Crack Speed vs. Time Right: Energy Release Rate vs. Time.....139

Figure 4-23 Normalized Energy Release Rate vs. Normalized Crack Speed.....140

Figure 4-24 Elasto-Plastic Material Model.....141

Figure 4-25 Top: Von-Mises Stress Contour and Crack Speed at Different Stage of Crack Extension. Left: Crack Speed vs. Time for Mode. Right: Energy Release Rate vs. Time (E=1, ε0=0.05, σvm=0.08, Fixed Grip Boundary Condition, Mode I Crack) 142

Figure 4-26 Left: Elasto-Plastic Material Model. Right: Mixed Mode Loading Configuration 142

Figure 4-27 Left: Von-Mises Contour with Elastic Material Model. Right: Von-Mises Contour with Elasto-Plastic Material Model 143

List of Tables

Table 1-1 Crack tip Stress Estimated by Small Strain and Large Strain FEM.....26

Table 2-1 Ratio between Energy Release Rate is the Ratio between Surface Energy of different direction for Graphene.....40

Table 2-2 Energy Release Rate of Graphene Calculated by Different Method.....50

Chapter 1

Introduction: Limitation of linear elastic fracture mechanics.

1.1 Introduction

Fracture is a complex problem in continuum mechanics due to geometry discontinuity at crack tip. In linear elastic fracture mechanics (LEFM), several assumptions need to be made in order to achieve a close form solution. Analytical solution derived by Airy stress function and Westgaard functional theory(H. M. Westergaard 1939) made the following assumptions (Sun, Jin et al. 2012). The material is considered continuous, homogeneous, isotropic and linear elastic. The formulation is in small strain, two dimensional, static, with no thermal, plasticity or viscosity effect. Under such a frame work, the analytical solution is achieved such that the stress, strain and displacement of any point can be calculated. If the traction-free boundary condition is imposed on an elliptical void, the result yield the famous Inglis' solution (C. E. Inglis 1913). Such result is quite complex in terms of derivation and implication. To simplify the problem, Irwin imposed the traction free boundary condition on a line crack (Sun, Jin et al. 2012). Not only the initial crack is assumed to be a line, even after the loading is applied the traction free boundary condition is still specified on the original line. The result of the line crack problem encounters an infinite stress at the crack tip, often referred as crack tip singularity. Usually the assumption of stationary line crack is within the scope of small-strain. The concept of singularity is widely accepted in the fracture mechanics community(Suo 1990, Mubashar

2014, Hui, Ruina 1985) and many numerical method are based on the character of the singular field (Zi 2003, Ma 2009, Duflot 2004, Miao 2010).

Nature forbids naked singularity (Barve 1997). It is unrealistic for the stress to have an infinite value. Studies with molecular dynamic simulation, considered having a higher resolution than continuum mechanics, has not reported infinite stress on the crack tip (Buehler 2006, Ma 2006, Rösner 2009, Zhang 2014). Therefore, singularity is introduced with assumptions made to simplify the realistic problem to a continuum LEFM problem. This work suggests that the small-strain assumption is one of the possible causes of singularity.

1.2 LEFM Analytical Solution of Line Crack

Under LEFM framework, the closed form solution for mode I and mode II crack is derived by Airy stress function and Westgaard functional theory utilizing Kolosov and Muskhelishvili method (Sih 1966, Synge 1955). The processes are summarized as follows by (Sun, Jin et al. 2012). For mode I crack, the problem is formulated as an infinite plane with a line crack of length $2a$ subjected to biaxial stress σ_0 at infinity as shown in figure 1.1. The boundary conditions

$$\sigma_{xy} = \sigma_{yy} = 0 \text{ at } |x| \le a \text{ and } y = 0 \tag{1.1}$$

represents the traction free crack surface.

$$\sigma_{xx} = \sigma_{yy} = \sigma_0 \text{ , } \sigma_{xy} = \sigma_{yx} = 0 \text{ at } x^2 + y^2 \to \infty \tag{1.2}$$

resembles the tensile stress at far field. The underline assumption made here is that the displacement is small so crack surface remains a line crack at original position after deformation. Notice that $|x| \le a$ and $y = 0$ represents crack surface only at undeformed shape. Crack surface will move away from its original position immediately after some loading is applied. Realistically, boundary conditions need to be satisfied at the deformed stage at which the equilibrium is reached and governing equation satisfied. If large strain theory is utilized, the traction free boundary condition needs to be applied on the deformed crack surface of which shape is accordance with the calculated displacement field.

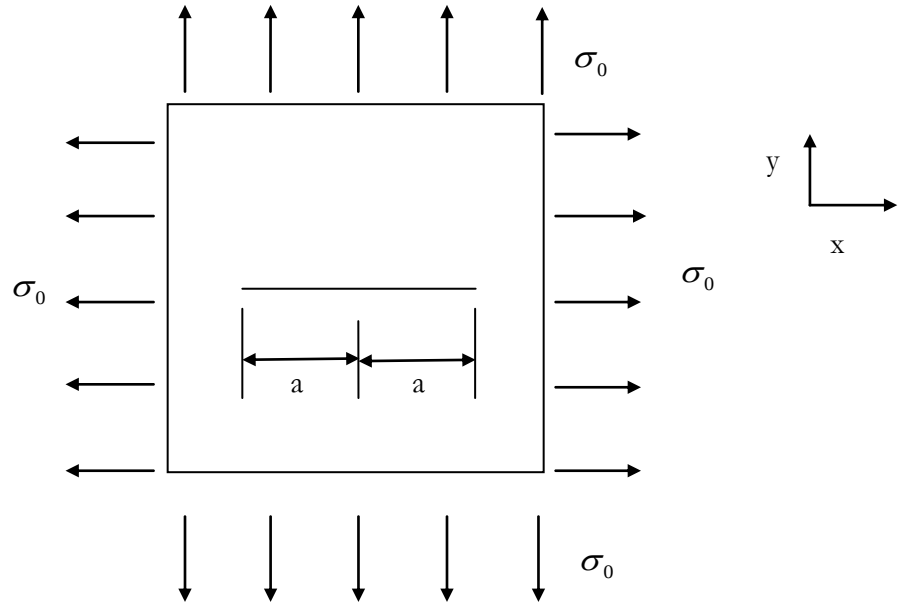

Figure 1-1 Mode I Crack Configuration

Kolosov-Muskhelishvili function of mode I crack is(Sun, Jin et al. 2012):

$$\sigma_{xx} = \mathrm{Re}\{Z_I\} - y\,\mathrm{Im}\{Z_I'\} + 2A \tag{1.3}$$

$$\sigma_{yy} = \mathrm{Re}\{Z_I\} + y\,\mathrm{Im}\{Z_I'\} \tag{1.4}$$

$$\sigma_{xy} = -y\,\mathrm{Re}\{Z_I'\} \tag{1.5}$$

$$2\mu u_x = \frac{\kappa-1}{2}\mathrm{Re}\{\hat{Z}_I\} - y\,\mathrm{Im}\{Z_I\} + \frac{1}{2}(\kappa+1)Ax \tag{1.6}$$

$$2\mu u_y = \frac{\kappa+1}{2}\mathrm{Im}\{\hat{Z}_I\} - y\,\mathrm{Re}\{Z_I\} + \frac{1}{2}(\kappa-3)Ay \tag{1.7}$$

where Z_I is Westgaard function for mode I

$$Z_I(z) = \frac{\sigma_0 z}{\sqrt{z^2 - a^2}} \tag{1.8}$$

$$\frac{D\hat{Z}_I}{Dz} = Z_I \tag{1.9}$$

$\kappa \equiv 3-4\upsilon$ (plain strain), $\kappa \equiv (3-\upsilon)/(1+\upsilon)$ (plane stress).

The stress field associated with A is uniform uniaxial stress $\sigma_{xx} - \sigma_{yy} = 2A$ at $y = 0$ (Sun, Jin et al. 2012). $A = 0$ if uniform tension is applied at x and y directions with equal magnitude. Notice the crack doesn't open if tension is applied only on x direction, therefore the solution of such problem is identical to simple tension problem. In case of uniform tension with non-equal magnitude, one may apply principle of superposition to divide the problem into two parts: a mode I uniaxial stress with equal magnitude and a simple tension problem on the x direction. The result is equal to the summation of the two independent problems.

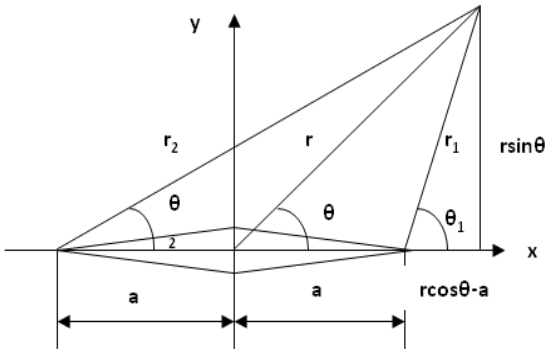

Figure 1-2 Elliptical Coordinate Definitions

Recall eq. (1.8) and further derivation leads to

$$Z_I(z) = \frac{\sigma_0 a}{\sqrt{z^2 - a^2}} \tag{1.10}$$

$$z = re^{i\theta} \tag{1.11}$$

$$z - a = r_1 e^{i\theta_1} \tag{1.12}$$

$$z + a = r_2 e^{i\theta_2} \tag{1.13}$$

$$x = r\cos\theta, y = r\sin\theta \tag{1.14}$$

$$Z_I = \frac{\sigma_0 z}{\sqrt{z+a}\sqrt{z-a}} = \frac{\sigma_0 r}{\sqrt{r_1 r_2}} \exp\left[i\left(\theta - \frac{1}{2}\theta_1 - \frac{1}{2}\theta_2 \right)\right] \tag{1.15}$$

$$Z_I = \frac{\sigma_0 r}{\sqrt{r_1 r_2}} \left[\cos\left(\theta - \frac{1}{2}\theta_1 - \frac{1}{2}\theta_2 \right) + i\sin\left(\theta - \frac{1}{2}\theta_1 - \frac{1}{2}\theta_2 \right)\right] \tag{1.16}$$

$$\hat{Z}_I' = Z_I \tag{1.17}$$

$$\hat{Z}_I = \sigma_0 \sqrt{z+a}\sqrt{z-a} = \sigma_0 \sqrt{r_2 e^{i\theta_1}}\sqrt{r_1 e^{i\theta_2}} = \sigma_0 \sqrt{r_1 r_2}\exp\left[i\left(1/2\theta_1 + 1/2\theta_2\right)\right] \tag{1.18}$$

$$\hat{Z}_I = \sigma_0 \sqrt{r_1 r_2}\cos\left(1/2\theta_1 + 1/2\theta_2\right) + i\sigma_0 \sqrt{r_1 r_2}\sin\left(1/2\theta_1 + 1/2\theta_2\right) \tag{1.19}$$

$$\mathrm{Re}\{\hat{Z}_I\} = \sigma_0 \sqrt{r_1 r_2}\cos(1/2\theta_1 + 1/2\theta_2) \tag{1.20}$$

$$\mathrm{Im}\{\hat{Z}_I\} = \sigma_0 \sqrt{r_1 r_2}\sin(1/2\theta_1 + 1/2\theta_2) \tag{1.21}$$

$$\mathrm{Re}\{Z_I\} = \frac{\sigma_0 r}{\sqrt{r_1 r_2}}\cos(\theta - 1/2\theta_1 - 1/2\theta_2) \tag{1.22}$$

$$\mathrm{Im}\{Z_I\} = \frac{\sigma_0 r}{\sqrt{r_1 r_2}}\sin(\theta - 1/2\theta_1 - 1/2\theta_2) \tag{1.23}$$

$$\mathrm{Re}\{Z_I'\} = -\frac{\sigma_0 a^2}{(r_1 r_2)^{3/2}}\cos\frac{3}{2}(\theta_1 + \theta_2) \tag{1.24}$$

$$\mathrm{Im}\{Z_I'\} = \frac{\sigma_0 a^2}{(r_1 r_2)^{3/2}}\sin\frac{3}{2}(\theta_1 + \theta_2) \tag{1.25}$$

The solution becomes

$$\begin{aligned}\sigma_{xx} &= \mathrm{Re}\{Z_I\} - y\,\mathrm{Im}\{Z_I'\} + 2A \\ &= \frac{\sigma_0 r}{\sqrt{r_1 r_2}}\left[\cos\left(\theta - \frac{1}{2}\theta_1 - \frac{1}{2}\theta_2\right) - \frac{a^2}{r_1 r_2}\sin\theta\sin\frac{3}{2}(\theta_1 + \theta_2)\right] + 2A\end{aligned} \tag{1.26}$$

$$\begin{aligned}\sigma_{yy} &= \mathrm{Re}\{Z_I\} + y\,\mathrm{Im}\{Z_I'\} \\ &= \frac{\sigma_0 r}{\sqrt{r_1 r_2}}\left[\cos\left(\theta - \frac{1}{2}\theta_1 - \frac{1}{2}\theta_2\right) + \frac{a^2}{r_1 r_2}\sin\theta\sin\frac{3}{2}(\theta_1 + \theta_2)\right]\end{aligned} \tag{1.27}$$

$$\begin{aligned}\sigma_{xy} &= -y\,\mathrm{Re}\{Z_I'\} \\ &= \frac{\sigma_0 r}{\sqrt{r_1 r_2}}\left[\frac{a^2}{r_1 r_2}\sin\theta\cos\frac{3}{2}(\theta_1 + \theta_2)\right]\end{aligned} \tag{1.28}$$

$$\begin{aligned}2\mu u_x &= \frac{\kappa - 1}{2}\mathrm{Re}\{\hat{Z}_I\} - y\,\mathrm{Im}\{Z_I\} + \frac{1}{2}(\kappa + 1)Ax \\ &= \frac{\kappa - 1}{2}\sigma_0\sqrt{r_1 r_2}\cos\left(\frac{\theta_1 + \theta_2}{2}\right) - \sin\theta\frac{\sigma_0 r^2}{\sqrt{r_1 r_2}}\sin\left(\theta - \frac{1}{2}\theta_1 - \frac{1}{2}\theta_1\right) + \frac{1}{2}(\kappa + 1)Ax\end{aligned} \tag{1.29}$$

$$2\mu u_y = \frac{\kappa+1}{2}\mathrm{Im}\{\hat{Z}_I\} - y\,\mathrm{Re}\{Z_I\} + \frac{1}{2}(\kappa-3)Ay$$
$$= \frac{\kappa+1}{2}\sigma_0\sqrt{r_1 r_2}\sin\left(\frac{1}{2}\theta_1+\frac{1}{2}\theta_2\right) - \sin\theta\frac{\sigma_0 r^2}{\sqrt{r_1 r_2}}\cos\left(\theta-\frac{1}{2}\theta_1-\frac{1}{2}\theta_2\right)+\frac{1}{2}(\kappa-3)Ay \quad (1.30)$$

For Mode II crack as shown in figure 1.3

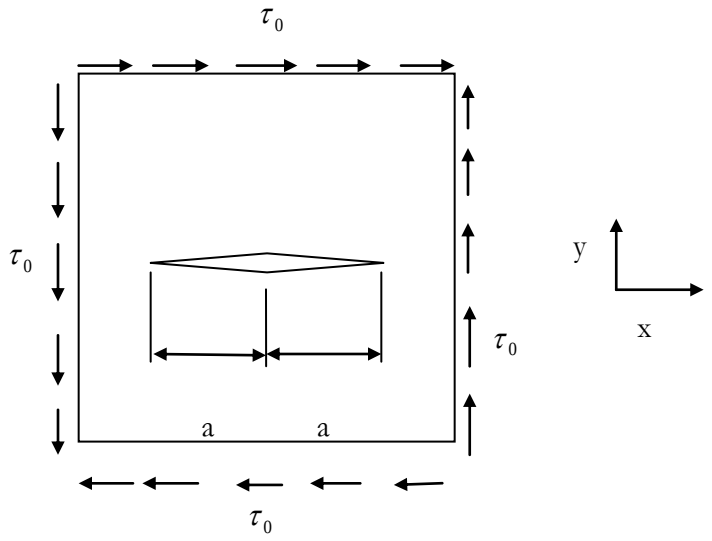

Figure 1-3 Mode II Crack

Kolosov-Muskhelishvili function of mode II crack is:

$$\sigma_{xx} = 2\,\mathrm{Im}\{Z_{II}\} + y\,\mathrm{Re}\{Z_{II}^{'}\} \quad (1.31)$$

$$\sigma_{yy} = -y\,\mathrm{Re}\{Z_{II}^{'}\} \quad (1.32)$$

$$\sigma_{xy} = \mathrm{Re}\{Z_{II}\} - y\,\mathrm{Im}\{Z_{II}^{'}\} \quad (1.33)$$

$$2\mu u_x = \frac{\kappa+1}{2}\mathrm{Im}\{\hat{Z}_{II}\} + y\,\mathrm{Re}\{Z_{II}\} + \frac{\kappa+1}{2}By \quad (1.34)$$

$$2\mu u_y = -\frac{1}{2}(\kappa-1)\mathrm{Re}\{\hat{Z}_{II}\} - y\,\mathrm{Im}\{Z_{II}\} - \frac{\kappa+1}{2}Bx \quad (1.35)$$

where Z_{II} is Westgaard function for mode I

$$Z_{II}(z)=\frac{\sigma_0\tau}{\sqrt{z^2-a^2}} \tag{1.36}$$

$$\hat{Z}_{II}'=\frac{D\hat{Z}_I}{Dz}=Z_{II} \tag{1.37}$$

$\kappa\equiv 3-4\upsilon$ (plain strain), $\kappa\equiv(3-\upsilon)/(1+\upsilon)$ (plane stress).

The last term of displacement equations represents a rigid body motion. For convenience, set $B=0$

$$Z_{II}=\frac{\tau_0 z}{\sqrt{z+a}\sqrt{z-a}}=\frac{\tau_0 r}{\sqrt{r_1 r_2}}\exp\left[i\left(\theta-\frac{1}{2}\theta_1-\frac{1}{2}\theta_2\right)\right] \tag{1.38}$$

$$\hat{Z}_{II}'=Z_{II} \tag{1.39}$$

$$\hat{Z}_{II}=\tau_0\sqrt{z+a}\sqrt{z-a}=\tau_0\sqrt{r_2e^{i\theta_1}}\sqrt{r_1e^{i\theta_2}}=\tau_0\sqrt{r_1r_2}\exp\left[i(1/2\theta_1+1/2\theta_2)\right] \tag{1.40}$$

$$\hat{Z}_{II}=\tau_0\sqrt{r_1r_2}\cos(1/2\theta_1+1/2\theta_2)+i\tau_0\sqrt{r_1r_2}\sin(1/2\theta_1+1/2\theta_2) \tag{1.41}$$

$$\mathrm{Re}\{\hat{Z}_{II}\}=\tau_0\sqrt{r_1r_2}\cos(1/2\theta_1+1/2\theta_2) \tag{1.42}$$

$$\mathrm{Im}\{\hat{Z}_{II}\}=\tau_0\sqrt{r_1r_2}\sin(1/2\theta_1+1/2\theta_2) \tag{1.43}$$

$$\mathrm{Re}\{Z_{II}\}=\frac{\tau_0 r}{\sqrt{r_1r_2}}\cos(\theta-1/2\theta_1+1/2\theta_2) \tag{1.44}$$

$$\mathrm{Im}\{Z_{II}\}=\frac{\tau_0 r}{\sqrt{r_1r_2}}\sin(\theta-1/2\theta_1+1/2\theta_2) \tag{1.45}$$

$$\mathrm{Re}\{Z_{II}'\}=-\frac{\tau_0 a^2}{(r_1r_2)^{3/2}}\cos\frac{3}{2}(\theta_1+\theta_2) \tag{1.46}$$

$$\mathrm{Im}\{Z_{II}'\}=\frac{\tau_0 a^2}{(r_1r_2)^{3/2}}\sin\frac{3}{2}(\theta_1+\theta_2) \tag{1.47}$$

$$x=r\cos\theta,\ y=r\sin\theta \tag{1.48}$$

It leads to the following solutions

$$\begin{aligned}\sigma_{xx} &= 2\,\mathrm{Im}\{Z_{II}\} + y\,\mathrm{Re}\{Z_{II}'\} \\ &= 2\frac{\tau_0 r}{\sqrt{r_1 r_2}}\sin\left(\theta - 1/2\theta_1 + 1/2\theta_2\right) - r\frac{\tau_0 a^2}{\left(r_1 r_2\right)^{3/2}}\sin\theta\cos\frac{3}{2}\left(\theta_1+\theta_2\right)\end{aligned} \tag{1.49}$$

$$\begin{aligned}\sigma_{yy} &= -y\,\mathrm{Re}\{Z_{II}^{'}\} \\ &= \frac{\tau_0 a^2 r}{\left(r_1 r_2\right)^{3/2}}\sin\theta\sin\frac{3}{2}\left(\theta_1+\theta_2\right)\end{aligned} \tag{1.50}$$

$$\begin{aligned}\sigma_{xy} &= \mathrm{Re}\{Z_{II}\} - y\,\mathrm{Im}\{Z_{II}^{'}\} \\ &= \frac{\tau_0 r}{\sqrt{r_1 r_2}}\cos\left(\theta - 1/2\theta_1 + 1/2\theta_2\right) - r\frac{\tau_0 a^2}{\left(r_1 r_2\right)^{3/2}}\sin\theta\sin\frac{3}{2}\left(\theta_1+\theta_2\right)\end{aligned} \tag{1.51}$$

$$\begin{aligned}2\mu u_x &= \frac{\kappa+1}{2}\mathrm{Im}\{\hat{Z}_{II}\} + y\,\mathrm{Re}\{Z_{II}\} \\ &= \frac{\kappa+1}{2}\tau_0\sqrt{r_1 r_2}\sin\left(1/2\theta_1 + 1/2\theta_2\right) + r\frac{\tau_0 r}{\sqrt{r_1 r_2}}\sin\theta\cos\left(\theta - 1/2\theta_1 - 1/2\theta_2\right)\end{aligned} \tag{1.52}$$

$$\begin{aligned}2\mu u_y &= -\frac{1}{2}\left(\kappa-1\right)\mathrm{Re}\{\hat{Z}_{II}\} - y\,\mathrm{Im}\{Z_{II}\} \\ &= -\frac{1}{2}\left(\kappa-1\right)\tau_0\sqrt{r_1 r_2}\cos\left(1/2\theta_1 + 1/2\theta_2\right) - r\frac{\tau_0 r}{\sqrt{r_1 r_2}}\sin\theta\sin\left(\theta - 1/2\theta_1 - 1/2\theta_2\right)\end{aligned} \tag{1.53}$$

Combine the solution of mode I and mode II, mixed mode solution can be achieved as follows

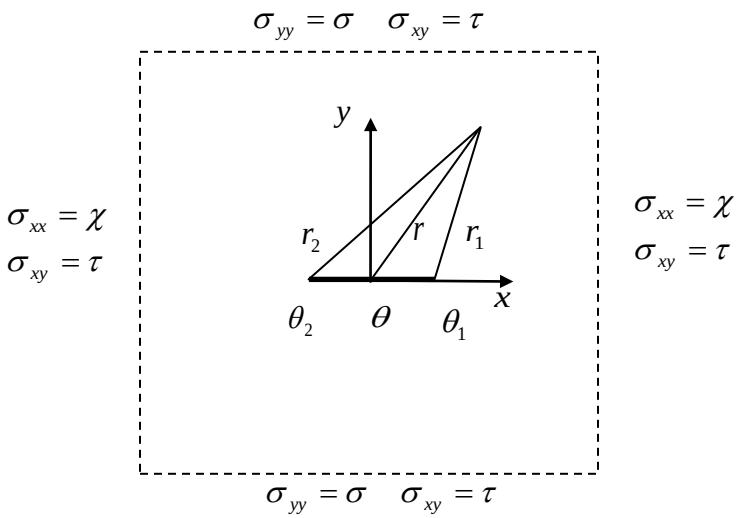

Figure 1-4 Parameter definitions in Westgaard functional theory for a mixed mode crack

$$\begin{aligned} 4\mu u_x =& K_I S\left[(\kappa-1) r_1 r_2 \cos\alpha - 2r^2 \sin\theta \sin\beta\right] \\ &+ K_2 S\left[(\kappa+1) r_1 r_2 \sin\alpha + 2r^2 \sin\theta \cos\beta\right] \\ &- (\sigma-\chi)(\kappa+1) r \cos\theta/2 \end{aligned} \tag{1.54}$$

$$\begin{aligned} 4\mu u_y =& K_1 S[(\kappa+1) r_1 r_2 \sin\alpha - 2r^2 \sin\theta \cos\beta] \\ &+ K_2 S\left[(1-\kappa) r_1 r_2 \cos\alpha - 2r^2 \sin\theta \sin\beta\right] \\ &- (\sigma-\chi)(\kappa-3) r \sin\theta/2 \end{aligned} \tag{1.55}$$

$$\begin{aligned} \sigma_{xx} =& K_1 S\left[r\cos\beta - a^2 \sin\theta_1 \sin 3\alpha / r_2\right] \\ &+ K_2 S\left[2r\sin\beta - a^2 \sin\theta_1 \cos 3\alpha / r_2\right] \\ &+ \chi - \sigma \end{aligned} \tag{1.56}$$

$$\begin{aligned} \sigma_{yy} =& K_1 S\left[r\cos\beta + a^2 \sin\theta_1 \sin 3\alpha / r_2\right] \\ &+ K_2 S a^2 \sin\theta_1 \sin 3\alpha / r_2 \end{aligned} \tag{1.57}$$

$$\begin{aligned} \sigma_{xy} =& K_1 S\left[a^2 \sin\theta_1 \cos 3\alpha / r_2\right] \\ &+ K_2 S\left[r\cos\beta - a^2 \sin\theta_1 \sin 3\alpha / r_2\right] \end{aligned} \tag{1.58}$$

where

$$S \equiv 1/\sqrt{ar_1r_2} \tag{1.59}$$

$$\alpha \equiv (\theta_1 + \theta_2)/2 \ , \ \beta \equiv \theta - (\theta_1 + \theta_2)/2 \tag{1.60}$$

The stress intensity factor for first and second mode

$$K_1 \equiv \sigma_0\sqrt{a} \ , \ K_2 \equiv \tau_0\sqrt{a} \tag{1.61}$$

$$\kappa \equiv 3-4\upsilon \text{ (plain strain)} \ , \ \kappa \equiv (3-\upsilon)/(1+\upsilon) \text{ (plane stress).} \tag{1.62}$$

$$\lambda = \upsilon E/(1+\upsilon)(1-2\upsilon) \ \ \mu = 0.5E/(1+\upsilon) \tag{1.63}$$

$$E = \mu(3\lambda + 2\mu)(\lambda + \mu) \ , \ \upsilon = 0.5\lambda/(\lambda + \mu) \tag{1.64}$$

At right crack surface

$$\theta = 0, \quad \theta_1 = \pi, \quad \theta_2 = 0 \tag{1.65}$$

$$r = x \ , r_1 = a - x \ , r_2 = a + x \tag{1.66}$$

gives

$$S = 1/\sqrt{a(a-x)(a+x)} \tag{1.67}$$

$$\alpha = \pi/2 \text{ and } \ \beta = -\pi/2 \tag{1.68}$$

$$\begin{aligned} 4\mu u_x =& K_I S\left[(\kappa-1)r_1r_2\cos\alpha - 2r^2\sin\theta\sin\beta\right] \\ &+ K_2 S\left[(\kappa+1)r_1r_2\sin\alpha + 2r^2\sin\theta\cos\beta\right] \\ &- (\sigma-\chi)(\kappa+1)r\cos\theta/2 \end{aligned} \tag{1.69}$$

$$4\mu u_x = K_2\frac{(\kappa+1)(a-x)(a+x)}{\sqrt{a(a-x)(a+x)}} - (\sigma-\chi)(\kappa+1)x/2 \tag{1.70}$$

$$4\mu u_y = K_1 S[(\kappa+1)(a-x)(a+x)] \tag{1.71}$$

$$4\mu u_x = \tau(\kappa+1)\sqrt{(a-x)(a+x)} - (\sigma-\chi)(\kappa+1)x/2 \tag{1.72}$$

$$4\mu u_y = \sigma(\kappa+1)\sqrt{(a-x)(a+x)} \tag{1.73}$$

At crack surface $y=0$, the deformed crack surface coordinates $\hat{x}$ and $\hat{y}$

$$\hat{x} = x + u_x = x + \frac{1}{4\mu}\left[\tau(\kappa+1)\sqrt{(a-x)(a+x)} - (\sigma-\chi)(\kappa+1)x/2\right] \tag{1.74}$$

$$\hat{y} = y + u_y = \frac{1}{4\mu}\sigma(\kappa+1)\sqrt{(a-x)(a+x)} \tag{1.75}$$

Notice the deformed shape of mode I crack ($\tau = 0$)

$$\hat{x} = x + u_x = x - \frac{(\sigma-\chi)(\kappa+1)x}{8\mu} = \frac{[8\mu-(\sigma-\chi)(\kappa+1)]x}{8\mu} \tag{1.76}$$

$$x = \frac{8\mu}{[8\mu-(\sigma-\chi)(\kappa+1)]}\hat{x} \tag{1.77}$$

$$\hat{y}^2 = \frac{1}{16\mu^2}\sigma^2(\kappa+1)^2(a^2-x^2) \tag{1.78}$$

$$\hat{y}^2 = \frac{1}{16\mu^2}\sigma^2(\kappa+1)^2\left(a^2 - \frac{64\mu^2}{[8\mu-(\sigma-\chi)(\kappa+1)]^2}\hat{x}^2\right) \tag{1.79}$$

$$\frac{\hat{x}^2}{\left[\frac{8\mu-(\sigma-\chi)(\kappa+1)}{8\mu}\cdot a\right]^2} + \frac{\hat{y}^2}{\left[\frac{\sigma(\kappa+1)}{4\mu}\cdot a\right]^2} = 1 \tag{1.80}$$

Notice that eq. (1.80) is an elliptical equation. Therefore it is proved by this work that that the deformed shape of pure mode I crack is an ellipse.

Pure mode II crack problem gives $\sigma = 0$, $\chi = 0$

$$\hat{x} = x + u_x = x + \frac{1}{4\mu}\left[\tau(\kappa+1)\sqrt{(a-x)(a+x)}\right] \tag{1.81}$$

$$\hat{y} = y + u_y = 0 \tag{1.82}$$

Notice $\hat{y}=0$ means the deformed shape mode II is still a line crack.

$$u_x = \frac{1}{4\mu}\left[\tau(\kappa+1)\sqrt{(a-x)(a+x)}\right] \tag{1.83}$$

gives

$$16\mu^2 u_x^2 = \tau^2(\kappa+1)^2 a^2 - \tau^2(\kappa+1)^2 x^2 \tag{1.84}$$

$$\frac{u_x^2}{\left(\frac{\tau(\kappa+1)a}{4\mu}\right)^2} + \frac{x^2}{a^2} = 1 \tag{1.85}$$

At crack tip x = a , $u_x = 0$ indicates deformed crack is of the same length as original crack.

General deformed shape of mixed mode crack is derived as follows.

$$\hat{x} = x + u_x = x + \frac{1}{4\mu}\left[\tau(\kappa+1)\sqrt{(a-x)(a+x)} - (\sigma-\chi)(\kappa+1)x/2\right] \tag{1.86}$$

$$\hat{y} = y + u_y = \frac{1}{4\mu}\sigma(\kappa+1)\sqrt{(a-x)(a+x)} \tag{1.87}$$

$$\hat{y}^2 = \frac{1}{16\mu^2}\sigma^2(\kappa+1)^2(a^2-x^2) \tag{1.88}$$

$$\frac{16\mu^2\hat{y}^2}{\sigma^2(\kappa+1)^2} = a^2 - x^2 \tag{1.89}$$

$$x^2 = a^2 - \frac{16\mu^2\hat{y}^2}{\sigma^2(\kappa+1)^2} \tag{1.90}$$

$$\hat{x} = x + \frac{1}{4\mu}\left[\tau(\kappa+1)\sqrt{(a^2-x^2)} - (\sigma-\chi)(\kappa+1)x/2\right] \tag{1.91}$$

$$\hat{x} = \sqrt{a^2 - \frac{16\mu^2\hat{y}^2}{\sigma^2(\kappa+1)^2}} + \frac{1}{4\mu}\left[\tau(\kappa+1)\frac{4\mu\hat{y}}{\sigma(\kappa+1)} - (\sigma-\chi)(\kappa+1)\sqrt{a^2 - \frac{16\mu^2\hat{y}^2}{\sigma^2(\kappa+1)^2}}/2\right] \tag{1.92}$$

$$\hat{x} = x + \frac{1}{4\mu}\tau(\kappa+1)\sqrt{a^2-x^2} - \frac{1}{8\mu}(\sigma-\chi)(\kappa+1)x \tag{1.93}$$

$$\begin{aligned}\hat{x}^2 = {} & x^2 + \frac{\mathrm{x}}{4\mu}\tau(\kappa+1)\sqrt{a^2-x^2} - \frac{1}{8\mu}(\sigma-\chi)(\kappa+1)x^2 \\ & + \frac{\mathrm{x}}{4\mu}\tau(\kappa+1)\sqrt{a^2-x^2} + \frac{\tau^2(\kappa+1)^2}{16\mu^2}(a^2-x^2) - \frac{1}{32\mu^2}\tau(\kappa+1)^2\sqrt{a^2-x^2}(\sigma-\chi)x \\ & - \frac{1}{8\mu}(\sigma-\chi)(\kappa+1)x^2 - \frac{1}{32\mu^2}\tau(\kappa+1)^2\sqrt{a^2-x^2}(\sigma-\chi)x - \frac{1}{64\mu^2}(\sigma-\chi)^2(\kappa+1)^2x^2\end{aligned} \tag{1.94}$$

$$\begin{aligned}\hat{x}^2 = {} & x^2 + \frac{\tau^2(\kappa+1)^2}{16\mu^2}(a^2-x^2) + \frac{1}{64\mu^2}(\sigma-\chi)^2(\kappa+1)^2x^2 + \frac{\mathrm{x}}{2\mu}\tau(\kappa+1)\sqrt{a^2-x^2} \\ & - \frac{1}{4\mu}(\sigma-\chi)(\kappa+1)x^2 - \frac{1}{16\mu^2}\tau(\kappa+1)^2\sqrt{a^2-x^2}(\sigma-\chi)x\end{aligned} \tag{1.95}$$

Substituting $x^2 = a^2 - \dfrac{16\mu^2\hat{y}^2}{\sigma^2(\kappa+1)^2}$ into the previous equation, it leads to the followings.

When $\sigma \neq \chi$, the general term is not an ellipse. Notice the last term is a nonlinear term. When $\sigma = \chi, \tau = 0$ the formula represents an ellipse. Figure 1.5 gives the deformed crack surface shape of mixed mode with different tensile to shear ratio.

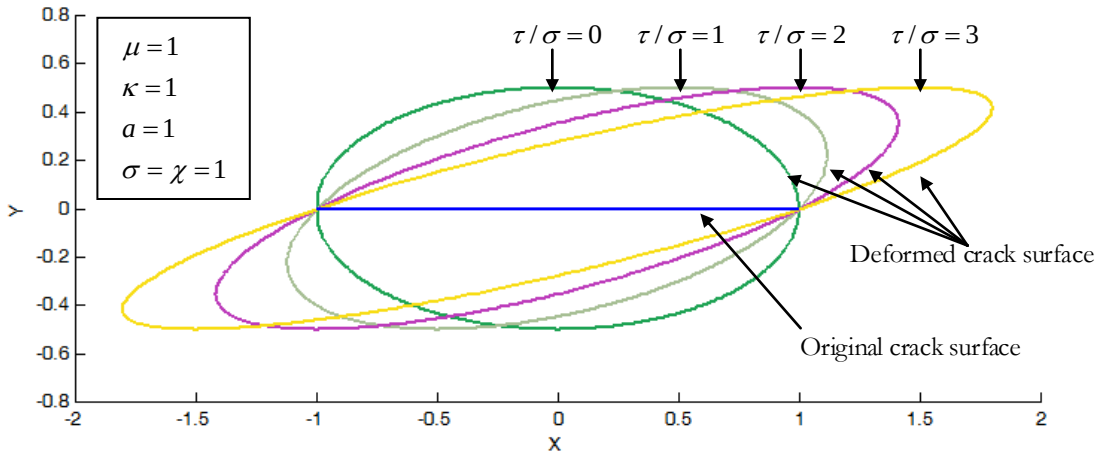

Figure 1-5 Deformed Crack Surface Shape of

Mixed Mode Line Crack

This dissertation is not the first to identify the deformed shape of line crack. Similar result with different procedure is also reported by others(Theocaris, Pazis et al. 1986).

1.3 LEFM Analytical Solution of Elliptical Crack

In this section, the deformed shape of an elliptical void is evaluated by analytical solution. Brown (Brown 1977) summarized the explicit function of deformed shape of an elliptical hole follows Inglis(Inglis 1913) elliptical hole solution as such

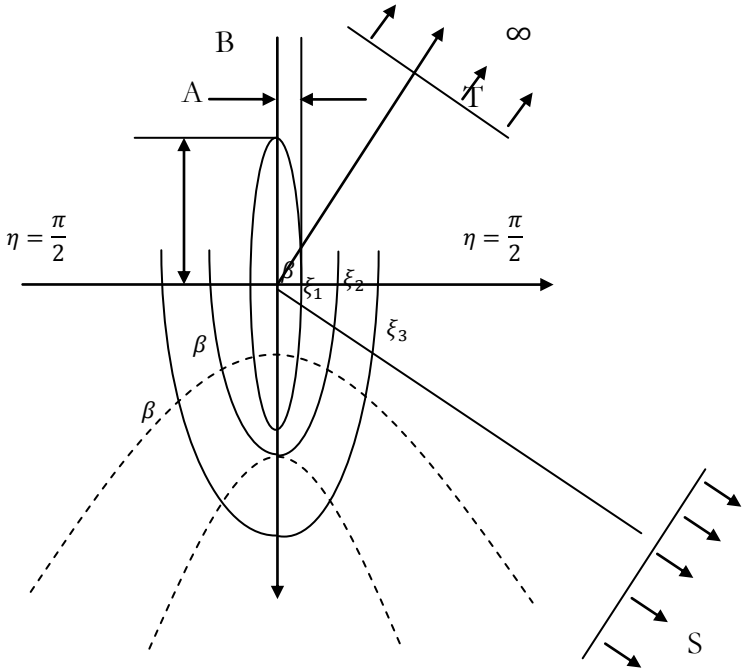

Figure 1-6 Elliptical Coordinate Definitions

$$u = \frac{SC}{8nG}[HLDA \cdot \sinh\xi\cos\eta + HLDB \cdot \cosh\xi\sin\eta \qquad (1.96)$$

$$v = \frac{SC}{8nG}[HLDA \cdot \cosh\xi \sin\eta - HLDB \cdot \sinh\xi \cos\eta \tag{1.97}$$

where

$$\begin{aligned} HLDA = e^{2\xi_1} \cos 2\beta (&K \sinh 2\xi - K \cosh 2\xi + K \cos 2\eta \\ &+ \cosh 2\xi - 2\sinh\xi \cosh\xi + \cos 2\eta) \\ &+ K(\cosh 2\xi - \cos 2\eta) \\ &- \cosh 2\xi - \cos 2\eta + 2\cosh 2\xi_1 - 2\cos 2\beta \\ &+ 2e^{2\xi_1}(\cos 2\eta \cos 2\beta + \sin 2\eta \sin 2\beta) \\ &\times (\cosh 2\xi_1 \sinh 2\xi - \sinh 2\xi_1 \cosh 2\xi) \end{aligned} \tag{1.98}$$

$$\begin{aligned} HLDB = e^{2\xi_1} [&\cos 2\beta (K \sinh 2\eta - 2\sin\eta \cos\eta) + \sin 2\beta \\ &\times (K \cosh 2\xi - K \cos 2\eta + \cosh 2\xi + \cos 2\eta) \\ &- 2(\cos 2\eta \sin 2\beta - \sin 2\eta \cos 2\beta) \\ &\times (\cosh 2\xi_1 \cos 2\xi - \sinh 2\xi_1 \sinh 2\xi)] \end{aligned} \tag{1.99}$$

and u denotes the displacement on x direction, v denotes displacements on y direction

$$K = \begin{cases} (3-\upsilon)/(1+\upsilon) \text{ plane stress} \\ 3 - 4\upsilon \quad \text{plain strain} \end{cases} \tag{1.100}$$

The solution becomes

$$\begin{aligned} 4\mu u_x = &K_I S\left[(\kappa - 1) r r_2 \cos\alpha - 2r_1^2 \sin\theta_1 \sin\beta\right] \\ &+ K_2 S\left[(\kappa + 1) r r_2 \sin\alpha + 2r_1^2 \sin\theta_1 \cos\beta\right] \\ &- (\sigma - \chi)(\kappa + 1) r_1 \cos\theta_1 / 2 \end{aligned} \tag{1.101}$$

$$\begin{aligned} 4\mu u_y = &K_1 S[(\kappa + 1) r r_2 \sin\alpha - 2r_1^2 \sin\theta_1 \cos\beta] \\ &+ K_2 S\left[(1 - \kappa) r r_2 \cos\alpha - 2r_1^2 \sin\theta_1 \sin\beta\right] \\ &- (\sigma - \chi)(\kappa - 3) r_1 \sin\theta_1 / 2 \end{aligned} \tag{1.102}$$

$$\begin{aligned} \sigma_{xx} = &K_1 S\left[r_1 \cos\beta - a^2 \sin\theta \sin 3\alpha / r_2\right] \\ &+ K_2 S\left[2r_1 \sin\beta - a^2 \sin\theta \cos 3\alpha / r_2\right] \\ &+ \chi - \sigma \end{aligned} \tag{1.103}$$

$$\sigma_{yy} = K_1 S\left[r_1 \cos\beta + a^2 \sin\theta \sin 3\alpha / r_2\right] + K_2 S a^2 \sin\theta \sin 3\alpha / r_2 \tag{1.104}$$

$$\sigma_{xy} = K_1 S\left[a^2 \sin\theta \cos 3\alpha / r_2\right] + K_2 S\left[r_1 \cos\beta - a^2 \sin\theta \sin 3\alpha / r_2\right] \tag{1.105}$$

where

$$S \equiv 1/\sqrt{arr_2} \tag{1.106}$$

$$\alpha \equiv (\theta + \theta_2)/2 \ , \ \beta \equiv \theta_1 - (\theta + \theta_2)/2 \tag{1.107}$$

$$K_1 \equiv \sigma_0 \sqrt{a} \ , \ K_2 \equiv \tau_0 \sqrt{a} \tag{1.108}$$

$$\kappa \equiv 3 - 4\upsilon \text{ (plain strain)} \ , \ \kappa \equiv (3-\upsilon)/(1+\upsilon) \text{ (plane stress)} \tag{1.109}$$

$$\lambda = \upsilon E/(1+\upsilon)(1-2\upsilon) \ , \ \mu = 0.5E/(1+\upsilon) \tag{1.110}$$

$$E = \mu(3\lambda + 2\mu)(\lambda + \mu) \ , \ \upsilon = 0.5\lambda/(\lambda + \mu) \tag{1.111}$$

If we plot the deformed crack surface shape of a mode I crack against the original shape as seen in figure 1.7, it is numerically verified that the deformed shape is an ellipse.

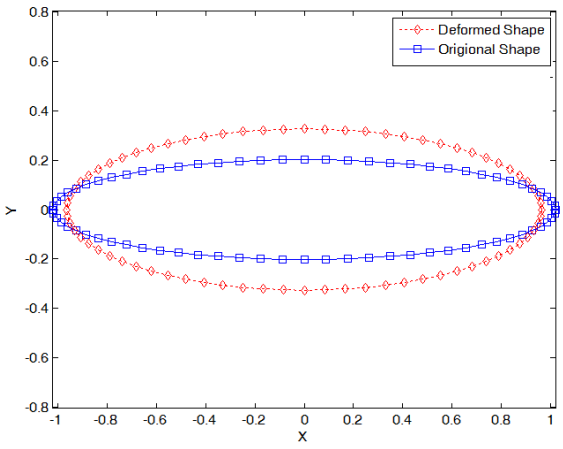

Figure 1-7 Comparison between original shape and deformed shape of ellipsoid void in mode I tension.

1.4 Discussion

For 2D mode I crack, we demonstrated with LEFM that the line crack will deform into an ellipse upon loading. An elliptical crack will deform into another ellipse upon loading. Notice a minimum external loading will cause the line crack to deform into an ellipsoid shape, and further loading will be calculated with the traction free boundary condition on a ellipsoid void of which the stress singularity does not appear. It is suggested that the singularity comes from the traction free boundary condition over a fixed line crack:

$$\sigma_{xy} = \sigma_{yy} = 0 \text{ at } |x| \le a \text{ and } y = 0 \text{ (crack surface)}$$

A more realistically definition of the crack surface should be

$$\sigma_{xy} = \sigma_{yy} = 0 \text{ at crack surface. (Crack surface is moving)}$$

Of course, such boundary condition is beyond the scope of small strain formulation and may not be analytically solved. Noticed that the original and deformed coordinate are not distinguished in small-strain formulation. It is suggested the difference between these two type of boundary conditions are significant(Dunn 1994). Notice that the deformed shape of line crack being an ellipse is also confirmed with large strain FEM simulation (Krishnan, Hui et al. 2008) and experiment (Bouchbinder, Goldman et al. 2014). Therefore Inglis elliptical solution is better in describing fracture.

1.5 Small Strain and Large Strain Finite Element Formulation

In this section, the small-strain and large-strain formulation are elaborated to find their influence upon crack tip stress. The small-strain definition is summarized as such:

Balance of linear momentum

$$t_{ij,i} + \rho f_j = \rho \ddot{u}_j \tag{1.112}$$

where t_{ij} is the stress tensor, ρ is the mass density f_j is the external force. u_j is the displacement.

$$t_{ij} = a_{ijkl}\tilde{e}_{kl} \tag{1.113}$$

where $\tilde{e}_{kl}$ is infinitesimal strain tensor(small strain); a_{ijkl} is a fourth order tensor describe the strain stress relation.

The small strain approximation gives

$$\tilde{e}_{kl} \approx \frac{1}{2}\left(u_{k,l} + u_{l,k}\right) \tag{1.114}$$

The variation principle yields

$$\int \left(t_{ij,i} + \rho f_j - \rho \ddot{u}_j\right)\delta u_j = 0 \tag{1.115}$$

$$\int t_{ij,i}\delta u_j dv + \int \rho f_j \delta u_j dv - \int \rho \ddot{u}_j \delta u_j dv = 0 \tag{1.116}$$

Let us define

$$\begin{aligned} I &\equiv \int t_{ij,i}\delta u_j dv \\ &= \int \left\{\left(t_{ij}\delta u_j\right)_{,i} - t_{ij}\delta u_{j,i}\right\} dv \\ &= \oint_s t_{ij}\delta u_j n_i ds - \int t_{ij}\delta e_{j,i} dv \end{aligned} \tag{1.117}$$

If u_i are interpreted by finite element shape function N_α, i.e.

$$u_i = N_\alpha U_{\alpha i} \tag{1.118}$$

where $U_{\alpha i}$ is the i-th component of the nodal value of the displacement at the $\alpha - th$ node of the element.

$$u_{i,j} = \left(N_\alpha U_{\alpha i}\right)_{,j} = N_{\alpha,j} U_{\alpha i} \tag{1.119}$$

$$\begin{aligned} \tilde{e}_{ij} &= \frac{1}{2}\left[u_{i,j} + u_{j,i}\right] \\ &= \frac{1}{2}\left[\left(N_\alpha U_{\alpha i}\right)_{,j} + \left(N_\alpha U_{\alpha j}\right)_{,i}\right] \\ &= \frac{1}{2}\left[N_{\alpha,j} U_{\alpha i} + N_{\alpha,i} U_{\alpha j}\right] \end{aligned} \tag{1.120}$$

$$\begin{aligned} I &= \delta U_{\alpha j} \int_s t_{ij} n_i N_\alpha ds - \int t_{ij} \delta u_{j,i} dv \\ &= \delta U_{\alpha j} \int_s \bar{t}_j N_\alpha ds - \int t_{ij} \delta u_{j,i} dv \\ &= \delta U_{\alpha j} \int_s \bar{t}_j N_\alpha ds - \delta U_{\alpha j} \int N_{\alpha,i} a_{ijkl} N_{\beta,l} U_{\beta l} dv \\ &= \delta U_{\alpha j} \int_s \bar{t}_j N_\alpha ds - \delta U_{\alpha j} U_{\beta l} \int N_{\alpha,i} N_{\beta,l} a_{ijkl} dv \\ &\equiv \delta U_{\alpha j} \left\{F^1_{\alpha j} - K_{\alpha\beta jl} U_{\beta l}\right\} \end{aligned} \tag{1.121}$$

$$\begin{aligned} II &= \int \rho^o f_j \delta u_j dv \\ &= \delta U_{\alpha j} \int N_\alpha \rho^o f_j dv \\ &\equiv \delta U_{\alpha j} F^2_{\alpha j} \end{aligned} \tag{1.122}$$

$$\begin{aligned} III &= \int \rho^o \ddot{u}_j \delta u_j dv \\ &= \int \rho^o N_\beta \ddot{U}_{\beta j} N_\alpha \delta U_{\alpha j} dv \\ &= \delta U_{\alpha j} \left\{\int \rho^o N_\beta N_\alpha dv\right\} \ddot{U}_{\beta j} \\ &\equiv \delta U_{\alpha j} M_{\alpha\beta} \ddot{U}_{\beta j} \end{aligned} \tag{1.123}$$

If we rewrite term I, II and III, it yields

$$M_{\alpha\beta}\ddot{U}_{\beta j} + K_{\alpha\beta jl}U_{\beta l} = F^1_{\alpha j} + F^2_{\alpha j} \tag{1.124}$$

$$M_{\alpha\beta}\ddot{U}_{\beta j} + K_{\alpha\beta jl}U_{\beta l} = F_{\alpha j} \tag{1.125}$$

Where $F_{\alpha j} = F^1_{\alpha j} + F^2_{\alpha j}$. From this equation the displacement $U_{\beta l}$ can be readily solved with central difference method

The small strain formulation is summarized by (Sadd 2009). The large-strain formulation is summarized by Lee(Chen, Lee et al. 2006). The Cauchy stress and the first and second order Piola-Kirchhoff stress have the following relationship

$$t_{kl} = j^{-1}x_{k,K}T_{Kl} = j^{-1}x_{k,K}x_{l,L}T_{KL} \tag{1.126}$$

$$T_{Kl} = jX_{K,k}t_{kl} = T_{KL}x_{l,L} \tag{1.127}$$

$$T_{KL} = T_{Kl}X_{L,l} = jX_{K,k}X_{L,l}t_{kl} \tag{1.128}$$

$$t_{ij,i} + \rho f_j = \rho\ddot{u}_j \tag{1.129}$$

$$\left(j^{-1}x_{i,K}x_{j,L}T_{KL}\right)_{,j} + \rho\left(f_j - \ddot{u}_j\right) = 0 \tag{1.130}$$

$$\left(j^{-1}x_{j,L}x_{i,K}T_{KL}\right)_{,j} + \rho^o j\left(f_j - \ddot{u}_j\right) = 0 \tag{1.131}$$

$$\left(j^{-1}x_{j,L}\right)_{,j}x_{i,K}T_{KL} + j^{-1}x_{j,L}\left(x_{i,K}T_{KL}\right)_{,j} + \rho^o j^{-1}\left(f_j - \ddot{u}_j\right) = 0 \tag{1.132}$$

because

$$(j^{-1}x_{j,L})_{,j} = 0 \tag{1.133}$$

Therefore

$$\left(T_{KL}x_{k,L}\right)_{,K} + \rho^o\left(f_k - \dot{v}_k\right) = 0 \tag{1.134}$$

The weak form is

$$\int_V \left\{ \left(T_{KL} x_{k,L} \right)_{,K} + \rho^o \left(f_k - \dot{v}_k \right) \right\} \delta u_k dV = 0 \tag{1.135}$$

$$\int_V \left(T_{KL} x_{k,L} \right)_{,K} \delta u_k dV + \int_V \rho^o f_k \delta u_k dV - \int_V \rho^o \dot{v}_k \delta u_k dV = 0 \tag{1.136}$$

Let us define

$$I \equiv \int_V \left(T_{KL} x_{k,L} \right)_{,K} \delta u_k dV \tag{1.137}$$

$$II \equiv \int_V \rho^o f_k \delta u_k dV \tag{1.138}$$

$$III \equiv \int_V \rho^o \dot{v}_k \delta u_k dV \tag{1.139}$$

Finite element approximation with shape function

$$u_i = N_\alpha U_{i\alpha} \quad , \quad u_{i,k} = N_{\alpha,k} U_{i\alpha} \tag{1.140}$$

Let us first derive a useful relationship between displacement vector and position vector.

$$\begin{aligned} u_k &= x_k - \delta_{kK} X_K + b_k \\ u_{k,L} &= x_{k,L} - \left(\delta_{kK} X_K \right)_{,L} \\ u_{k,L} &= x_{k,L} - \delta_{kK} \delta_{KL} \\ u_{k,L} &= x_{k,L} - \delta_{kL} \end{aligned}$$

$$x_{k,L} = u_{k,L} + \delta_{kL} \tag{1.141}$$

And also the Lagrangian strain and second order Piola-Kirchhoff stress in term of nodal displacement $U_{k\alpha}$

$$\begin{aligned} E_{KL} &= \left(U_{K,L} + U_{L,K} + U_{M,K} U_{M,L} \right) / 2 \\ &= \left(C_{KL} - \delta_{KL} \right) / 2 \\ &= \left(x_{k,K} x_{k,L} - \delta_{KL} \right) / 2 \\ &= \left[(u_{k,K} + \delta_{kK})(u_{k,L} + \delta_{kL}) - \delta_{KL} \right] / 2 \\ &= \left[(N_{\alpha,K} U_{k\alpha} + \delta_{kK})(N_{\alpha,L} U_{k\alpha} + \delta_{kL}) - \delta_{KL} \right] / 2 \end{aligned} \tag{1.142}$$

$$
\begin{aligned}
T_{KL} &= A_{IJKL} E_{KL} \\
&= A_{IJKL}[(N_{\alpha,K} U_{k\alpha} + \delta_{kK})(N_{\alpha,L} U_{k\alpha} + \delta_{kK}) - \delta_{KL}]/2
\end{aligned}
\tag{1.143}
$$

$$
\begin{aligned}
I &\equiv \int_V \left\{ \left(T_{KL} x_{k,L} \delta u_k \right)_{,K} - T_{KL} x_{k,L} \delta u_{k,K} \right\} dV \\
&= \oint_S n_K T_{KL} x_{k,L} \delta u_k dS - \int_V T_{KL} (u_{k,L} + \delta_{kL}) \delta u_{k,K} dV \\
&= \delta U_{k\alpha} \int_S \bar{T}_L x_{k,L} N_\alpha dS - \int_V T_{KL} \left[(N_\alpha U_{k\alpha})_{,L} + \delta_{kL} \right] \delta (N_\alpha U_{k\alpha})_{,K} dV \\
&= \delta U_{k\alpha} \int_S \bar{T}_L x_{k,L} N_\alpha dS - \int_V T_{KL} \left(\delta_{kL} + N_{\alpha,L} U_{k\alpha} \right) \delta N_{\alpha,K} U_{k\alpha} dV \\
&= \delta U_{k\alpha} \int_S \bar{T}_L x_{k,L} N_\alpha dS - \delta U_{k\alpha} \int_V T_{KL} \left(\delta_{kL} + N_{\alpha,L} U_{k\alpha} \right) N_{\alpha,K} dV \\
&= \delta U_{k\alpha} \int_S \bar{T}_L x_{k,L} N_\alpha dS \\
&\quad - \delta U_{k\alpha} \int_V A_{IJKL} [(N_{\alpha,K} U_{k\alpha} + \delta_{kK})(N_{\alpha,L} U_{k\alpha} + \delta_{kK}) - \delta_{KL}]/2 \left(\delta_{kL} + N_{\alpha,L} U_{k\alpha} \right) N_{\alpha,K} dV \\
&\equiv \delta U_{k\alpha} \left\{ F^2_{k\alpha} - F^{int}_{ka} \right\}
\end{aligned}
\tag{1.144}
$$

$$
\begin{aligned}
II &\equiv \int_V \rho^o f_k \delta u_k dV \\
&= \delta U_{k\alpha} \int_V \rho^o N_\alpha f_k dV \\
&\equiv \delta U_{k\alpha} F^1_{k\alpha}
\end{aligned}
\tag{1.145}
$$

$$
\begin{aligned}
III &\equiv \int_V \rho^o \dot{v}_k \delta u_k dV \\
&= \delta U_{k\alpha} \dot{V}_{k\beta} \int_V \rho^o N_\alpha N_\beta dV \\
&\equiv \delta U_{k\alpha} \ddot{U}_{k\beta} M_{\alpha\beta}
\end{aligned}
\tag{1.146}
$$

Variation principle gives

$$
\int_V \left\{ \left(T_{KL} x_{k,L} \right)_{,K} + \rho^o \left(f_k - \dot{v}_k \right) \right\} \delta u_k dV = 0 \tag{1.147}
$$

which leads to

$$
M_{\alpha\beta} \ddot{U}_{k\beta} = F^1_{k\alpha} + F^2_{k\alpha} - F^{\text{int}}_{k\alpha} \tag{1.148}
$$

Define

$$F_{k\alpha} \equiv F_{k\alpha}^{1} + F_{k\alpha}^{2} - F_{k\alpha}^{\text{int}} \tag{1.149}$$

$$M_{\alpha\beta}\ddot{U}_{k\beta} = F_{k\alpha} \tag{1.150}$$

Notice the difference between the small-strain and large-strain formulation lays at the treatment of displacement gradient tensor. The small strain formulation made an approximation and gets the infinitesimal strain directly

$$\tilde{e}_{kl} = \left(x_{k,l} + x_{l,k}\right)/2 \tag{1.151}$$

While the large strain formulation use the exact formula.

$$\begin{aligned} E_{KL} &= \left(U_{K,L} + U_{L,K} + U_{M,K}U_{M,L}\right)/2 \\ &= \left(C_{KL} - \delta_{KL}\right)/2 \\ &= \left(x_{k,K}x_{k,L} - \delta_{KL}\right)/2 \end{aligned} \tag{1.152}$$

Recall that the subscript k stands for the three degree of freedom and α stands for the node ID. If we rearrange these two dimensional matrix as

$$M_{\alpha\beta}\ddot{U}_{k\beta} = F_{k\alpha}^{1} + F_{k\alpha}^{2} - F_{k\alpha}^{\text{int}} \tag{1.153}$$

$$U_i \equiv \left[U_{11}\ U_{21}\ U_{31}\ U_{12}\ U_{22}\ U_{32}\ U_{33}\ \cdots U_{K1}\ U_{K2}\ U_{K3}\right] \tag{1.154}$$

$$M_i \equiv \left[M_1\ M_1\ M_1\ M_2\ M_2\ M_2\ \cdots M_K\ M_K\ M_K\right] \tag{1.155}$$

$$f_i \equiv \left[f_{11}\ f_{21}\ f_{31}\ f_{12}\ f_{22}\ f_{32}\ f_{33}\ \cdots f_{K1}\ f_{K2}\ f_{K3}\right] \tag{1.156}$$

It yields

$$M_i\ddot{U}_i = F_i^{1} + F_i^{2} - F_i^{\text{int}} \tag{1.157}$$

The finite element analysis is used to explain the difference between small strain formulation and large strain formulation. Mode I simple tension tests of four different

loading levels is modeled with three different mesh size. The von Mises stress of the crack tip element is recorded with large strain formulations and small strain formulation. Notice the physical problem is identical between each large strain and small strain cases being compared. As shown in Table 1-1, "LSTRAIN" is a large strain finite element code developed by the author and his advisor. "RADIOSS" is a commercial small strain finite element software developed by Altair Inc. The Von Misses stress of the element closest to the crack tip is recorded and compared. The stress calculated by the large strain formulation is considered as the benchmark value. The crack tip stress calculate with the small strain formulation is compared with the large strain result and the percentage of difference is shown in the bracket.

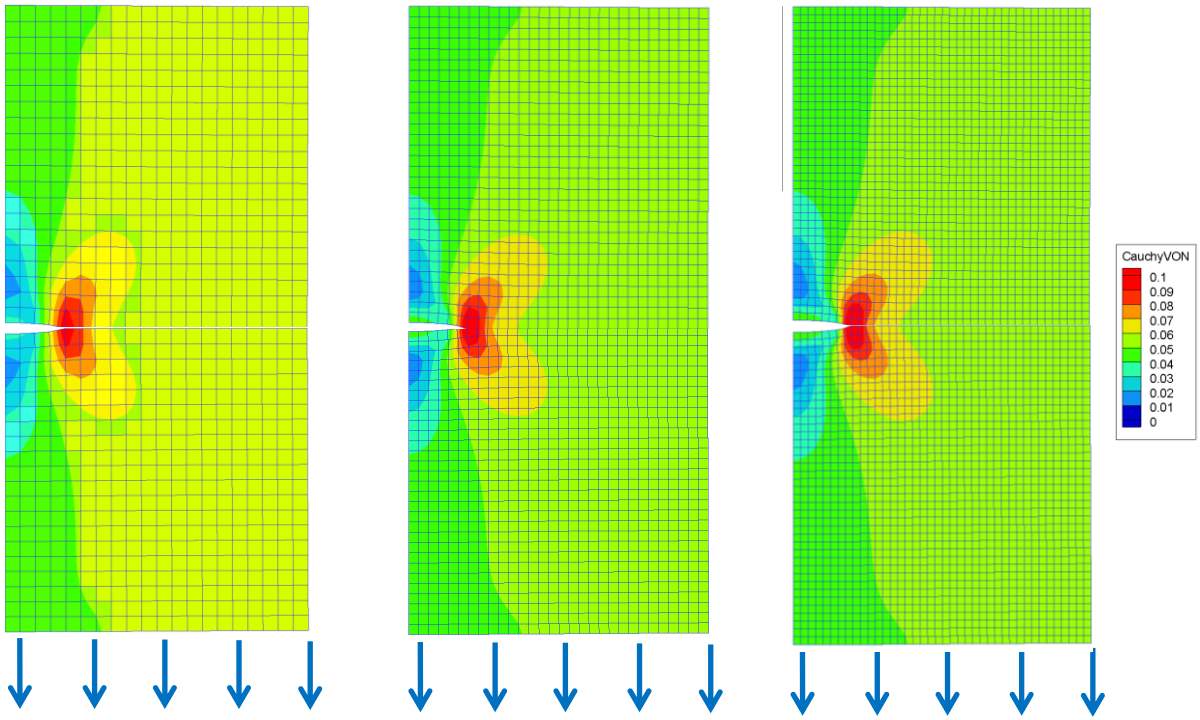

Figure 1-8 Crack Tip Von Misses Stress Contour with three different meshes

		Mesh Size 5 Von Misses stress measures at crack tip element Δx=2.5 Δy=2.5		**Mesh Size 3.3 Von Misses stress measures at crack tip element Δx=1.65 Δy=1.65**		**Mesh size 2.5 Von Misses stress measures at crack tip element Δx=1.25 Δy=1.25**	
ϵ_a	σ_a	σmax Large Strain (LSTRAIN)	σmax Small Strain (RADIOSS)	σmax Large Strain (LSTRAIN)	σmax Small Strain (RADIOSS)	σmax Large Strain (LSTRAIN)	σmax Small Strain (RADIOSS)
0.05	0.05	0.0962012 (100%)	0.09955 (103%)	0.111705 (100%)	0.1187 (106%)	0.12471 (100%)	0.1329 (107%)
0.1	0.1	0.190391 (100%)	0.1991 (104%)	0.218403 (100%)	0.2347 (107%)	0.241 (100%)	0.2658 (110%)
0.2	0.2	0.374892 (100%)	0.3982 (106%)	0.407491 (100%)	0.4695 (115%)	0.42195 (100%)	0.5316 (125%)

Table 1-1 Crack tip Stress Estimated by Small Strain and Large Strain FEM

The study shows that the small strain FEM in general overestimate the stress at the crack tip. This overestimation is more severe with higher applied loading or closer the probing site to the crack tip. In the worst scenario of this study, the error can be up to 25% at the probing site 1.25 to the crack tip when the applied strain is up to 0.2 as shown in Figure 1-8 and Table 1-1. Therefore the method that utilizes the LEFM singular field is not suitable for treating large strain problem or describing the field in the immediate neighborhood of the crack tip. Other researchers has states that the $1/\sqrt{r}$ singularity field associate with LEFM's stress intensity factor K field is not valid within close neighborhood around the crack tip as well (Bouchbinder, Livne et al. 2009, Krishnan, Hui et al. 2008). In fact at the

immediate neighborhood of the crack tip, the crack tip stress is a finite value and non of the singularity field works. The comparison between LEFM analytical solution and large strain FEM result are presented in Figure 1-9. One may not use LEFM formulation to describe the near tip field of the crack because the error can be excessive. Noticed that the stress intensity factor K is based on LEFM analytical solution. Many fracture mechanics finite element utilizing the "singular field" around the crack tip also based on LEFM formulation. These methods are not accurate in large strain or in the close neighborhood of crack tip.

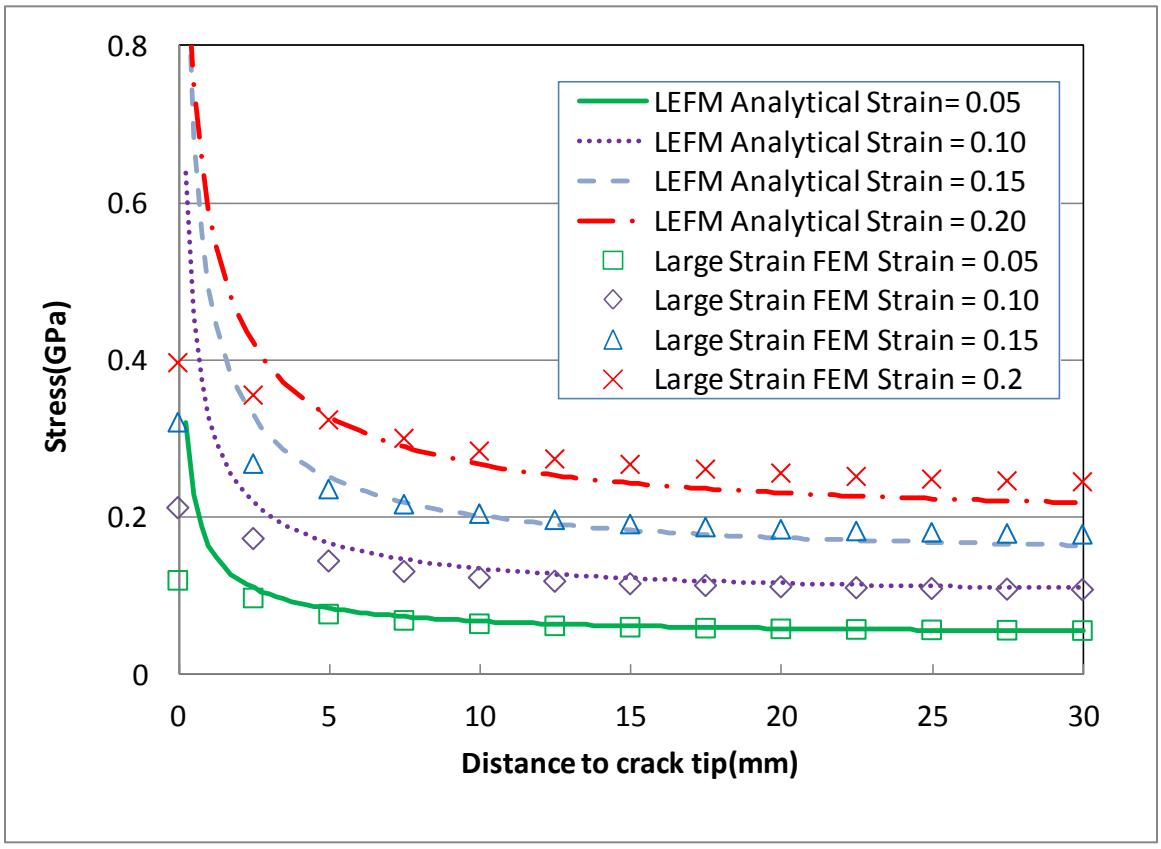

Figure 1-9 LEFM Analytical Solution

Overestimates Crack Tip Stress

1.6 Conclusion

Crack tip singularity is studied by utilizing both analytical and numerical method. In mode I , It is proved that the deformed shape of a line crack is an ellipse; deformed shape of an ellipse is another ellipse. In mixed mode, the deformed shape of a line crack is not an ellipse. A small loading will cause the line crack to deform to elliptical shape and further loading needs to be calculated on the elliptical void, which will eliminate singularity. It is suggested that the asymptotic field analyzed by Irwin's method overestimates the stress level at the crack tip by imposing a traction free boundary condition on a stationary line crack. In the more accurate large-strain theory, traction free boundary condition is imposed on the deformed shape of crack surface(Chen, Lee et al. 2006). To verify this statement, the small-strain and large-strain finite element formulations are presented. The numerical results confirmed the small-strain approximation overestimates the stress at the crack tip. This overestimation is more severe if the strain is large or the probing site is closer to the crack tip. Thus it is suggested that Irwin's LEFM analytical solution overestimates the crack tip stress field. Because the stress intensity factor is built upon Irwin's LEFM solution of the line crack assumption (cf. eq.(1.1)), it is predicted that the stress intensity factor overestimate the stress level of the crack tip. Therefore the stress intensity factor is not accurate in modeling large strain or close neighborhood to the crack tip. In next chapter, the energy concept will be introduced to overcome the theoretical difficulties of the LEFM-based fracture mechanics.

Chapter 2

Energy Release Rate Interpreted by Molecular Dynamics

2.1 Introduction

Fracture mechanics is widely used in failure prediction for many engineering applications. The most important part of a fracture theory lays at its failure criteria. In chapter one, it is shown that the stress intensity factor (K) based criterion is limited to the linear elastic fracture mechanics (LEFM). Among various fracture criteria (Sun, Jin et al. 2012, Mecholsky 1995), the critical energy release rate fracture criterion has the most clear physical meaning and can be readily extend beyond LEFM. In this chapter, the author modified Griffith's energy release rate approach by taking atomistic point of view. Energy release rate is defined as the decrease of potential energy associated with creating unit new crack surface when crack is assumed to extend at current stage. Critical energy release rate is defined as the decrease of potential energy associated with creating unit new crack surface when crack extends naturally. The energy release rate failure criterion is defined as such: the crack will extend when energy release rate reaches the critical energy release rate. Examples are presented for calculating the energy release rate of graphene.

Traditionally, critical energy release rate is equivalent to surface energy in brittle material(Griffith 1921). Surface energy in fracture mechanics is read as the increase of potential energy per unit new surface generation (Swadener 2002). Surface energy can be calculated as the bond energy at lattice constant times the bond number density on the

failure plane(Cima 2012). Surface energy is a material constant since both bond energy at lattice parameter and bond number density are fixed numbers. It is seen that the crystalline material has different values of surface energy at different direction of failure planes. The ratio between surface energy is the ratio between the number density of bond for different planes. In molecular dynamics simulation, the surface energy can be calculated by the difference of potential energy of the stress-free stage between the cracked specimen and the original specimen. The energy release rate can be calculated by the decrease of potential energy right before and immediately after the crack extension. It is noticed that the surface energy increases with crack extension but the potential energy decreases with crack extension. It is noted that the critical energy release rate is not related to surface energy. By taking atomistic point of view, it is seen that the surface energy is part of total potential energy, the comparison between total potential energy and part of total potential energy (surfaces energy) is not meaningful. According to conservation of energy, the decrease of potential energy during crack extension must be the increase of kinetic and thermo energy for an isolated system. In other words, the strain energy release rate is also the thermo and kinetic energy generation rate. Therefore the fracture phenomenon is a kinetic and thermal problem in nature. It is improper to view fracture process as a quasi-static elastic problem even if the crack growth is slow. It will be proved in next chapter that the interatomic potential energy is equivalent to strain energy. By then, the interatomic potential energy release rate can be equivalent to strain energy release rate. It is observed that the potential energy will transform to the kinetic energy at the event of bond breaking followed by the relaxation of lattice. The breaking of the bond happened at the crack tip as well as in the plastic zone surrounding the crack tip. In the general case of brittle and ductile fracture, the

critical energy release rate is a material constant as long as the crack grows self-similarly, defined as the configuration (size and shape) of the plastic zone are identical regardless of crack position, crack speed, crack length, loading condition etc. Notice that there may be other events other than fracture that involves plasticity for a single specimen under some loading condition. Therefore a proper region needs to be selected to calculate energy release rate and J-integral. Such region should enclose the crack tip plastic zone and the part of the elastic zone that involves lattice relaxation, but exclude the plastic zone not related to crack.

2.2 Surface Energy Calculation

The term "surface energy" is often ambiguous because the term is widely used in chemistry and physics to describe a variety of phenomena, which may or may not carry the same meaning. Here we interpret Griffith's "surface energy" as the2 (Cima 2012, Sun, Jin et al. 2012). Surface energy may be rewritten as

$$2\gamma = \frac{U_{bond}}{S_{bond}} = U_{bond} n_{bond} \tag{2.1}$$

where U_{bond} is the chemical bond energy, denotes the energy necessary to break one bond with bond length being the lattice constant; S_{bond} is the new crack surface generated with one bond broken; n_{bond} is the bond number density defined as

$$n_{bond} \equiv \frac{\text{Total Number of Broken Bonds}}{\text{Total Area of New Surface}} \tag{2.2}$$

Notice $n_{bond} = 1/S_{bond}$. Because chemical bond energy U_{bond} at lattice parameter is a constant. New crack surface S_{bond} created in a certain direction with breaking single bond is also a fixed number. Therefore their ratio, named surface energy, is a constant as well. For a crystalline material, every failure direction with different bond number density has a different value of energy release rate. Notice that the surface energy can be calculated easily since atomic density for each failure direction is known and the bond energy can be calculated from interatomic potential. Since the chemical bond energy can be calculated by a valid interatomic potential function in MD,

$$2\gamma_{\langle 100\rangle} = \frac{\Delta U}{\Delta A} = \frac{U^{ij}(a)}{S_{\langle 100\rangle}} \tag{2.3}$$

where $\gamma_{\langle 100\rangle}$ is the surface energy at <100> direction. $S_{\langle 100\rangle}$ is the new crack surface created due to crack advances one atom forward on <100> direction. Equation (2.3) indicates the surface energy is a function of interatomic potential U, lattice constant a, and direction θ

$$2\gamma = 2\gamma(U, a, \theta) \tag{2.4}$$

Because theoretically, bond length a is also a function of interatomic potential U, and temperature T, i.e.,

$$a = a(U, T) \tag{2.5}$$

and S also depends on bond length and failure surface direction θ,

$$S = S(\theta, a) \tag{2.6}$$

Therefore

$$2\gamma = 2\gamma(U, a, S) = 2\gamma(U, a, \theta, T) \tag{2.7}$$

which means the surface energy is a material constant depending on interatomic potential, lattice constant, direction and temperature.

2.2.1. Surface energy Calculation from Bond Energy

It is possible to calculate surface energy by knowing the chemical bond energy U_{bond} and atomistic density S_{bond} at fracture direction.

$$2\gamma = \frac{U_{bond}}{S_{bond}} \tag{2.8}$$

Take graphene as an example, it is known that graphene has sp2 bond (Stankovich, Dikin et al. 2006). The C-C single bond has an energy of 347 kJ/mol. the C=C double bond has energy of 614 kJ/mol (Zumdahl, Zumdahl 2007). For simplicity, we use the average between C=C bond and C-C bond, 480.5kJ/mol , for calculation. This averaging method may be rough, therefore we cross check with the value calculated by Tersoff potential as a verification. The result gives that the $C \simeq C$ bond in graphene has an average bond energy of 484 kJ/mol. Here we utilize the value of 480.5kJ/mol as bond energy because this value comes from chemical bond energy. The length of a graphene bond is a = 0.142 nm (RozpŁoch 2007). Graphene thickness is t=0.335 nm (Ni, Wang et al. 2007) . The surface created with broken single bond for zigzag and armchair directions are

$$S_{zig} = 1/n_{zig} = 2\sqrt{3}a \cdot t/2 = 8.24 \times 10^{-20} m^2 / \text{bond} \tag{2.9}$$

$$S_{arm} = 1/n_{arm} = 3a \cdot t/2 = 7.14 \times 10^{-20} m^2 / \text{bond} \tag{2.10}$$

The bond energy released is obtained as

$$U_{bond} = 480.5kJ / mol = 480.5 / 6.02 \times 10^{23} = 7.9817 \times 10^{-19} J / atom \quad (2.11)$$

$$2\gamma_{zig} = \frac{U_{bond}}{S_{zig}} = \frac{7.9817 \times 10^{-19} J / atom}{8.24 \times 10^{-20} m^2 / \text{atom}} = 9.682 J / m^2 \quad (2.12)$$

$$2\gamma_{arm} = \frac{U_{bond}}{S_{arm}} = \frac{7.9817 \times 10^{-19} J / atom}{7.14 \times 10^{-20} m^2 / \text{atom}} = 11.1789 J / m^2 \quad (2.13)$$

2.2.2. Surface Energy Calculation from Molecular Dynamics

Noticed that, under stress free condition, a specimen with the crack has higher potential energy than the specimen without crack. This is because the potential energy will decrease when free atoms form a crystal. A material body with more surface area yields a higher potential energy. Surface energy can be calculated as the potential energy difference divided by new surface area. An example is given in Figure 2-1 to calculate surface energy with molecular dynamics. Assume graphene cracks in brittle manner and the crack surface has a clean cut boundary. For case one (cf. Figure 2-2(a)), a single layer graphene sheet with a slit is simulated with no external loading. Damping is applied to damp out all kinetic energy and the specimen reaches absolute zero temperature. Damping is then removed and the initial potential energy of U_1 is recorded. For case two (cf. Figure 2-2(b)), The graphene sheet is manually separated into two sheets with a clean cut crack surface. The total potential energy of the separated configuration is calculated as E_2. The clean cut crack surface represents a brittle fracture, which is defined as the fracture that only involves the bond breaking between the crack tip atoms. Notice that, the atom at the new crack surface will inevitably distort due to edge effect; Such distortion can be viewed as plasticity in

continuum mechanics because there are permanent shape changes after loading is removed. Thus there are permanent shape changes even for the brittle fracture.

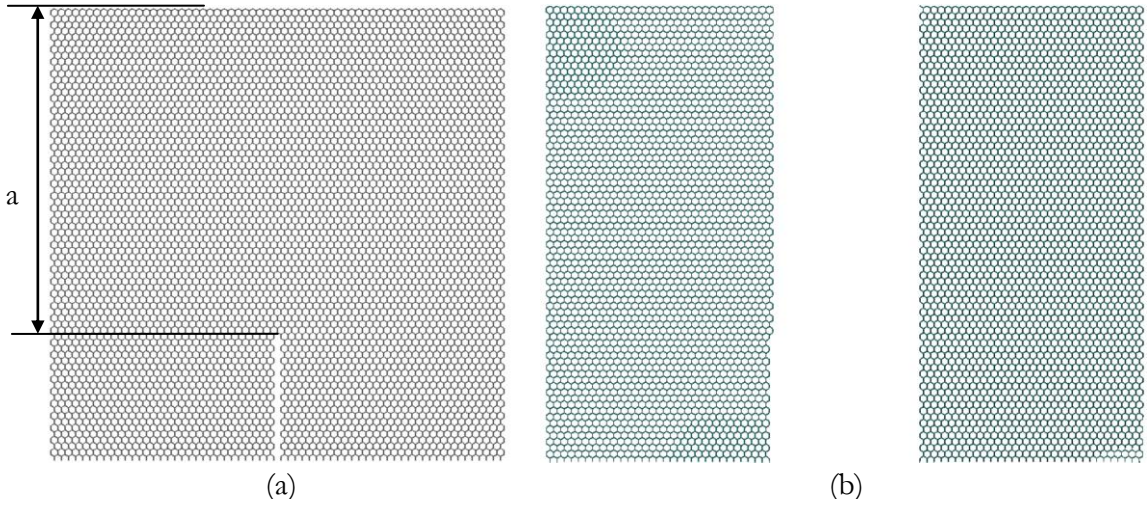

Figure 2-1 (a) original specimen of graphene at stress free stage. (b) cracked specimen of graphene at stress free stage.

The total potential energy of the original specimen under stress free condition is

$$U_1 = -2575.3831AU \tag{2.14}$$

The total potential energy of the cracked specimen under stress free condition is

$$U_2 = -2566.0573AU \tag{2.15}$$

where AU is atomic unit. Notice that the cracked specimen has a higher potential energy

$$U_2 > U_1 \tag{2.16}$$

The difference in potential energy between the initial and the cracked specimens is the surface energy.

$$\begin{aligned}\Delta U &= U_2 - U_1 = (-2566.0573AU + 2575.3831AU) \times 4.3598 \times 10^{-18} \\ &= 4.0674411 \times 10^{-17}\ J\end{aligned} \tag{2.17}$$

The created surface area is

$$\begin{aligned}\Delta A &= a \cdot t = 214.833504AU \times 5.2917721092 \times 10^{-11} m / AU \times 0.34 \times 10^{-9} m \\ &= 3.8652898 \times 10^{-18} m^2\end{aligned} \tag{2.18}$$

The surface energy calculated is

$$2\gamma_{arm} = \frac{\Delta U}{\Delta A} = \frac{4.0674411 \times 10^{-17}\ J}{3.8652898 \times 10^{-18} m^2} = 10.5229913162 J / m^2 \tag{2.19}$$

where a stands for the crack extension length; t is the thickness of the single layer graphene sheet, which is 0.34nm. The surface energy calculated with simulation is in good agreement with that calculated by chemical bond(c.f. eq. (2.13)). Notice that the surface energy calculate by molecular dynamics simulation, $10.52299 J / m^2$,is slightly smaller than that calculated from bond energy $11.1789 J / m^2$. This is because the surface energy calculated by chemical bond counts on the potential energy difference between original and the cracked specimen of perfect lattice shape (c.f. Figure 2-7 (a) (c)). In molecular dynamics, the edge effect of lattice distortion is counted, causing a decrease of system total potential energy. The potential energy difference is calculated between original and the cracked specimen of the relaxed stage (c.f. Figure 2-7 (a) (d)).

In reality, a naturally formed cracked surface of graphene does not have a clean cut boundary(c.f. Figure 2-2(b)). A molecular dynamics simulation is carried out to calculate the surface energy of graphene on a naturally formed crack surface. The initial total potential energy after relaxation , U_1 , is recorded. Afterword, the graphene sheet is gradually pulled apart until crack extension naturally. Later on, the artificial damping is

introduced to damp out all kinetic energy. After the specimen reaches zero temperature again, damping is removed and the final total potential energy, U_5, is recorded. The potential energy decrease is calculated between the original and the naturally cracked specimen of the relaxed stage.

$$\begin{aligned}\Delta U &= U_5 - U_1 = (-2558.7575AU - (-2575.3831AU)) \times 4.3598 \times 10^{-18} \\ &= 7.2484291 \times 10^{-17}\ J\end{aligned} \tag{2.20}$$

$$\begin{aligned}\Delta A &= a \cdot t = 214.833504AU \times 5.2917721092 \times 10^{-11} m / AU \times 0.34 \times 10^{-9} m \\ &= 3.8652898 \times 10^{-18} m^2\end{aligned} \tag{2.21}$$

$$2\gamma = \frac{\Delta U}{\Delta A} = \frac{7.2484291 \times 10^{-17}\ J}{3.8652898 \times 10^{-18} m^2} = 18.7526148751 J / m^2 \tag{2.22}$$

Notice that the surface energy is the potential energy increase of the stress-free specimen before and after crack formation.

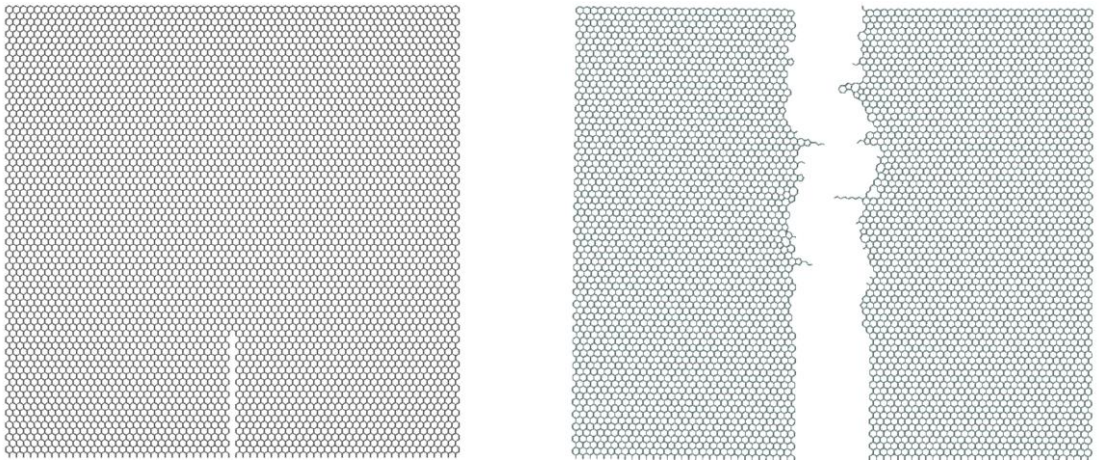

(a) (b)

Figure 2-2 (a) Graphene with a pre manufactured crack (b) The stress free graphene specimen after natural crack propagation through the length.

2.2.3 Ratio between surface energy of different directions

It is noticed that the atomic bond density $n_{<100>} \equiv S_{<100>}^{-1}$ is different along each possible failure plane. Therefore each possible crack propagation direction has its own surface energy. One may converts surface energy from one direction to another based on the information of the failure plane. For example, if crack extends on (1 1 0) direction,

$$2\gamma_{\langle 110\rangle} = \frac{U_{bond}}{S_{\langle 110\rangle}} = \frac{U^{ij}(a)}{\left(\sqrt{2}a\right)^2} = \frac{U^{ij}(a)}{2a^2} \tag{2.23}$$

and the ratio between surface energy of different directions

$$\frac{\gamma_{\langle 110\rangle}}{\gamma_{\langle 100\rangle}} = \frac{S_{\langle 100\rangle}}{S_{\langle 110\rangle}} = \frac{n_{\langle 110\rangle}}{n_{\langle 100\rangle}} \tag{2.24}$$

To demonstrate eqs. (2.3) ,(2.24), we calculate the ratio between surface energy of different directions for graphene. Let t denotes the thickness of grapheme sheet and a denotes the bond length of graphene.

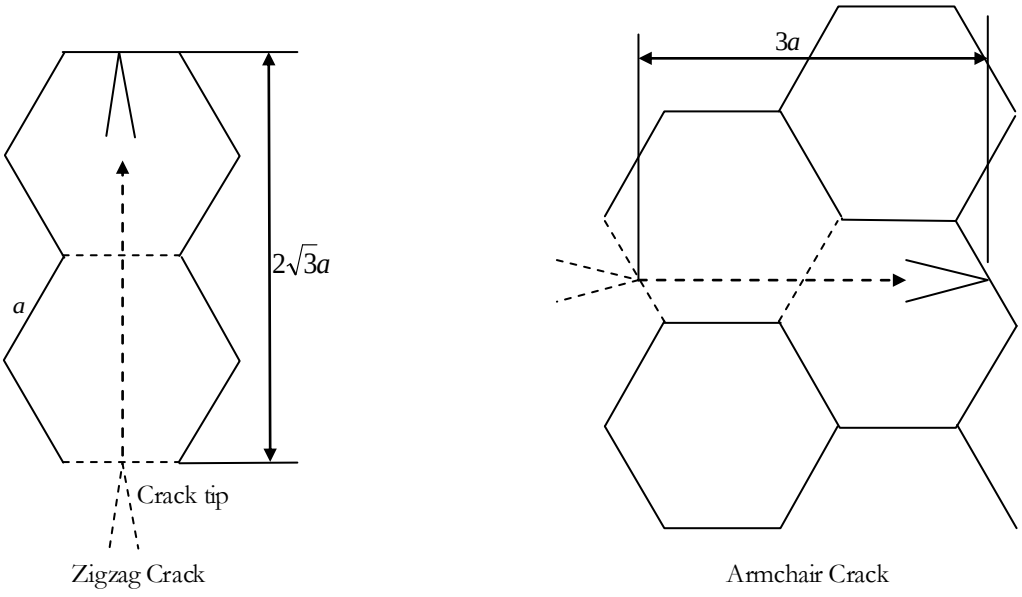

Figure 2-3 Zigzag and Armchair crack direction of grapheme

Let E_b denotes the C=C bond energy in graphene. There are 2 broken bonds when the crack advances from original crack tip (dash line) to current crack tip (solid line) in both armchair and zigzag directions as shown in Figure 2-3. However The atomic density of these two directions are different . The surface energy of zigzag direction is

$$2\gamma_{zig} = \frac{2E_b}{2S_{\langle zig\rangle}} = E_b n_{\langle zig\rangle} = \frac{2E_b}{2\sqrt{3}a \cdot t} = \frac{E_b}{\sqrt{3}a \cdot t} \tag{2.25}$$

where $S_{\langle zig\rangle}$ is the new surface area generated with crack extends one atom forward; $n_{\langle zig\rangle}$ is the bond number density in the zigzag direction. Surface Energy of armchair direction is

$$2\gamma_{arm} = \frac{2E_b}{2S_{\langle arm\rangle}} = E_b n_{\langle arm\rangle} = \frac{2E_b}{2S_{\langle arm\rangle}} = \frac{2E_b}{3a \cdot t} \tag{2.26}$$

where $S_{\langle arm\rangle}$ is the new surface area generated with crack extends one atom forward; $n_{\langle arm\rangle}$ is the bond number density of armchair direction. The ratio between energy release rates of the two directions are

$$\chi_{theroy} \equiv \frac{2\gamma_{armr}}{2\gamma_{zig}} = \frac{n_{\langle arm\rangle}}{n_{\langle zig\rangle}} = \frac{2E_b}{3a \cdot t}\frac{\sqrt{3}a \cdot t}{E_b} = \frac{2}{\sqrt{3}} = 1.154 \tag{2.27}$$

Zhang (Zhang 2014) calculates the graphene energy release rate with MD simulation

$$G_{arm} = 33.18 \tag{2.28}$$

$$G_{zig} = 29.45 \tag{2.29}$$

If we calculate the ratio

$$\chi_{simulation} = \frac{G_{armchair}}{G_{zigzag}} = \frac{33.18}{29.45} = 1.127 \tag{2.30}$$

It is interesting to notice that the ratio of energy release rate between different directions is the ratio of surface energy of such directions. Here we summarize the ratio between surface energy and the ratio between energy release rate calculated by various method in

Table 2-1. LEFM relation $G = K_{IC}^2 / E$ is utilized to convert all results to energy releaser rate (Xu 2012a). The Young's modulus is 1GPa and Poisson's ratio is 0.22 (Zhang 2014).

Method	Zigzag (J/m^2)	Armchair (J/m^2)	Ratio
CM/FEM(Xu 2012b)	G=16.31	G=13.1681	1.2386
DFT(Jun 2008)	G=7.3332	G=5.6829	1.2333
MD(Zhang 2014)	G=33.18	G=29.45	1.127
Surface Energy Calculated with Chemical Bond	2γ=11.1789	2γ=9.682	1.154

Table 2-1 Ratio between Energy Release Rate is the Ratio between Surface Energy of different direction for Graphene

2.3 Revisit Griffith's Energy Release Rate

Griffith's strain energy release rate criterion states that the crack will extend if strain energy release rate G, defined as the strain energy decrease, ΔE, per newly created crack surface area, ΔA, greater than or equals to the surface energy 2γ (Griffith 1921).

$$2\gamma = -\frac{\Delta E}{\Delta A} = -\frac{E_2 - E_1}{A_2 - A_1} \tag{2.31}$$

where E_1 is the strain energy before crack extension. E_2 is the strain energy after crack extension. A_1 is the crack surface area before crack extension. A_2 is the crack surface area after crack extension. Griffith assumed a completely static fracture, where no kinetic energy is involved. Under such condition, he proposed the conservation between the potential energy and surface energy.

$$E_1 + 2\Gamma_1 = E_2 + 2\Gamma_2 \tag{2.32}$$

$$2\Gamma_1 - 2\Gamma_2 = E_2 - E_1 \tag{2.33}$$

where $\Gamma \equiv \gamma A$. Because surface energy is a material constant.

$$2\gamma A_1 - 2\gamma A_2 = E_2 - E_1 \tag{2.34}$$

$$2\gamma = -\frac{E_2 - E_1}{A_2 - A_1} = -\frac{\Delta E}{\Delta A} \tag{2.35}$$

which yield his original statement that the critical energy release rate equals to the surface energy. There are several fundamental flaws within Griffith derivation: Surface energy is part of system total potential energy. The conservation of energy cannot be applied to potential energy and part of potential energy. In fact, there is no need to know surface energy when calculating interatomic potential energy difference before and after crack extension(c.f. Figure 2-4). It is observed that the strain energy decreases with crack extension but surface energy increases with crack extension (c.f. Figure 2-6). Equation (2.32) and Equation (2.35) are erroneous. Conservation of energy needs to be applied to all forms of energy. There are only two forms of energy in molecular dynamics, which are potential energy and kinetic energy. Consider a fixed-grip boundary condition, in which

there is no external work done to the system. The decrease of potential energy (strain energy) is the increase of kinetic energy. If written correctly, equation (2.32) should be

$$E_1 + K_1 = E_2 + K_2 \tag{2.36}$$

where K_1 and K_2 are kinetic energy before and after crack extension respectively. If energy release rate G is defined as

$$G \equiv -\frac{\Delta E}{\Delta A} \tag{2.37}$$

It also implies the energy release rate is also the kinetic energy generation rate.

$$G = -\frac{E_2 - E_1}{A_2 - A_1} = \frac{K_2 - K_1}{A_2 - A_1} \tag{2.38}$$

$$G = -\frac{\Delta E}{\Delta A} = \frac{\Delta K}{\Delta A} \tag{2.39}$$

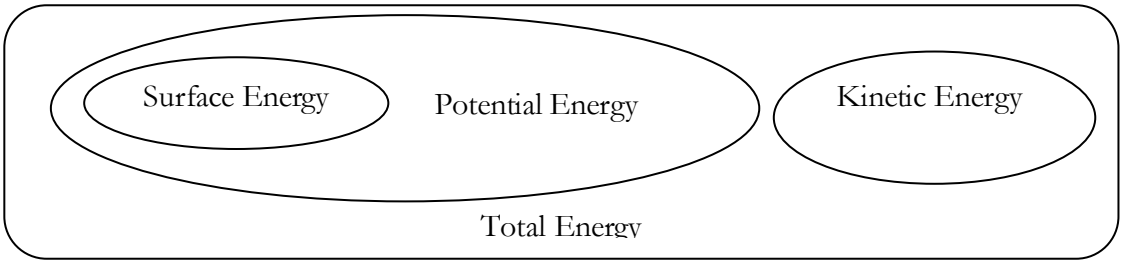

Figure 2-4 The logical diagram of surface energy, potential energy and kinetic energy

From fracture mechanics point of view, only the decrease of potential energy right before and immediately after the crack growth is related to energy release rate. Surface energy is not related to energy release rate.

2.3.1 Magnitude of Energy Release Rate and Surface Energy

It has been demonstrated in previous section that the surface energy is not related to energy release rate. A fair question to ask is: If surface energy is utilized to study fracture, would the value calculated be an overestimation or underestimation of energy release rate? Recall that the energy release rate is the potential energy decrease associated with crack growth right before and immediately after crack extension. Surface energy can be calculated as the bond breaking energy times the bond number density. The surface energy is part of the total potential energy after crack extension.

A molecular dynamics simulation is used to verify the magnitude of energy release rate is always greater than the magnitude of surface energy even in perfect brittle fracture. A single layer graphene sheet is pulled apart until crack extends naturally. The fixed grip boundary condition is imposed after the crack initiation. Referring to Figure 2-5, the stage right before crack extend (green) and the stage immediately after crack extend (red) are overlaid on top of each other for the convince of comparison. For crack extend two atoms forward, bond A and bond B are broken. The bond C and D are pulled almost to the cut-off distance right before the crack extension. bond C and D are relaxed to the lattice constant after crack extension,. The decrease of potential energy for bond C and D is the chemical bond energy U_{bond} at lattice constant.

$$U_C \approx U_D \approx U_{bond} \tag{2.40}$$

Recall that the surface energy can be calculated with bond energy times the bond number density on the crack surface and $U_C = U_D$

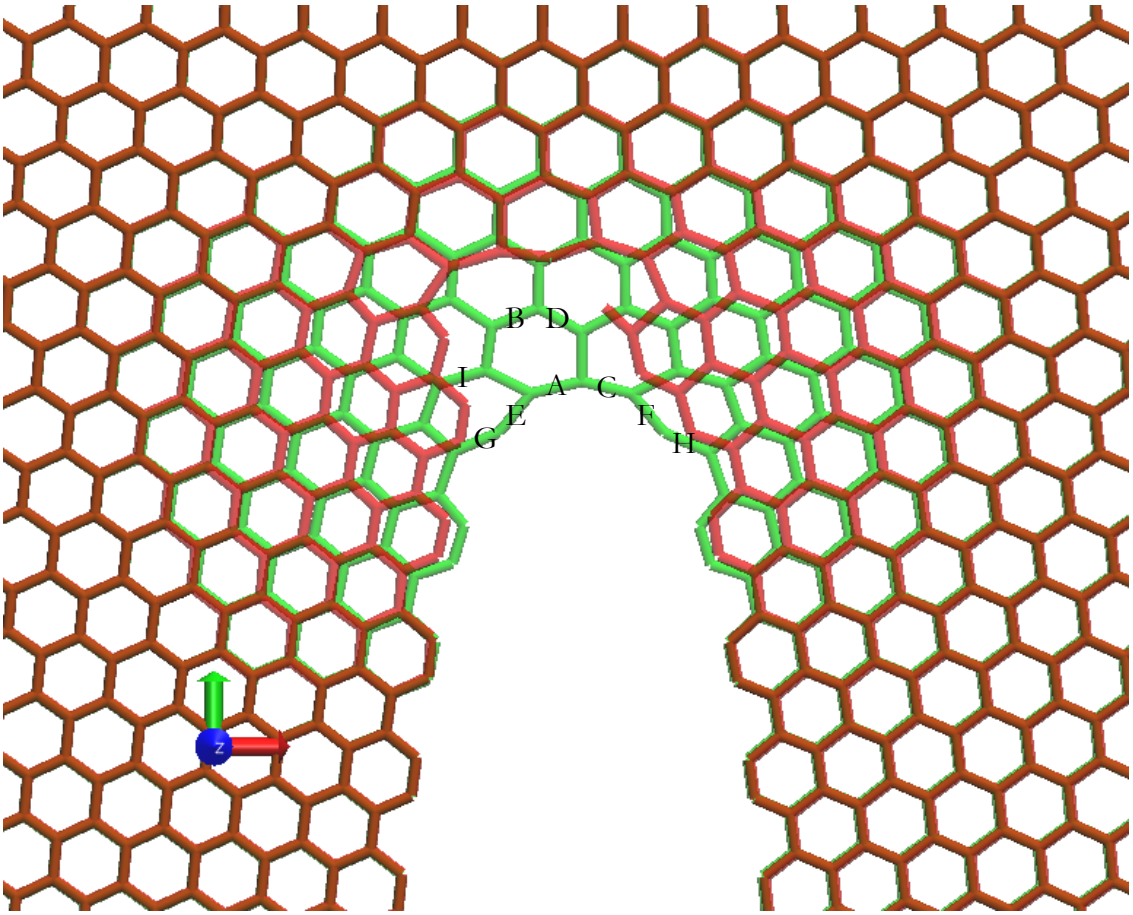

Figure 2-5 Graphene specimen before and after crack extension

Therefore

$$2\gamma = \frac{U_A}{A} = \frac{U_{bond}}{A} = \frac{U_C}{A}\ , \quad 2\gamma = \frac{U_B}{A} = \frac{U_{bond}}{A} = \frac{U_D}{A} \tag{2.41}$$

$$2\gamma = \frac{U_C + U_D}{2A} \tag{2.42}$$

For calculating energy release rate, the decrease of potential energy are contributed by the decrease of bond length of all bonds.

$$G = \frac{U_C + U_D + U_E + U_F + U_I + \ldots}{2A} \tag{2.43}$$

In fact, all the bonds that change length in Figure 2-5 go through a sudden relaxation process, causing the potential energy to decrease and the kinetic energy to increase. Therefore the magnitude of energy release rate is greater than surface energy even in perfect brittle fracture

$$G > 2\gamma \tag{2.44}$$

Right before crack extends, the system has no kinetic energy due to the quasi-static process. However the atomic configuration after bond breaking is not stable because the force is not balanced due to the absent of bond A. The lattice will mobilized to try to reach the equilibrium again. Notice that this relaxation procedure is dynamic in nature. No matter how slow the loading force, one cannot control the speed for the lattice to reorient. The potential energy is transformed to kinetic energy; therefore the strain energy is "released". In terms of plastic fracture, the decrease of total potential energy is attributed to broken bonds at the crack tip as well as dislocations in the plastic zone surrounding the crack tip, which is again not related to surface energy.

2.4 Modified Energy Release Rate Fracture Criterion

To be more precise and clear from ambiguity, allow us to redefine energy release rate, critical energy release rate and energy-release-rate fracture criterion with atomistic point of view.

Energy Release Rate, G : The decrease of interatomic potential energy associated with creating unit new crack surface when crack is assumed to extend at current stage.

$$G = -\frac{dU}{dA} \tag{2.45}$$

$$G = -\frac{dU}{dA} = -\frac{\Delta U}{\Delta a} = -\frac{U(a+\Delta a) - U(a)}{\Delta A} \tag{2.46}$$

where Δa is the distance of crack moving one atom forward; $U(a)$ is the interatomic potential energy at crack length a, referring to the potential energy of the stretched specimen right before crack extension; $U(a+\Delta a)$ is the interatomic potential energy at crack length $a+\Delta a$, referring to the potential energy of the specimen after crack extended a distance Δa; ΔA is the new crack surface area. Noticed the energy release rate can be directly calculated with MD simulation because potential energy is known at any moment. The bond of the crack tip atom can be artificially broken to trigger the crack extending one atom forward and the potential energy decrease associated with this procedure can be measured. This method is similar to the virtual crack closure technique (Yang 2005) except the crack is assumed to be open, not close.

In chapter 3, interatomic potential energy is shown to be equivalent to strain energy. By then, interatomic potential energy release rate is strain energy release rate. The value of energy release rate may also be calculated with node release method in continuum mechanics as described later in chapter 4. In small deformation cases, strain energy release rate calculated by eq. (2.45) is identical to that calculated from stress intensity factor in LEFM as verified in chapter 4 example 3.

Critical Energy Release Rate, G_{cr} : The decrease of interatomic potential energy associated with creating unit new crack surface when crack extends naturally.

$$G_{cr} = -\frac{\Delta U}{\Delta S} \tag{2.47}$$

$$G_{cr} = -\frac{dU}{dA} = -\frac{\Delta U}{\Delta a} = -\frac{U(a+\Delta a) - U(a)}{\Delta A} \tag{2.48}$$

where ΔU is the decrease of interatomic potential energy with crack extension; ΔS is the new crack surface generated with crack extension; ΔU refers to the potential energy difference between the moment of the stretched specimen right before crack extension and the moment of potential energy at crack length $a + \Delta a$.

Energy Release Rate Fracture Criterion: Crack will extend if energy release rate equals to the critical energy release rate, i.e.

$$\begin{cases} G < G_{cr} & \text{Crack Stationary} \\ G = G_{cr} & \text{Crack Extend} \\ G > G_{cr} & \text{Impossible} \end{cases} \tag{2.49}$$

It is claimed that the energy release rate cannot be greater than the critical energy release rate.

2.5 Energy Release Rate Calculation for Brittle and Non-Brittle Material.

In principle, the critical energy release rate criterion is valid for both elastic and plastic fracture. Recall that the critical energy release rate is defined as the difference between potential energy right before and immediately after crack advance. Notice that the decrease

of potential energy is caused by lattice relaxation after bond breaking. In brittle fracture, only the bond at the crack tip breaks. In ductile fracture, bonds breaks at the crack tip as well as in the plastic zone surrounding the crack tip. It is suggested that, as long as the crack growth is self-similar, the critical energy release rate is still a constant in ductile material. Here self-similar means the plastic zone shape, size and the configuration around crack tip are identical regardless the crack speed, crack length, loading condition, crack shape, etc. Assume that the experiment confirmed this assumption, then the amount of the potential energy decrease associated with crack extension is a constant. The energy release rate is also a material constant. A numerical method is introduced to calculated energy release rate with molecular dynamics simulation. The MD program "POLY", developed by James. D. Lee and Zidong Yang, is used to simulate graphene fracture.

Critical energy release rate G_{cr} can be calculated by utilizing molecular dynamic simulation to calculate potential energy difference right before and immediately after crack propagation. Single layer graphene is studied under mode I fracture. Tersoff potential is adopted.

A specimen is gradually loaded until crack extend naturally. System total potential energy right before crack extends, U_3, is recorded. The crack is then spontaneously extends all the way through the specimen. System potential energy right after crack extends, U_4, is recorded.

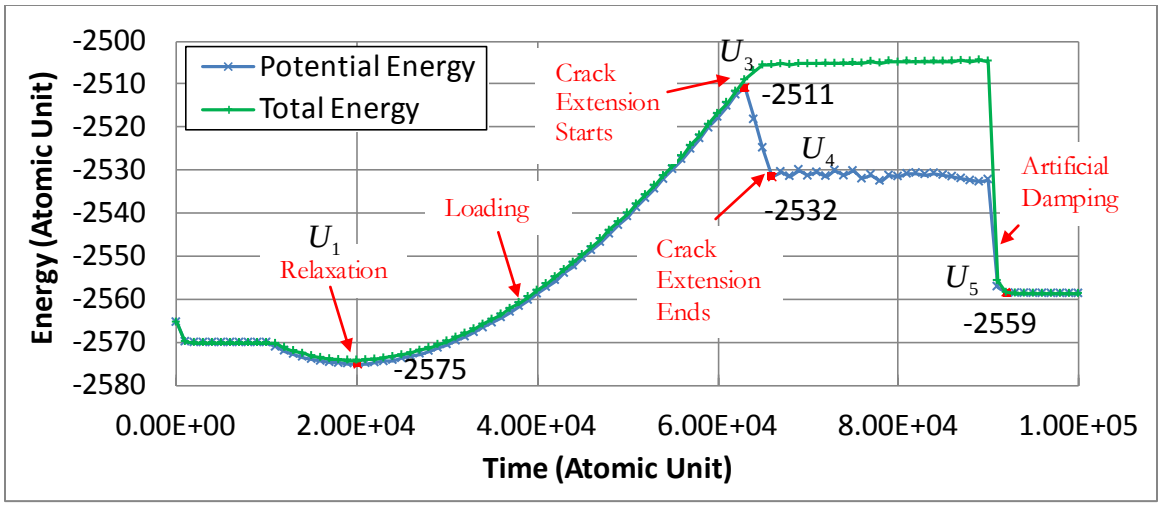

Figure 2-6 Potential Energy and Total Energy of Graphene Fracture

It is observed that the fracture of graphene is not completely brittle. As shown in Figure 2-2(b), the natural crack surface involves not only the bond breaking on the edge, but also the dislocations near the edge. The irregular shape of many pentagon and hexagon formations represents dislocations generated during crack propagation. When taking continuum point of view, this means plasticity appears on the crack surface. If we assume the amount of plasticity generated per unit crack advance is a constant, or in other words, the crack grows self-similarly, it is possible to calculate the constant value of critical energy release rate accordingly. Recall the energy differences are calculated for the moment right before and after crack extension

$$\begin{aligned}\Delta U &= U_4 - U_3 = (-2531.47880AU - (-2510.89320AU)) \times 4.3598 \times 10^{-18} \\ &= -8.9749 \times 10^{-17}\ J\end{aligned} \tag{2.50}$$

$$\Delta A = a \cdot t = 3.8652898 \times 10^{-18} m^2 \tag{2.51}$$

$$G_{arm} = -\frac{\Delta U}{\Delta A} = -\frac{-8.9749 \times 10^{-17}\ J}{3.8652898 \times 10^{-18} m^2} = 23.2186 J / m^2 \tag{2.52}$$

which shows the realistic energy release rate is much larger than the energy release rate calculated with brittle fracture assumption, in other words, graphene is not a brittle material. The energy release rate calculated by other method are present for comparison as shown in

Table 2-2. The relation between energy release rate and stress intensity factor $G = K_{IC}^2 / E$ is utilized to convert all results to energy releaser rate (Xu 2012a). The Young's modulus is 1GPa and Poisson's ratio is 0.22 (Zhang 2014).

Method	G_{arm} (J/m^2)
MD(Ky 2014)	10.24
CM/FEM(Xu 2012b)	13.1681
DFT(Jun 2008)	5.6829
MD(Zhang 2014)	29.45
This Work	23.2186

Table 2-2 Energy Release Rate of Graphene Calculated by Different Method

2.6 Discussion

We redefine energy release rate of fracture mechanics as follows: The instantaneous energy release rate *G* is defined as the potential energy would be released associated with unit crack surface creation if the crack extended at current stage. The critical energy release rate is defined as the release of potential energy associated with unit crack surface

creation when crack grow naturally. The critical energy release rate failure criterion is rewritten as: Crack is stationary if the energy release rate is smaller than the critical energy release rate. Crack will extend if energy release rate reaches the critical potential energy release rate; It is impossible for energy release rate to exceed the critical energy release rate. This definition is valid for both brittle fracture and ductile fracture. In next chapter, the strain energy will be equivalent to interatomic potential energy. Therefore the critical energy release rate is the critical strain energy release rate and is also the critical interatomic potential energy release rate.

The surface energy can be calculated as the chemical bond energy multiplied by the bond number density of a particular failure plane. Surface energy can also be calculated with molecular dynamics by counting the potential energy increase before and after crack extension at the stress free stage. For crystalline material, the surface energy may have different values determined by the different bond number density on each failure plane. Energy release rate can be calculated by molecular dynamics by counting the decrease of potential energy right before and immediately after crack extension.

Critical energy release rate fracture criterion also suggested that the fracture is a dissipative process, which is associated with temperature raise. Notice that there are only two forms of energy in MD: potential energy U and kinetic and thermo energy K. (Kinetic and thermo energy are not distinguished in MD). Due to conservation of energy, The "loss" of potential energy has to be equivalent to the "gain" of the thermo energy and kinetic energy add together for an isolated system. Therefore energy release rate as a material constant also implies the kinetic and thermo energy generation rate is also a material constant.

$$\Delta U + \Delta K = \Delta W \tag{2.53}$$

$\Delta W = 0$ for a fixed grip boundary condition

$$\Delta U = -\Delta K \tag{2.54}$$

$$G = -\frac{\Delta U}{\Delta A} = \frac{\Delta K}{\Delta A} \tag{2.55}$$

If we consider the kinetic energy will eventually be dissipated to thermo energy, then the critical energy release rate is also the heat generation rate in fixed grip condition. Thus the heat generation rate of a material with crack extension is also a constant in fixed grip condition. This statement can be readily checked with experiment.

Surface energy is interpreted as the potential energy stored at the edge of the crystal. It is worthwhile to mention that surface energy is usually calculated with perfect lattice. The lattice distortion due to edge effect is not included in surface energy calculation. A molecular dynamics simulation procedure is suggested to determine the surface energy considering the edge effect. Surface energy is the potential energy increase with new surface area creation(cf. eq. (2.50)). Energy release rate is the potential energy loss with new surface creation. Surface energy is part of system total potential energy, therefore the comparison between surface energy and total potential energy decrease is not meaningful. Surface energy has no direct relationship with energy release rate. In brittle material, the energy release rate is still greater than surface energy.

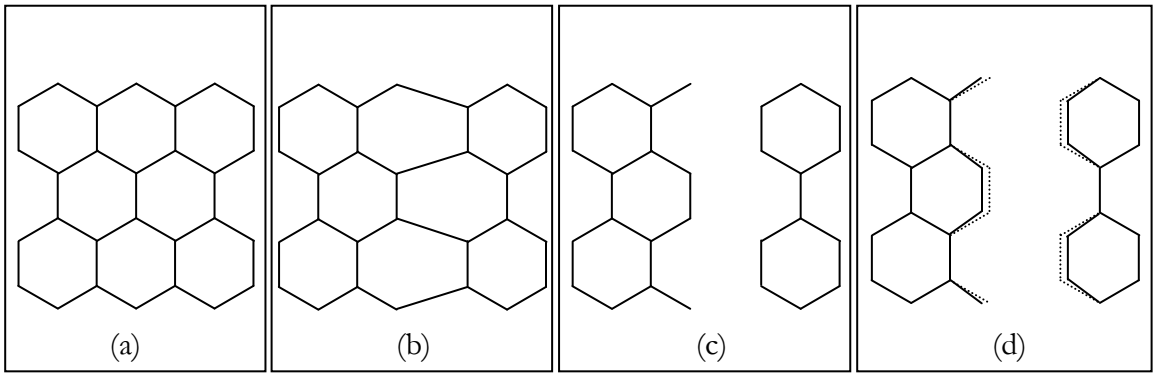

Figure 2-7 (a) Graphene at initial state. (b) Graphene right before bonds broken. (c) Graphene right after bond broken. (d) Lattice reorientation after bond broken

It can be seen that all fractures involve plastic deformation, even in brittle fracture which only involves broken bond at crack tip, (no dislocation or other plastic deformation associated with crack extension). Notice that the lattice distortion (cf. Figure 2-7 (d)) will inevitability change the shape of the newly created crack surface. This change, when viewed from continuum mechanics, is the plastic deformation because the shape permanently changes after loading is removed. (The original shape is a perfect hexagon and the final shape is a distorted hexagon) (cf. Figure 2-7 (d)). Since the material yield minimum potential energy at the relaxed configuration, lattice distortion at the surface will cause the decrease of total potential energy at the final stage. Crack extension process is irreversible even for brittle fracture, which indicates the crack cannot close back if the external loading is reversed. Due to thermodynamic first law of energy conservation, the decrease of potential energy is exactly the increase of kinetic and thermo energy for an isolated system. Due to thermodynamic second law of irreversibility, the kinetic and

thermo energy cannot transform back to potential energy when the loading process is reversed. In addition, the distortion of natural crack surface due to boundary effect will cause a mismatch of lattice when compression load is applied (Figure 2-7 (d)). In real world observation, we never see crack close back for brittle material under any loading condition. For example, glass is usually viewed as a brittle material. It is not possible to fix a cracked glass by compressing it. The non-existence of self-healing phenomenon clearly endorsed the statement that even brittle fracture is associated with dissipative plasticity effect and heat generation(c.f. (2.55).

It is important to specify the proper region to calculate energy release rate. Griffith didn't specify the size of the specimen. Since Inglis elliptical hole solution is utilized to derive energy balance, he implicitly states that the specimen is an infinitely plate under uniform tension. Consider that a dog-bone specimen contains a crack as shown in Figure 2-8(a)

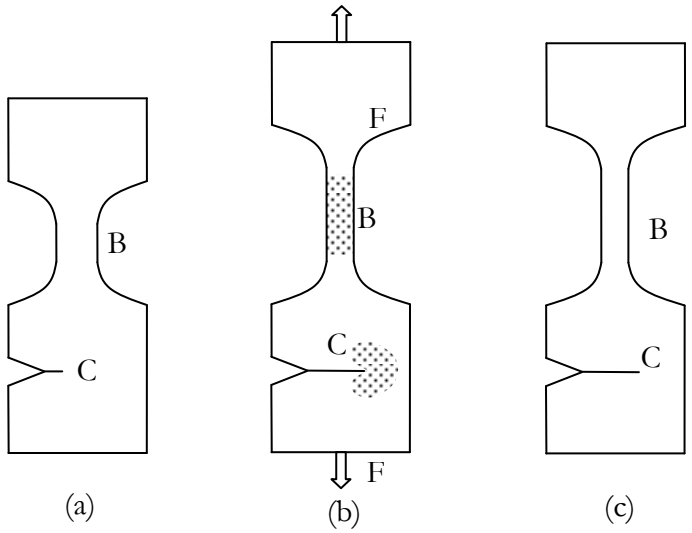

Figure 2-8 (a) Tensile and Fracture Combined Specimen. (b) Specimen undergo plastic deformation in area C and crack extends in area B (c) specimen after loading is removed.

The specimen is loaded with force *F* such that the material in neck area C undergoes plastic deformation at the same time the crack in area B extends. (cf. Figure 2-8). The total energy loss is the shaded area enclosed by force-displacement curve of the grip (cf. Figure 2-9). When calculating global energy release rate, the work done by the grip force (shaded area enclosed by force-displacement curve) is dived by the increase of crack length to calculate energy release rate. The value of energy release rate calculated with this method is not correct. Notice that the potential energy decrease due to plastic deformation in neck area B also contributes to the decrease of total potential energy. Since the plastic deformation in necking area B is not related to crack in area B, the potential energy loss in area B should be excluded when calculating energy release at the crack tip.

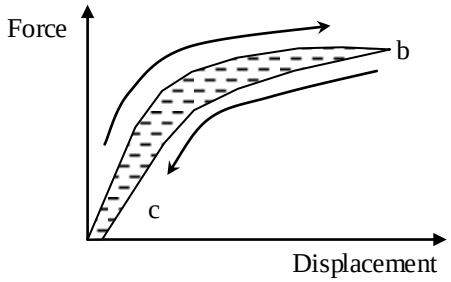

Figure 2-9 Force Displacement Curve of Tension Crack Combined Specimen

It is suggested that the energy release rate should be calculated in a region close enough to the crack tip where no plasticity appears other than that caused by the crack (cf. Figure 2-10(a)). Also, such region has to be big enough so that the whole plastic zone and the

elastic zone involves lattice relaxation after bond breaking are enclosed in the region (cf. Figure 2-10(b)).

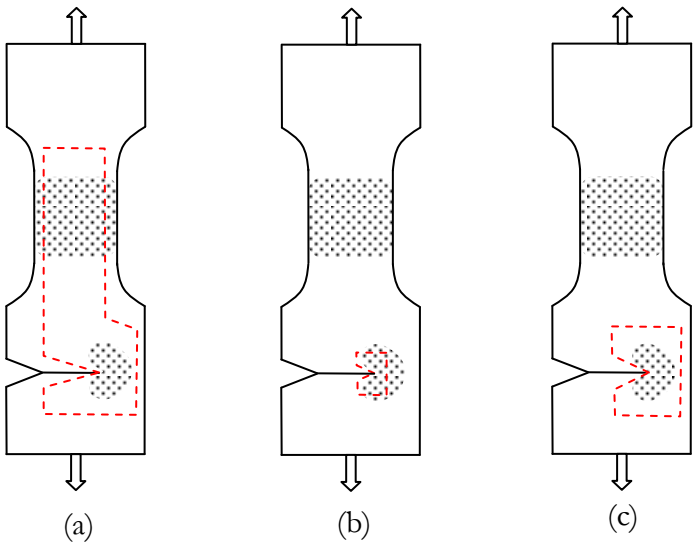

Figure 2-10 Region Selection in Energy Release Rate Calculation. (a) Inappropriate selection: Contain plastic zone not associate with crack. (b) Inappropriate selection: Does not contain the whole plastic zone associates with crack. (c) Appropriate selection: Contains the whole plastic zone caused by crack and part of the elastic zone involves the lattice relaxation after bond breaking but excludes the plastic zone not caused by crack. The shaded area represents the plastic zone and the elastic zone that involves lattice relaxation after bond breaking.

Recall that J-integral calculates the energy flux on the edge of a close-loop integral path (Freund 1990). If the integral path encloses the plastic region unrelated to crack (cf. Figure 2-10 (a), or the integral path does not enclose all plastic region of the crack tip (cf. Figure 2-10 (b)), The J-integral and the energy release rate calculated does not represents a property of the crack. It is the strain energy reduced due to a mixture of events in the

specimen. It can be seen that *J-integral is NOT path independent if plasticity is considered*. An integral path that is too close to the crack tip will exclude potential energy decrease in part of the crack tip plastic zone that are not enclosed by the integral path (cf. Figure 2-10 (b)). A integral path that is too far away from crack tip will include the potential energy decrease of other phenomenon not related to the crack extension (cf. Figure 2-10 (a)). The proper integral path should enclose the entire crack tip plastic zone but exclude plastic zone not related to the crack (cf. Figure 2-10 (c)).

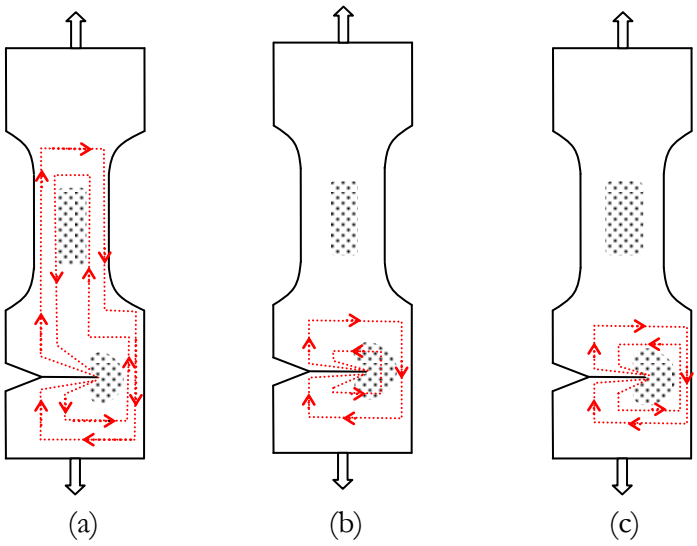

Figure 2-11 Integral Path Selection for J-Integral. Shaded area represents the plastic zone. (a) Inappropriate selection: Integral path enclose the plastic zone not caused by crack. (b) Inappropriate selection: Integral path does not enclose entire plastic zone caused by the crack. (c) Appropriate selection: Integral path remains in elastic region and contains the whole plastic zone caused by crack but excludes the plastic zone not caused by crack.

Chapter 3

Work Conjugacy between Stresses and Strains in Molecular Dynamics

3.1. Introduction

Atomistic stresses and strains are important measurement to bridge the gap between molecular dynamics (MD) and continuum mechanics (CM). Since Clausius and Maxwell first derived the virial theory (Clausius 1870, Maxwell 1870), many researchers made significant progresses in defining stress and strain in molecular dynamic (Shenoy 1999, Subramaniyan 2008, Zhou 2003, Cheung 1991, Zimmerman, WebbIII et al. 2004, Miller, Tadmor 2002, Zimmerman, Bammann et al. 2009, Cheng 2014). Because virial theory is derived from macroscopic equilibrium (Murdoch 2007, Cheung 1991), difficulties have arisen to define the stress at each atom (Sun 2006). To avoid using virial theory, this work is built upon the strain calculation from a two-atom system and the equivalence between the strain energy in CM and the interatomic potential energy in MD.

In this work, only the material system at absolute zero temperature is considered. It is noticed that there are two methods to calculate potential energy of an atomistic system. The first one is to calculate the interatomic potential directly. The second one is to convert the atomistic force and displacement to stress and strain and then calculate from their strain energy. Since MD and CM describe the same physical phenomenon, it is believed that the potential energy calculated from MD should be identical to the potential energy calculated from CM in all conditions. In order to calculate the strain energy, certain stress and strain

have to be defined from atomic force and displacement. Only a specific stress and strain pair, called conjugate pair, forms a scalar valued strain energy function, which should be equal to the interatomic potential energy. A two-atom system is first considered. Since atomistic displacement field is well defined in such system, various forms of strain can be obtained accordingly, e.g., Eulerian strain, Lagrangian strain, Hencky strain, deformation gradient, etc. Among them, atomistic Hencky strain and atomistic Kirchhoff stress are proved to be a thermodynamic conjugate pair and their corresponding strain energy equals to the interatomic potential energy. Since Hencky strain and Kirchhoff stress are a conjugate pair in continuum mechanics (Fitzgerald 1980, Xiao 1999, Norris 2008) and atomistic Hencky strain is considered to be equivalent to Hencky Strain in CM, atomistic Kirchhoff stress in MD is equivalent to Kirchhoff stress in continuum mechanics. Following this idea, the atomistic second order Piola-Kirchhoff (PK2) stress is defined and proved to be conjugate to atomistic Lagrangian strain. Later on, these definitions and proof of conjugacy are generalized to multi-atom system with the stress taking summation and the strain taking average of the influence from all other atoms. The result indicates that the atomistic Kirchhoff stress is nothing but virial stress defined at the undeformed volume occupied by each atom summing up the influence of all other atoms. It is noticed that the atomistic Kirchhoff stress is the potential part of the "atomic level stress" named by some researchers(Cheung 1991).

To begin with, we propose a method to define conjugate stress and strain for a pair of atoms; later we generalize this method to system with many atoms.

3.2 . Work Conjugacy between Stress and Strain

Various strain measures can be adopted to describe a displacement field in continuum mechanics (Tong 2001, Eringen 1989), for example:

Deformation gradient $$F_{kK} \equiv x_{k,K} \quad , \quad F^{-1}_{Kk} = X_{K,k} \tag{3.1}$$

Green deformation tensor $$C_{KL} \equiv x_{k,K} x_{k,L} \tag{3.2}$$

Cauchy deformation tensor $$c_{kl} \equiv X_{K,k} X_{K,l} \tag{3.3}$$

Lagrangian strain $$E_{KL} \equiv \frac{1}{2}\left(C_{KL} - \delta_{KL}\right) \tag{3.4}$$

Eulerian strain $$e_{kl} \equiv \frac{1}{2}\left(\delta_{kl} - c_{kl}\right) \tag{3.5}$$

Right Cauchy-Green deformation tensor $$B_{KL} \equiv X_{K,k} X_{L,k} \tag{3.6}$$

Left Cauchy-Green stretch tensor $$b_{kl} \equiv x_{k,K} x_{l,K} \tag{3.7}$$

Similar to strain, various stress tensors can be defined, for example:

Cauchy stress tensor $$t_{kl} \equiv \frac{df_l}{da} n_k \tag{3.8}$$

Kirchhoff stress tensor $$\tau_{kl} \equiv j t_{kl} \tag{3.9}$$

First-order Piola-Kirchhoff stress (PK1) $$T_{Kl} \equiv \frac{df_l}{dA} N_K = j t_{kl} X_{K,k} \tag{3.10}$$

Second-order Piola-Kirchhoff stress (PK2) $$T_{KL} \equiv \frac{dF_L}{dA} N_K = j t_{kl} X_{K,k} X_{L,l} \tag{3.11}$$

where $j \equiv \det(x_{k,K})$; f_l is force in Eulerian coordinate; A and a are areas in undeformed and deformed configurations, respectively; n_k and N_K are unit vectors normal to the

deformed and undeformed areas. It is worthwhile to mention that $T_{Kl}dA_K = t_{kl}da_k = f_l$, which implies T_{Kl} is the engineering stress, equals to force per undeformed area.

A hyperelastic material refers to a material which has a scalar-valued strain energy function $\sum$ and a stress tensor $\mathbf{S}$ can be obtained from the derivative of the strain energy function with respect to the conjugated strain tensor $\mathbf{E}$ (Hashiguchi 2013), i.e.

$$\mathbf{S} = \frac{\partial \sum}{\partial \mathbf{E}} \tag{3.12}$$

As a consequence, the work done by the stress is independent of the loading path. It is noticed that, in MD, all materials that can be described by an interatomic potential have the same characteristics in hyperelastic material. Because, in MD, the existence of an interatomic potential *U* enables one to find the interatomic force through a potential and the work done by the force is independent of the loading path. One may claim that the interatomic force $\mathbf{f}^{\alpha}$ and displacement $\mathbf{r}^{\alpha}$ are a conjugate pair because of

$$\mathbf{f}^{\alpha} = -\frac{\partial U}{\partial \mathbf{r}^{\alpha}} \tag{3.13}$$

In continuum mechanics, the stress and strain of a hyperelastic material have to satisfy work conjugacy as defined by Hill (Hill 1970).

$$\dot{\Sigma} = \frac{\partial \Sigma}{\partial \mathbf{E}} : \dot{\mathbf{E}} = \mathbf{S} : \dot{\mathbf{E}} \tag{3.14}$$

The work done per unit volume by the stress can be obtained as

$$\int_0^{\mathbf{E}} \mathbf{S} : d\mathbf{E} = \int_0^{\mathbf{E}} \frac{\partial \Sigma}{\partial \mathbf{E}} : d\mathbf{E} = \int_0^{\mathbf{E}} d\Sigma = \Sigma(\mathbf{E}) - \Sigma^o \tag{3.15}$$

It is emphasized that not any stress and any strain can form a conjugate pair. In fact, we may list a few famous stress-strain conjugate pairs as follows.

First order Piola Kirchhoff stress (PK1) T_{Kl} and deformation gradient $x_{l,K}$

$$T_{Kl} = \rho^0 \frac{\partial \psi}{\partial x_{l,K}} = \frac{\partial \Sigma}{\partial x_{l,K}} \tag{3.16}$$

Second order Piola Kirchhoff stress (PK2) T_{KL} and Lagrangian Strain E_{KL}

$$T_{KL} = \rho^0 \frac{\partial \psi}{\partial E_{KL}} = \frac{\partial \Sigma}{\partial E_{KL}} \tag{3.17}$$

Kirchhoff Stress and Hencky Strain

$$\boldsymbol{\tau} = \frac{\partial \Sigma}{\partial \mathbf{h}} \tag{3.18}$$

where ρ_0 and ρ are mass densities in undeformed and deformed states, respectively; $\psi \equiv \Sigma / \rho_0$ is the Helmholtz free energy density.

It is seen that, from eqs. (3.19)(3.20)(3.21), Cauchy stress is not conjugate to deformation gradient, left Cauchy-Green stretch tensor or Eulerian strain tensor (Xiao 1999, Xiao,H., Bruhns,O.T. and Meyers, M.,M. 1998).

$$t_{kl} = \rho \frac{\partial \psi}{\partial x_{l,K}} x_{k,K} = j^{-1} \frac{\partial \Sigma}{\partial x_{l,K}} x_{k,K} \tag{3.19}$$

$$t_{kl} = 2\rho b_{km} \frac{\partial \psi}{\partial b_{ml}} = 2 j^{-1} b_{km} \frac{\partial \Sigma}{\partial b_{ml}} \tag{3.20}$$

$$t_{kl} = \rho \frac{\partial \psi}{\partial e_{km}} c_{lm} = j^{-1} \frac{\partial \Sigma}{\partial e_{km}} c_{lm} \tag{3.21}$$

3.3 Hencky Strain

Ludwik defined one dimensional Hencky strain as "small increment of length divided by the instantaneous length" (Ludwik 1909)

$$d\varepsilon_h \equiv dr / r \tag{3.22}$$

One dimensional Hencky strain may be derived from one dimensional engineering stress $\varepsilon_{eng} \equiv (r - r_0) / r$ as

$$\varepsilon_h = \int_{r_0}^{r} \frac{dr}{r} = \ln r \Big|_{r_0}^{r} = \ln \frac{r}{r_0} = \ln\left(1 + \frac{r - r_0}{r_0}\right) = \ln(1 + \varepsilon_{eng}) \tag{3.23}$$

where r_0 and r denote the original and current lengths, respectively. Hencky strain is also referred as logarithmic strain. It is not straightforward to define a shear logarithmic strain. As a generalization of Ludwik's idea, a rigorous definition of 3-D Hencky strain is summarized by Fitzgerald as follows (Fitzgerald 1980). Recall that deformation gradient F_{kK} can be polar decomposed to a right stretch tensor U_{LK} followed by a rigid rotation R_{kL} or a rigid rotation R_{lK} followed by a left stretch tensor V_{kl} (Eringen 1989, Truesdell, Noll 2004, Davies 2003)

$$F_{kK} = R_{kL} U_{LK} = V_{kl} R_{lK} \tag{3.24}$$

Then one may find the eigenvalue matrix $\mathbf{\Lambda}$ and eigenvector matrix $\mathbf{Q}$ by j

$$\mathbf{\Lambda} = \mathbf{Q}\mathbf{V}\mathbf{Q}^{\mathbf{T}} \tag{3.25}$$

$$\mathbf{V} = \mathbf{Q}^{\mathbf{T}}\mathbf{\Lambda}\mathbf{Q} \tag{3.26}$$

where $\mathbf{\Lambda} = \begin{bmatrix} \lambda_1 & 0 & 0 \\ 0 & \lambda_2 & 0 \\ 0 & 0 & \lambda_3 \end{bmatrix}; \mathbf{Q} = \begin{bmatrix} \begin{pmatrix} \\ \mathbf{q_1} \\ \\ \end{pmatrix} & \begin{pmatrix} \\ \mathbf{q}_2 \\ \\ \end{pmatrix} & \begin{pmatrix} \\ \mathbf{q}_3 \\ \\ \end{pmatrix} \end{bmatrix}; \mathbf{q_1}, \mathbf{q_2}, \mathbf{q_3}$ are the three eigenvectors corresponding to the three eigenvalues $\lambda_1, \lambda_2, \lambda_3$ of matrix $\mathbf{V}$. Now the logarithm can be performed on the diagonal elements

$$\ln(\mathbf{\Lambda}) = \ln\begin{bmatrix} \lambda_1 & 0 & 0 \\ 0 & \lambda_2 & 0 \\ 0 & 0 & \lambda_3 \end{bmatrix} = \begin{bmatrix} \ln\lambda_1 & 0 & 0 \\ 0 & \ln\lambda_2 & 0 \\ 0 & 0 & \ln\lambda_3 \end{bmatrix} \tag{3.27}$$

Then $\mathbf{\Lambda}$ is rotated back by $\mathbf{Q}^{\mathbf{T}}$. Finally, the generalized Hencky strain is defined as(Fitzgerald 1980, Davies 2003)

$$\mathbf{h} \equiv \ln(\mathbf{V}) = \mathbf{Q}^{T} \ln\left(\mathbf{\Lambda}\right)\mathbf{Q} \tag{3.28}$$

One may prove that Hencky strain $\mathbf{h}$ and Kirchhoff stress $\boldsymbol{\tau}$ is a thermodynamic pair (Xiao 1999, Norris 2008, Fitzgerald 1980). Fitzgerald, utilizing stress power along with Clausius-Duhem inequality (Fitzgerald 1980), proved that, when the material is isotropic elastic (Hoger 1987), Hencky strain and Kirchhoff stress commute, i.e.

$$\boldsymbol{\tau}\mathbf{h} = \mathbf{h}\boldsymbol{\tau} \tag{3.29}$$

which leads to

$$\boldsymbol{\tau} = \frac{\partial \Sigma}{\partial \mathbf{h}} \tag{3.30}$$

3.4 . Stress and strain in simple tension case

A. Strain

Consider a simple tension case specified by (cf. Figure 3-1)

$$\begin{bmatrix} x \\ y \\ z \end{bmatrix} = \begin{bmatrix} k & 0 & 0 \\ 0 & m & 0 \\ 0 & 0 & n \end{bmatrix} \begin{bmatrix} X \\ Y \\ Z \end{bmatrix} \text{ or equivalently } \begin{bmatrix} X \\ Y \\ Z \end{bmatrix} = \begin{bmatrix} k^{-1} & 0 & 0 \\ 0 & m^{-1} & 0 \\ 0 & 0 & n^{-1} \end{bmatrix} \begin{bmatrix} x \\ y \\ z \end{bmatrix}$$

where $k \equiv x/X$, $m \equiv y/Y$, and $n \equiv z/Z$ are constants.

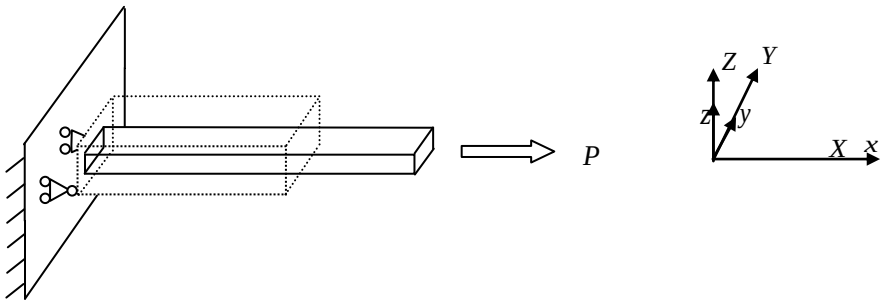

Figure 3-1 Three Dimensional Simple Tension Case

Therefore the Jacobian is obtained as

$$j = \frac{V}{V_0} = kmn = \frac{x}{X}\frac{y}{Y}\frac{z}{Z} \tag{3.31}$$

The displacements in Lagrangian coordinate U_K and Eulerian coordinate u_k are

$$U_K = \delta_{Kl} x_l - X_K \,,\; u_k = x_k - \delta_{Lk} X_L \tag{3.32}$$

which leads to

$$U_K = \begin{bmatrix} kX - X \\ mY - Y \\ nZ - Z \end{bmatrix},\; u_k = \begin{bmatrix} x - k^{-1}x \\ y - m^{-1}y \\ z - n^{-1}z \end{bmatrix} \tag{3.33}$$

$$U_{K,L} = \begin{bmatrix} k-1 & 0 & 0 \\ 0 & m-1 & 0 \\ 0 & 0 & n-1 \end{bmatrix},\; u_{k,l} = \begin{bmatrix} 1-k^{-1} & 0 & 0 \\ 0 & 1-m^{-1} & 0 \\ 0 & 0 & 1-n^{-1} \end{bmatrix} \tag{3.34}$$

It is straightforward to calculate the followings:

1. Deformation gradient and inverse deformation gradient

$$F_{kK} \equiv x_{k,K} = \begin{bmatrix} k & 0 & 0 \\ 0 & m & 0 \\ 0 & 0 & n \end{bmatrix},\; F_{K,k} \equiv X_{K,k} = \begin{bmatrix} k^{-1} & 0 & 0 \\ 0 & m^{-1} & 0 \\ 0 & 0 & n^{-1} \end{bmatrix} \tag{3.35}$$

2. Green deformation tensor and Lagrangian strain tensor

$$C_{KL} \equiv x_{k,K} x_{k,L} = \begin{bmatrix} k^2 & 0 & 0 \\ 0 & m^2 & 0 \\ 0 & 0 & n^2 \end{bmatrix},\; E_{KL} \equiv \frac{1}{2}\left(C_{KL} - \delta_{KL}\right) = \frac{1}{2}\begin{bmatrix} k^2-1 & 0 & 0 \\ 0 & m^2-1 & 0 \\ 0 & 0 & n^2-1 \end{bmatrix} \tag{3.36}$$

3. Cauchy deformation tensor and Eulerian strain tensor

$$c_{kl} \equiv x_{K,k} x_{K,l} = \begin{bmatrix} k^{-2} & 0 & 0 \\ 0 & m^{-2} & 0 \\ 0 & 0 & n^{-2} \end{bmatrix}, \; e_{kl} \equiv \frac{1}{2}\left(\delta_{kl} - c_{kl}\right) = \frac{1}{2}\begin{bmatrix} 1-k^{-2} & 0 & 0 \\ 0 & 1-m^{-2} & 0 \\ 0 & 0 & 1-n^{-2} \end{bmatrix} \quad (3.37)$$

4. Infinitesimal Lagrangian strain and Eulerian strain

$$\tilde{E}_{KL} \equiv \frac{U_{K,L} + U_{L,K}}{2} = \begin{bmatrix} k-1 & 0 & 0 \\ 0 & m-1 & 0 \\ 0 & 0 & n-1 \end{bmatrix}$$

$$\tilde{e}_{kl} \equiv \frac{u_{k,l} + u_{l,k}}{2} = \begin{bmatrix} 1-k^{-1} & 0 & 0 \\ 0 & 1-m^{-1} & 0 \\ 0 & 0 & 1-n^{-1} \end{bmatrix} \quad (3.38)$$

Recall eqs. (24-28), Hencky strain in simple tension case can be calculated as

$$V_{kl} = \begin{bmatrix} k & 0 & 0 \\ 0 & m & 0 \\ 0 & 0 & n \end{bmatrix}, \quad R_{lK} = \begin{bmatrix} 1 & 0 & 0 \\ 0 & 1 & 0 \\ 0 & 0 & 1 \end{bmatrix} \quad (3.39)$$

$$\mathbf{\Lambda} = \begin{bmatrix} k & 0 & 0 \\ 0 & m & 0 \\ 0 & 0 & n \end{bmatrix} \qquad \mathbf{Q} = \begin{bmatrix} 1 & 0 & 0 \\ 0 & 1 & 0 \\ 0 & 0 & 1 \end{bmatrix} \quad (3.40)$$

$$\mathbf{h} = \ln \mathbf{V} = \mathbf{Q} \ln(\mathbf{\Lambda}) \mathbf{Q}^T = \begin{bmatrix} \ln k & 0 & 0 \\ 0 & \ln m & 0 \\ 0 & 0 & \ln n \end{bmatrix} \tag{3.41}$$

Recall eqs. (3.38)(3.41), Hencky strain becomes

$$\mathbf{h} = \begin{bmatrix} \ln\left(1+\tilde{E}_{11}\right) & 0 & 0 \\ 0 & \ln(1+\tilde{E}_{22}) & 0 \\ 0 & 0 & \ln\left(1+\tilde{E}_{33}\right) \end{bmatrix} \tag{3.42}$$

In 1-D, engineering strain is defined as $\varepsilon_{eng} \equiv \tilde{E}_{11}$, which can also be calculated as

$$\varepsilon_{eng} \equiv \Delta r / r_0 = \frac{r - r_o}{r_o} = k - 1 \tag{3.43}$$

Therefore the 1-D Hencky strain becomes

$$h_{11} = \ln(k) = \ln\left(1+\varepsilon_{eng}\right) \tag{3.44}$$

which yields the classic 1-D formula given by Ludwik (Ludwik 1909). Here we have made no small-strain approximation although engineering strain (infinitesimal strain) is utilized to calculate the Hencky strain.

B. Stress Calculation

First order Piola-Kirchhoff stress T_{Kl} is defined as the force acting on a surface divided by the original area of the surface (cf. eq.(3.10)). This is why it is called the engineering stress. In simple tension case, T_{11} is the only non-zero term in first order Piola-Kirchhoff stress tensor, i.e.

$$\mathbf{T} = \begin{bmatrix} T_{11} & T_{12} & T_{13} \\ T_{21} & T_{22} & T_{23} \\ T_{31} & T_{32} & T_{33} \end{bmatrix} = \begin{bmatrix} T_{11} & 0 & 0 \\ 0 & 0 & 0 \\ 0 & 0 & 0 \end{bmatrix} \tag{3.45}$$

Referring to eqs. (3.9)(3.10)(3.11), Kirchhoff stress, Cauchy stress, and PK2 stress can be readily obtained as

$$\tau_{kl} = \begin{bmatrix} T_{11} & 0 & 0 \\ 0 & 0 & 0 \\ 0 & 0 & 0 \end{bmatrix} \begin{bmatrix} k & 0 & 0 \\ 0 & m & 0 \\ 0 & 0 & n \end{bmatrix} = \begin{bmatrix} kT_{11} & 0 & 0 \\ 0 & 0 & 0 \\ 0 & 0 & 0 \end{bmatrix} = \begin{bmatrix} \left(1+\tilde{E}_{11}\right)T_{11} & 0 & 0 \\ 0 & 0 & 0 \\ 0 & 0 & 0 \end{bmatrix} \tag{3.46}$$

$$\begin{aligned} t_{kl} &= \frac{1}{kmn} \begin{bmatrix} k & 0 & 0 \\ 0 & m & 0 \\ 0 & 0 & n \end{bmatrix} \begin{bmatrix} T_{11} & 0 & 0 \\ 0 & 0 & 0 \\ 0 & 0 & 0 \end{bmatrix} = \begin{bmatrix} T_{11}/mn & 0 & 0 \\ 0 & 0 & 0 \\ 0 & 0 & 0 \end{bmatrix} \\ &= \begin{bmatrix} T_{11}A_0/A & 0 & 0 \\ 0 & 0 & 0 \\ 0 & 0 & 0 \end{bmatrix} = \frac{V_o}{V} \begin{bmatrix} \tau_{11} & 0 & 0 \\ 0 & 0 & 0 \\ 0 & 0 & 0 \end{bmatrix} \end{aligned} \tag{3.47}$$

$$T_{KL} = \begin{bmatrix} k^{-1} & 0 & 0 \\ 0 & m^{-1} & 0 \\ 0 & 0 & n^{-1} \end{bmatrix} \begin{bmatrix} \tau_{11} & 0 & 0 \\ 0 & 0 & 0 \\ 0 & 0 & 0 \end{bmatrix} \begin{bmatrix} k^{-1} & 0 & 0 \\ 0 & m^{-1} & 0 \\ 0 & 0 & n^{-1} \end{bmatrix} = \begin{bmatrix} k^{-2}\tau_{11} & 0 & 0 \\ 0 & 0 & 0 \\ 0 & 0 & 0 \end{bmatrix} \tag{3.48}$$

It is seen that (cf. eq.(3.46))

$$\sigma_{Kirchhoff} = \sigma_{eng}\left(1+\varepsilon_{eng}\right) \tag{3.49}$$

One may also obtain

$$
\begin{aligned}
e_{kl} &= \frac{1}{2}\begin{bmatrix} 1-k^{-2} & 0 & 0 \\ 0 & 1-m^{-2} & 0 \\ 0 & 0 & 1-n^{-2} \end{bmatrix} \\
&= \frac{1}{2}\begin{bmatrix} \dfrac{2\tilde{E}_{11}+\tilde{E}_{11}^2}{1+2\tilde{E}_{11}+\tilde{E}_{11}^2} & 0 & 0 \\ 0 & \dfrac{2\tilde{E}_{22}+\tilde{E}_{22}^2}{1+2\tilde{E}_{22}+\tilde{E}_{22}^2} & 0 \\ 0 & 0 & \dfrac{2\tilde{E}_{33}+\tilde{E}_{33}^2}{1+2\tilde{E}_{33}+\tilde{E}_{33}^2} \end{bmatrix}
\end{aligned} \tag{3.50}
$$

In 1-D simple tension case, the results may be summarized as

$$\varepsilon_{true} = \varepsilon_{\log} = \varepsilon_{Hencky} = \ln(1+e_{eng}) \tag{3.51}$$

$$\sigma_{Kirchhoff} = \sigma_{eng}\left(1+e_{eng}\right) \tag{3.52}$$

$$e_{Euler} = \frac{2e_{eng}+e_{eng}^2}{2+4e_{eng}+2e_{eng}^2} \tag{3.53}$$

$$\sigma_{true} = \sigma_{Cauchy} = \sigma_{eng}A_0 / A \tag{3.54}$$

Although these results are for the special simple tension case, no approximation has been made.

For linear isotropic elastic material, the strain energy density function can be written as

$$\Sigma = \frac{1}{2}\lambda h_{mm}h_{nn} + \mu h_{kl}h_{kl} \tag{3.55}$$

where λ and μ are the two Lame constants. Then eq. (3.30) leads to the following Hencky strain – Kirchhoff stress relation

$$\tau_{ij} = \lambda h_{mm}\delta_{ij} + 2\mu h_{ij} \tag{3.56}$$

or

$$h_{kl} = \frac{1}{E}\left[\tau_{kl} - \nu\left(\tau_{mm}\delta_{kl} - \tau_{kl}\right)\right] \tag{3.57}$$

where E is the Young's modulus and ν is the Poisson's ratio. For simple tension case, the Young's modulus and the Poisson's ratio are obtained in terms of engineering stress T_{11}, elongation $\Delta X / X$, and lateral contraction $\Delta Y / Y$ as

$$E = \tau_{11} / h_{11} = T_{11}\left(1+\tilde{E}_{11}\right) / \ln\left(1+\tilde{E}_{11}\right) = T_{11}\left(1+\Delta X / X\right) / \ln\left(1+\Delta X / X\right) \tag{3.58}$$

$$\nu = \frac{-h_{22}E}{\tau_{11}} = -\frac{h_{22}}{h_{11}} = -\ln(1+\tilde{E}_{22}) / \ln(1+\tilde{E}_{11}) = -\ln(1+\Delta Y / Y) / \ln(1+\Delta X / X) \tag{3.59}$$

3.5 Interatomic potential and atomistic strain energy

One dimensional simple tension case is first presented to illustrate the idea that the strain energy and interatomic energy should be equivalent. The result of this simple case is then utilized in the derivation of general case.

Assume atom A and atom B are pulled from their original location $\mathbf{X}_o^A$ and $\mathbf{X}_o^B$ to their deformed position $\mathbf{X}^A$ and $\mathbf{X}^B$ respectively. $\mathbf{r}_o^{AB} \equiv \mathbf{X}_o^A - \mathbf{X}_o^B$ and $\mathbf{r}^{AB} \equiv \mathbf{X}^A - \mathbf{X}^B$. $\mathbf{r}_o^{AB}$ is always parallel to $\mathbf{r}^{AB}$ at all times representing a limiting case of simple tension (cf. fig.2). There are two methods to calculate the potential energy of atom A. The first method is to calculate the interatomic potential directly from the atomistic force as follows

$$\mathbf{f}^{AB} = -\frac{\partial U^{AB}}{\partial \mathbf{r}^A} = -\frac{\partial U^{AB}}{\partial r^{AB}}\frac{\partial r^{AB}}{\partial \mathbf{r}^A} = -\frac{\partial U^{AB}}{\partial r^{AB}}\frac{\mathbf{r}^A - \mathbf{r}^B}{r^{AB}} = -\frac{\partial U^{AB}}{\partial r^{AB}}\mathbf{i}^{AB} \tag{3.60}$$

$$U^{AB} = -\int_{r_0}^{r} \mathbf{f}^{AB} \cdot d\mathbf{r}^{AB} = \int_{r_0}^{r} dU = U\big|_r - U\big|_{r_0} \tag{3.61}$$

$$U^B = U^A \equiv \frac{1}{2}U^{AB} = \frac{1}{2}\left(U\big|_r - U\big|_{r_0}\right) \tag{3.62}$$

where $\mathbf{f}^{AB}$ is the force acting on A due to B; $\mathbf{i}^{AB}$ denotes the unit vector of $\mathbf{r}^{AB}$; $U\big|_r$ denotes the interatomic potential between A and B at distance r; $U\big|_{r_0}$ denotes the interatomic potential between A and B at initial distance r_0 . U^B and U^A are potential energy of atom B and atom A respectively. Let us distribute the total potential energy U^{AB} evenly between atom A and atom B, which gives eq. (3.62).

The second method of energy calculation is to calculate strain energy from conjugate stress and strain. Although not a necessity, we start from introducing virial stress at zero temperature. Virial stress s_{ij} at zero temperature of region Ω is defined as (Subramaniyan 2008, Zimmerman, WebbIII et al. 2004)

$$\mathbf{s} = -\frac{1}{2V_\Omega}\sum_{\alpha\in\Omega}\sum_{\beta\neq\alpha}^{N}\left(\mathbf{x}^\alpha - \mathbf{x}^\beta\right)\otimes\mathbf{f}^{\alpha\beta} \tag{3.63}$$

α is an atom in the domain Ω

β is an atom in the whole specimen, not just in the domain Ω

V_Ω is the volume of the whole domain

N is the number of atoms in the whole specimen, not just in the domain Ω

m^α is the mass of atom α

$\mathbf{x}^\alpha$ is the position vector of atom α

$\mathbf{f}^{\alpha\beta}$ is the force acting on atom α due to interaction with atom β

Notice that, reduction of the virial stress to two-atom system faces theoretical difficulties based on virial theorem (Murdoch 2007, Sun 2006). Here the atomistic stress $\mathbf{s}^A$ takes the form as in eq. (3.64) is solely based on the conjugate relation with respect to the atomistic Hencky strain as defined later by eq. (3.70). In two-atom case as shown in fig. 2, the atomistic Kirchhoff stress (local virial stress) of atom A

$$\mathbf{s}^A = -\frac{1}{2V_o}\left[\mathbf{r}^{AB}\otimes\mathbf{f}^{AB}\right] \tag{3.64}$$

where V_o is the initial volume of Wigner–Seitz cell for atom A. $\mathbf{s}^A$ is the "force part" of Cheung and Yip's "atomistic-level stress" (Cheung 1991), "local virial stress" and "BDT" stress if the volume refers to the undeformed state (Cheung 1991, Vitek 1987, BASINSKI 1971, Cormier 2001, Sun 2006). This stress is considered uniform within the volume V_o. Now we chose a special coordinate to study two-atom simple tension case.

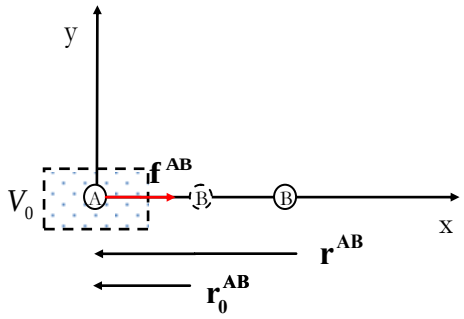

Figure 3-2 Atomistic Simple Tension Case

If the origin of coordinate is fixed at atom A, atom B is pulled apart along the X axis, (cf. fig.2). The position and force vectors of the original and deformed states become

$$\mathbf{r}_{\mathbf{oI}}^{AB} = \begin{bmatrix} r_o & 0 & 0 \end{bmatrix}^T \;,\; \mathbf{r}_{\mathbf{I}}^{AB} = \begin{bmatrix} r & 0 & 0 \end{bmatrix}^T \tag{3.65}$$

$$\mathbf{f}_{\mathbf{oI}}^{AB} = \begin{bmatrix} f_o & 0 & 0 \end{bmatrix}^T \;,\; \mathbf{f}_{\mathbf{I}}^{AB} = \begin{bmatrix} f & 0 & 0 \end{bmatrix}^T \tag{3.66}$$

where r_o and r are the only non-zero component of $\mathbf{r}_{\mathbf{I}}^{AB}$ and $\mathbf{r}_{\mathbf{oI}}^{AB}$ respectively. f_o and f are the only non-zero component of $\mathbf{f}_{\mathbf{I}}^{AB}$ and $\mathbf{f}_{\mathbf{oI}}^{AB}$ respectively. Notice that $r = \left|\mathbf{r}_{\mathbf{I}}^{\mathbf{AB}}\right|$, $r_o = \left|\mathbf{r}_{\mathbf{oI}}^{\mathbf{AB}}\right|$ since r and r_o are always positive. $f \neq \left|\mathbf{f}_{\mathbf{I}}^{AB}\right|$, $f_o \neq \left|\mathbf{f}_{\mathbf{oI}}^{AB}\right|$ because f can be a negative in compression. The atomistic Kirchhoff stress of atom A in this particular coordinate system (cf. eq. (3.46)) are

$$\mathbf{s}_{\mathbf{I}}^{AB} = -\frac{1}{2V_o}\mathbf{r}_{\mathbf{I}}^{AB} \otimes \mathbf{f}_{\mathbf{I}}^{AB} \tag{3.67}$$

$$\mathbf{s}_{\mathbf{I}} = -\frac{1}{2V_o}\begin{bmatrix} r_x^{AB} & 0 & 0 \\ 0 & 0 & 0 \\ 0 & 0 & 0 \end{bmatrix}\begin{bmatrix} f_x^{AB} & 0 & 0 \\ 0 & 0 & 0 \\ 0 & 0 & 0 \end{bmatrix} = -\frac{1}{2V_o}\begin{bmatrix} r_x^{AB} f_x^{AB} & 0 & 0 \\ 0 & 0 & 0 \\ 0 & 0 & 0 \end{bmatrix} \equiv -\frac{1}{2V_o}\begin{bmatrix} rf & 0 & 0 \\ 0 & 0 & 0 \\ 0 & 0 & 0 \end{bmatrix} \tag{3.68}$$

From CM point of view, in case of simple tension, the Lagrangian strain and the Hencky strain are obtained as (cf. eqs. (3.36),(3.41))

$$\mathbf{E}^A = \frac{1}{2}\begin{bmatrix} (r/r_0)^2 - 1 & 0 & 0 \\ 0 & m^2 - 1 & 0 \\ 0 & 0 & n^2 - 1 \end{bmatrix} \tag{3.69}$$

$$\mathbf{h}^A = \begin{bmatrix} \ln(r/r_0) & 0 & 0 \\ 0 & \ln m & 0 \\ 0 & 0 & \ln n \end{bmatrix} \tag{3.70}$$

The total strain energy Σ, integrated from Hencky strain h_{kl} and atomistic Kirchhoff stress (local virial stress) s_{kl} (cf. eqs. (3.62)(3.67)(3.70)), becomes

$$\begin{aligned} \Sigma &= \int_{r_0}^{r} s_{ij} dh_{ij} = -\frac{1}{2}\int_{r_0}^{r} \frac{1}{V_o} r f d\ln\left(\frac{r}{r_0}\right) \\ &= -\frac{1}{2V_o}\int_{r_0}^{r} f dr = \frac{1}{V_o}\frac{1}{2}\left(U\big|_r - U\big|_{r_0}\right) = \frac{U^A}{V_o} \end{aligned} \tag{3.71}$$

Notice that U^A calculated from interatomic potential (cf. eq.(3.62)) is identical to the strain energy ΣV_o (cf. eq.(3.71)). Therefore, atomistic Hencky strain and atomistic Kirchhoff stress (local virial stress) is a thermodynamic conjugate pair. Recall that Kirchhoff stress and Hencky strain is a thermodynamic conjugate pair in continuum mechanics (cf. eq. (3.30)). Therefore, virial stress, in 2-atom simple tension case, at zero temperature is equivalent to Kirchhoff stress

$$s_{ij} = \tau_{ij} \tag{3.72}$$

This conclusion is a crucial step to find the equivalence of virial stress in general case. For convenience, we write the PK2 stress and Cauchy stress in two atom simple tension case as follows (cf. eqs. (3.47)(3.48)(3.72))

$$T_{KL} = \begin{bmatrix} k^{-2}\tau_{11} & 0 & 0 \\ 0 & 0 & 0 \\ 0 & 0 & 0 \end{bmatrix} = -\frac{1}{2V_o}\begin{bmatrix} (r_0/r)^2 rf & 0 & 0 \\ 0 & 0 & 0 \\ 0 & 0 & 0 \end{bmatrix} \tag{3.73}$$

$$t_{kl} = \frac{V_o}{V}\begin{bmatrix} \tau_{11} & 0 & 0 \\ 0 & 0 & 0 \\ 0 & 0 & 0 \end{bmatrix} = -\frac{1}{2V}\begin{bmatrix} rf & 0 & 0 \\ 0 & 0 & 0 \\ 0 & 0 & 0 \end{bmatrix} \tag{3.74}$$

and the conjugacy of T_{KL} and E_{KL} in two atom simple tension case can also be proved with similar process

$$\begin{aligned} \Sigma &= \int_{r_0}^{r} T_{ij} dE_{ij} = -\frac{1}{2}\int_{r_0}^{r} \frac{1}{V_o}(r_0/r)^2 rf d\,\frac{1}{2}\left[(r/r_0)^2 - 1\right] \\ &= -\frac{1}{2}\int_{r_0}^{r} \frac{1}{V_o}(r_0/r)^2 rf\,\frac{r}{r_0^2} dr \\ &= -\frac{1}{2V_o}\int_{r_0}^{r} f dr = \frac{1}{V_o}\frac{1}{2}\left(U\big|_r - U\big|_{r_0}\right) = \frac{U^A}{V_o} \end{aligned} \tag{3.75}$$

3.6 Atomistic Kirchhoff stress/atomistic Hencky strain conjugate pair in general 3D case for 2-atom system

In previous Sections, local virial stress is proved to be Kirchhoff stress in simple tension case for two-atom system. Now we generalize this statement to three dimensional

case with arbitrary atomic configuration. Here the rotation refers to the rotation of a vector in a fixed coordinate.

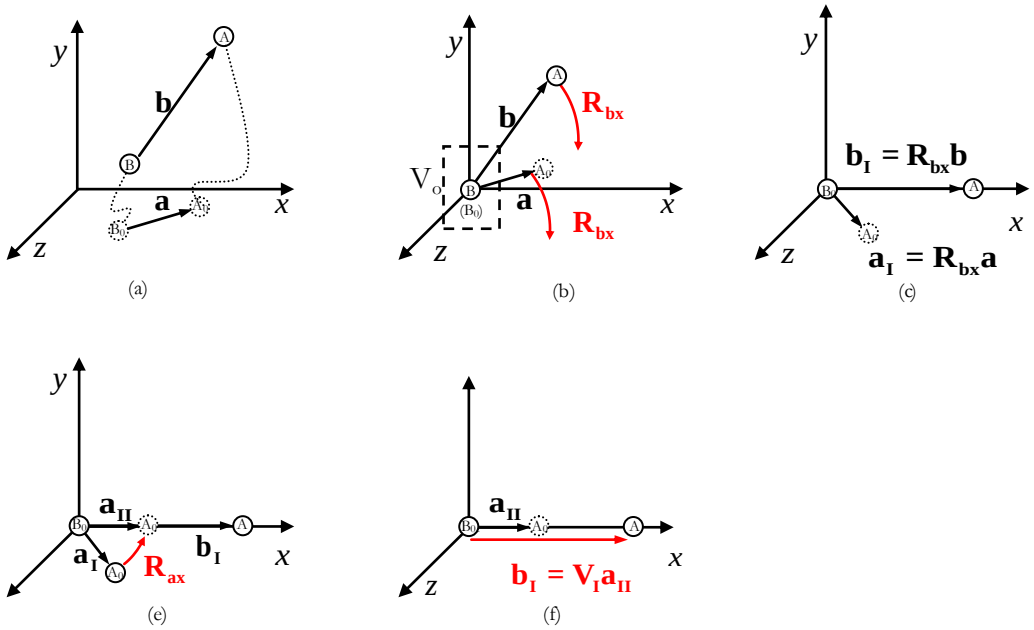

Figure 3-3 Deformation of two atoms: Atomistic Hencky Strain

A. Hencky Strain in General 3D case

Assume atom A and atom B moving from their original positions $\mathbf{X}^{A_o}$ and $\mathbf{X}^{B_o}$ to their current positions $\mathbf{X}^{A}$ and $\mathbf{X}^{B}$, respectively, (cf. figure 3a). Because atomistic stress and strain are calculated from the relative positions between atoms, the origin of the coordinate system can always be fixed at atom B without losing any generality. Define the relative original and current positions between atom A and atom B as (cf. figure 3b).

$$\mathbf{a} \equiv \mathbf{r}^{A_o B_o} = \mathbf{X}^{A_o} - \mathbf{X}^{B_o} \tag{3.76}$$

$$\mathbf{b} \equiv \mathbf{r}^{AB} = \mathbf{X}^{A} - \mathbf{X}^{B} \tag{3.77}$$

There always exists a special rotation matrix $\mathbf{R}_{\mathbf{bx}}$ that rotates $\mathbf{b}$ to $\mathbf{b}_{\mathbf{I}}$, which is aligned with x axis, i.e. (cf. figure 3c).

$$\mathbf{b}_{\mathbf{I}} = \mathbf{R}_{\mathbf{bx}}\mathbf{b} \tag{3.78}$$

Accordingly, $\mathbf{a}$ is rotated to $\mathbf{a}_{\mathbf{I}}$, i.e.

$$\mathbf{a}_{\mathbf{I}} = \mathbf{R}_{\mathbf{bx}}\mathbf{a} \tag{3.79}$$

Now we consider that vector $\mathbf{a}_{\mathbf{I}}$ is deformed into $\mathbf{b}_{\mathbf{I}}$

$$\mathbf{b}_{\mathbf{I}} = \mathbf{F}_{\mathbf{I}}\mathbf{a}_{\mathbf{I}} \tag{3.80}$$

where $\mathbf{F}_{\mathbf{I}}$ is the deformation gradient. Let the polar decomposition of $\mathbf{F}_{\mathbf{I}}$ be represented as:

$$\mathbf{F}_{\mathbf{I}} = \mathbf{V}_{\mathbf{I}}\mathbf{R}_{\mathbf{ax}} \tag{3.81}$$

which means $\mathbf{F}_{\mathbf{I}}$ can be decomposed into a pure rotation $\mathbf{R}_{\mathbf{ax}}$, which rotates vector $\mathbf{a}_{\mathbf{I}}$ to align with x-axis (cf. figure 3d), followed by a pure deformation $\mathbf{V}_{\mathbf{I}}$ (cf. figure 3e). It leads to

$$\mathbf{b}_{\mathbf{I}} = \mathbf{F}_{\mathbf{I}}\mathbf{a}_{\mathbf{I}} = \mathbf{V}_{\mathbf{I}}\mathbf{R}_{\mathbf{ax}}\mathbf{a}_{\mathbf{I}} \tag{3.82}$$

$$\mathbf{a}_{\mathbf{II}} \equiv \mathbf{R}_{\mathbf{ax}}\mathbf{a}_{\mathbf{I}} \tag{3.83}$$

$$\mathbf{b}_{\mathbf{I}} = \mathbf{V}_{\mathbf{I}}\mathbf{a}_{\mathbf{II}} \tag{3.84}$$

This indicates $\mathbf{V_I}$ is the deformation gradient between $\mathbf{b_I}$ and $\mathbf{a_{II}}$; now both are aligned with x axis (cf. figure 3e). The calculation of $\mathbf{h_1} \equiv \ln(\mathbf{V_I})$ is identical to that in simple-tension case between two atoms.

Recall that $\mathbf{H_1} = \mathbf{Q}^{\mathbf{T}} \ln(\mathbf{\Lambda_I})\mathbf{Q}$ and $\mathbf{\Lambda_I} = \mathbf{Q}\mathbf{V_I}\mathbf{Q}^{\mathbf{T}}$, and notice that $\mathbf{V_I}$ is diagonal by itself, therefore $\mathbf{Q}$ is an identical matrix. Now, we may in general write

$$\mathbf{V_I} = \mathbf{\Lambda_I} = \mathbf{F_{II}} = \begin{bmatrix} r/r_0 & 0 & 0 \\ 0 & m & 0 \\ 0 & 0 & n \end{bmatrix} \tag{3.85}$$

$$\mathbf{h_I} = \ln \mathbf{V_I} = \mathbf{Q}^T \ln \mathbf{\Lambda_I}\mathbf{Q} = \begin{bmatrix} \ln(r/r_0) & 0 & 0 \\ 0 & \ln m & 0 \\ 0 & 0 & \ln n \end{bmatrix} \tag{3.86}$$

where $r_0 = \sqrt{a_x{}^2 + a_y{}^2 + a_z{}^2}$ is the length of vector $\mathbf{a}$; $r = \sqrt{b_x{}^2 + b_y{}^2 + b_z{}^2}$ is the length of vector $\mathbf{b}$. Notice that $\mathbf{h_I}$ is independent of the rotation matrix $\mathbf{R_{ax}}$. This is because Hencky strain is independent of the rotational part of deformation gradient $\mathbf{F}$ (cf. eqs. (3.81)(3.82) (3.86)). In other words, the Hencky strain calculated from the simple tension case is identical to the Hencky strain in a general 3-D case viewed at the coordinate with $\mathbf{b}$ aligned with x-axis. Now another rotation is preformed to transfer $\mathbf{h_I}$ back to that in its original configuration (cf. Figure 3b, 3c). Notice that this transformation is due to coordinate rotation, not deformation, i.e.

$$\begin{aligned}\mathbf{h} &= \mathbf{R}_{\mathbf{bx}}^{-1}\mathbf{h}_{\mathbf{I}}\mathbf{R}_{\mathbf{bx}} = \mathbf{R}_{\mathbf{bx}}^{\mathbf{T}}\mathbf{h}_{\mathbf{I}}\mathbf{R}_{\mathbf{bx}} \\ &= \mathbf{R}_{\mathbf{bx}}^{\mathbf{T}}\begin{bmatrix}\ln(b/a) & 0 & 0\\ 0 & \ln m & 0\\ 0 & 0 & \ln n\end{bmatrix}\mathbf{R}_{\mathbf{bx}}\end{aligned} \tag{3.87}$$

Also one may readily verify that

$$\mathbf{R}_{\mathbf{bx}} = \begin{bmatrix} b_x/b & b_y/b & b_z/b \\ -b_y/b & \dfrac{1}{b_y^{\,2}+b_z^{\,2}}\left(b_z^{\,2}+\dfrac{b_x b_y^{\,2}}{b}\right) & \dfrac{b_y b_z}{b_y^{\,2}+b_z^{\,2}}\left(\dfrac{b_x}{b}-1\right) \\ -b_z/b & \dfrac{b_y b_z}{b_y^{\,2}+b_z^{\,2}}\left(\dfrac{b_x}{b}-1\right) & \dfrac{1}{b_y^{\,2}+b_z^{\,2}}\left(b_y^{\,2}+\dfrac{b_x b_z^{\,2}}{b}\right) \end{bmatrix} \tag{3.88}$$

where $\mathbf{b} = \begin{bmatrix} b_x & b_y & b_z \end{bmatrix}$ and $b = |\mathbf{b}|$. Note that we do not assume incompressibility here and we do not know the value of Poisson ration; hence m and n are undetermined quantities in the definition of strain between two atoms. For a two-atom system, any m and n are possible. For multiple-atom system, one is still unable to determine m and n rigorously. Moreover, in the next Section, it is seen that the end result of conjugacy is independent of m and n.

B. Atomistic Kirchhoff Stress(Local Virial Stress)

Atomistic Kirchhoff stress (local Virial Stress) of atom A between atom A and atom B at zero temperature can be obtained as (cf. eq. (3.67))

$$s_{ij} = -\frac{1}{2V_0} b_i \, f_j \tag{3.89}$$

Notice that, based on two-body interatomic potential, $\mathbf{f}$ and $\mathbf{b}$ has the same direction, i.e. $\mathbf{f} = \eta \mathbf{b}$; hence the atomistic Kirchhoff stress (local virial stress) tensor is symmetric. It leads to

$$\begin{aligned} \mathbf{s} &= -\frac{\eta}{2V_0} \mathbf{b} \otimes \mathbf{b}^{\mathbf{T}} = -\frac{\eta}{2V_0} \left(\mathbf{R}_{\mathbf{bx}}^{\mathbf{-1}} \mathbf{b}_{\mathbf{I}} \right) \otimes \left(\mathbf{R}_{\mathbf{bx}}^{\mathbf{-1}} \mathbf{b}_{\mathbf{I}} \right)^{\mathbf{T}} \\ &= -\frac{\eta}{2V_0} \mathbf{R}_{\mathbf{bx}}^{\mathbf{-1}} \mathbf{b}_{\mathbf{I}} \otimes \mathbf{b}_{\mathbf{I}}^{\mathbf{T}} \mathbf{R}_{\mathbf{bx}} = -\mathbf{R}_{\mathbf{bx}}^{\mathbf{-1}} \left(\frac{1}{2V_0} \mathbf{b}_{\mathbf{I}} \otimes \mathbf{f}_{\mathbf{I}}^{\mathbf{T}} \right) \mathbf{R}_{\mathbf{bx}} \\ &= \mathbf{R}_{\mathbf{bx}}^{\mathbf{-1}} \mathbf{s}_{\mathbf{I}} \mathbf{R}_{\mathbf{bx}} = \mathbf{R}_{\mathbf{bx}}^{\mathbf{T}} \mathbf{s}_{\mathbf{I}} \mathbf{R}_{\mathbf{bx}} \end{aligned} \tag{3.90}$$

where $\mathbf{R}_{\mathbf{bx}}$ is given in eq. (3.88). It is worthwhile to note that the virial stress $\mathbf{s}_{\mathbf{I}}$ is independent of the rotation $\mathbf{R}_{\mathbf{ax}}$ and can be expressed as

$$\mathbf{s}_{\mathbf{I}} = -\frac{1}{2V_0} \mathbf{r}_{\mathbf{I}} \otimes \mathbf{f}_{\mathbf{I}} \tag{3.91}$$

$$\mathbf{r}_{\mathbf{I}} = \mathbf{R}_{\mathbf{bx}} \mathbf{r} = \begin{bmatrix} r & 0 & 0 \end{bmatrix}^T \tag{3.92}$$

$$\mathbf{f}_{\mathbf{I}} = \mathbf{R}_{\mathbf{bx}} \mathbf{f} = \begin{bmatrix} f & 0 & 0 \end{bmatrix}^T \tag{3.93}$$

$$\mathbf{s}_{\mathbf{I}} = -\frac{1}{2V_0} \begin{bmatrix} rf & 0 & 0 \\ 0 & 0 & 0 \\ 0 & 0 & 0 \end{bmatrix} \tag{3.94}$$

where $\mathbf{f}_I = \mathbf{R}_{bx}\mathbf{f}$ denotes the force vector between atom A and B when $\mathbf{r}$ is rotated to align with X-axis, and f denotes the only non zero component of $\mathbf{f}_I = [f \quad 0 \quad 0]$; $r = |\mathbf{b}|$. The expression of local virial stress in eq. (3.89) is equivalent to that in eqs. (3.90)(3.91)

C. Work Conjugacy between Hencky strain and atomistic Kirchhoff stress (local virial stress) in discrete system

Now we are going to prove that $\mathbf{h}$ and $\mathbf{s}$ commute and $\mathbf{hs}$ is symmetric. First, we recall

$$\mathbf{h} = \mathbf{R}_{bx}^{-1}\mathbf{h}_I\mathbf{R}_{bx}, \quad \mathbf{s} = \mathbf{R}_{bx}^{-1}\mathbf{s}_I\mathbf{R}_{bx} \tag{3.95}$$

It is straightforward to have

$$\mathbf{hs} = \mathbf{R}_{bx}^{-1}\mathbf{h}_I\mathbf{R}_{bx}\mathbf{R}_{bx}^{-1}\mathbf{s}_I\mathbf{R}_{bx} = \mathbf{R}_{bx}^{-1}\mathbf{h}_I\mathbf{s}_I\mathbf{R}_{bx} \tag{3.96}$$

$$\mathbf{sh} = \mathbf{R}_{bx}^{-1}\mathbf{s}_I\mathbf{R}_{bx}\mathbf{R}_{bx}^{-1}\mathbf{h}_I\mathbf{R}_{bx} = \mathbf{R}_{bx}^{-1}\mathbf{s}_I\mathbf{h}_I\mathbf{R}_{bx} \tag{3.97}$$

From eqs. (3.86)(3.94) one may notice $\mathbf{h}_I$ and $\mathbf{s}_I$ are both diagonal. Therefore $\mathbf{h}_I\mathbf{s}_I = \mathbf{s}_I\mathbf{h}_I$, which implies $\mathbf{hs} = \mathbf{sh}$. In other words, it is proved that $\mathbf{h}$ and $\mathbf{s}$ commute. Notice that if $\mathbf{h}$ and $\mathbf{s}$ commute and both are symmetric, their product $\mathbf{hs}$ is symmetric.

It is well known that if $\mathbf{R}$ is rotational matrix, $\dot{\mathbf{R}}^{-1}\mathbf{R}$ and $\mathbf{R}\dot{\mathbf{R}}^{-1}$ are anti-symmetric. Now we prove the conjugacy between $\mathbf{h}$ and $\mathbf{s}$ following Fitzgerald's procedure (Fitzgerald 1980).

$$
\begin{aligned}
\mathbf{s}:\dot{\mathbf{h}} &= tr\left(\mathbf{s}^{\mathrm{T}}\dot{\mathbf{h}}\right) = tr\left[\mathbf{R}_{\mathbf{bx}}^{-1}\mathbf{s}_{\mathbf{I}}\mathbf{R}_{\mathbf{bx}}\left(\overline{\mathbf{R}_{\mathbf{bx}}^{-1}\mathbf{h}_{\mathbf{I}}\mathbf{R}_{\mathbf{bx}}}^{\cdot}\right)\right] \\
&= tr\left[\mathbf{R}_{\mathbf{bx}}^{-1}\mathbf{s}_{\mathbf{I}}\mathbf{R}_{\mathbf{bx}}\mathbf{R}_{\mathbf{bx}}^{-1}\dot{\mathbf{h}}_{\mathbf{I}}\mathbf{R}_{\mathbf{bx}} + \mathbf{R}_{\mathbf{bx}}^{-1}\mathbf{s}_{\mathbf{I}}\mathbf{R}_{\mathbf{bx}}\dot{\mathbf{R}}_{\mathbf{bx}}^{-1}\mathbf{h}_{\mathbf{I}}\mathbf{R}_{\mathbf{bx}} + \mathbf{R}_{\mathbf{bx}}^{-1}\mathbf{s}_{\mathbf{I}}\mathbf{R}_{\mathbf{bx}}\mathbf{R}_{\mathbf{bx}}^{-1}\mathbf{h}_{\mathbf{I}}\dot{\mathbf{R}}_{\mathbf{bx}}\right] \\
&= tr\left[\mathbf{R}_{\mathbf{bx}}^{-1}\mathbf{s}_{\mathbf{I}}\dot{\mathbf{h}}_{\mathbf{I}}\mathbf{R}_{\mathbf{bx}}\right] + tr\left[\mathbf{R}_{\mathbf{bx}}^{-1}\mathbf{s}_{\mathbf{I}}\mathbf{R}_{\mathbf{bx}}\dot{\mathbf{R}}_{\mathbf{bx}}^{-1}\mathbf{h}_{\mathbf{I}}\mathbf{R}_{\mathbf{bx}}\right] + tr\left[\mathbf{R}_{\mathbf{bx}}^{-1}\mathbf{s}_{\mathbf{I}}\mathbf{h}_{\mathbf{I}}\dot{\mathbf{R}}_{\mathbf{bx}}\right] \\
&\equiv I + II + III
\end{aligned}
\tag{3.98}
$$

It is seen that (cf. eq. (91))

$$
\begin{aligned}
II &= tr\left[\mathbf{R}_{\mathbf{bx}}^{-1}\mathbf{s}_{\mathbf{I}}\mathbf{R}_{\mathbf{bx}}\dot{\mathbf{R}}_{\mathbf{bx}}^{-1}\mathbf{h}_{\mathbf{I}}\mathbf{R}_{\mathbf{bx}}\right] \\
&= tr\left[\mathbf{R}_{\mathbf{bx}}^{-1}\mathbf{R}_{\mathbf{bx}}\mathbf{s}\mathbf{R}_{\mathbf{bx}}^{-1}\mathbf{R}_{\mathbf{bx}}\dot{\mathbf{R}}_{\mathbf{bx}}^{-1}\mathbf{R}_{\mathbf{bx}}\mathbf{h}\mathbf{R}_{\mathbf{bx}}^{-1}\mathbf{R}_{\mathbf{bx}}\right] \\
&= tr\left[\mathbf{s}\dot{\mathbf{R}}_{\mathbf{bx}}^{-1}\mathbf{R}_{\mathbf{bx}}\mathbf{h}\right] \\
&= tr\left[\dot{\mathbf{R}}_{\mathbf{bx}}^{-1}\mathbf{R}_{\mathbf{bx}}\mathbf{h}\mathbf{s}\right]
\end{aligned}
\tag{3.99}
$$

Since $\dot{\mathbf{R}}_{\mathbf{bx}}{}^{-1}\mathbf{R}_{\mathbf{bx}}$ is anti-symmetric and $\mathbf{hs}$ is symmetric, $II = 0$. Similarly, one can see that

$$
\begin{aligned}
III &= tr\left[\mathbf{R}_{\mathbf{bx}}^{-1}\mathbf{s}_{\mathbf{I}}\mathbf{h}_{\mathbf{I}}\dot{\mathbf{R}}_{\mathbf{bx}}\right] \\
&= tr\left[\mathbf{R}_{\mathbf{bx}}^{-1}\mathbf{R}_{\mathbf{bx}}\mathbf{s}\mathbf{R}_{\mathbf{bx}}^{-1}\mathbf{R}_{\mathbf{bx}}\mathbf{h}\mathbf{R}_{\mathbf{bx}}^{-1}\dot{\mathbf{R}}_{\mathbf{bx}}\right] \\
&= tr\left[\mathbf{s}\mathbf{h}\mathbf{R}_{\mathbf{bx}}^{-1}\dot{\mathbf{R}}_{\mathbf{bx}}\right] \\
&= 0
\end{aligned}
\tag{3.100}
$$

Therefore

$$
\mathbf{s}:\dot{\mathbf{h}} = tr\left[\mathbf{R}_{\mathbf{bx}}^{-1}\left(\mathbf{s}_{\mathbf{I}}\dot{\mathbf{h}}_{\mathbf{I}}\right)\mathbf{R}_{\mathbf{bx}}\right] = tr\left[\mathbf{s}_{\mathbf{I}}\dot{\mathbf{h}}_{\mathbf{I}}\right] = \mathbf{s}_{\mathbf{I}}:\dot{\mathbf{h}}_{\mathbf{I}} \tag{3.101}
$$

It is straightforward to derive (cf. eqs. (3.87)(3.94))

$$\mathbf{s}:\dot{\mathbf{h}} = \mathbf{s}_{\mathbf{I}}:\dot{\mathbf{h}}_{\mathbf{I}} = tr\left(\mathbf{s}_{\mathbf{I}}\dot{\mathbf{h}}_{\mathbf{I}}\right) = tr\left\{\begin{bmatrix} -rf/2V_0 & 0 & 0 \\ 0 & 0 & 0 \\ 0 & 0 & 0 \end{bmatrix}\frac{d}{dt}\begin{bmatrix} \ln(r/r_0) & 0 & 0 \\ 0 & \ln m & 0 \\ 0 & 0 & \ln n \end{bmatrix}\right\}$$
$$= tr\left\{\begin{bmatrix} -rf/2V_0 & 0 & 0 \\ 0 & 0 & 0 \\ 0 & 0 & 0 \end{bmatrix}\begin{bmatrix} \dot{r}/r & 0 & 0 \\ 0 & \dot{m}/m & 0 \\ 0 & 0 & \dot{n}/n \end{bmatrix}\right\} = -\frac{f}{2V_0}\frac{dr}{dt} \tag{3.102}$$

or equivalently, $\mathbf{s}:d\mathbf{h} = -\dfrac{f}{2V_0}dr$. Now strain energy density becomes

$$\Sigma = \int_{r_0}^{r}\mathbf{s}:d\mathbf{h} = -\int_{r_0}^{r}\frac{f}{2V_0}dr = -\frac{1}{2V_0}\int_{r_0}^{r}fdr = \frac{1}{2V_0}\int_{r_0}^{r}dU = \frac{1}{2V_0}\left(U\big|_r - U\big|_{r_0}\right) \tag{3.103}$$

where $U_{atom}\big|_r$ and $U_{atom}\big|_{r_0}$ denotes the interatomic potential between atom A and B at distance r and r_0 respectively. Notice that the strain energy Σ is considered a constant throughout the virtual specimen geometry; therefore it can be pull out of integration. The total Energy of system when taking continuum point of view

$$U^B = \int_{V_0}\Sigma dV_0 = \Sigma\int_{V_0}dV_0 = \Sigma V_0 = \frac{1}{2}\left(U\big|_r - U\big|_{r_0}\right) \tag{3.104}$$

Thus one may see that the energy calculated from interatomic potential is identical to the energy calculated from strain energy (cf. eqs. (3.62)(3.104)) where the stress and strain are taken to be atomistic Kirchhoff stress (local virial stress) and atomistic Hencky strain, respectively. Thus we have proved that atomistic Hencky Strain and atomistic Kirchhoff stress form a work conjugate pair. Recall that, in continuum mechanics, Hencky strain and Kirchhoff stress form a work conjugate pair. Therefore, one may conclude that atomistic

Kirchhoff stress (local virial stress) is Kirchhoff stress in atomistic level. It is worthwhile to mention that, in this work, we only consider the potential part of the stress, and also the volume in the expression of atomistic Kirchhoff stress (local virial stress), Ω, is taken to be the volume of undeformed state.

3.7 The conjugate pair of Atomistic second order Piola-Kirchhoff stress and atomistic Lagrangian strain in general 3D case for 2-Atom

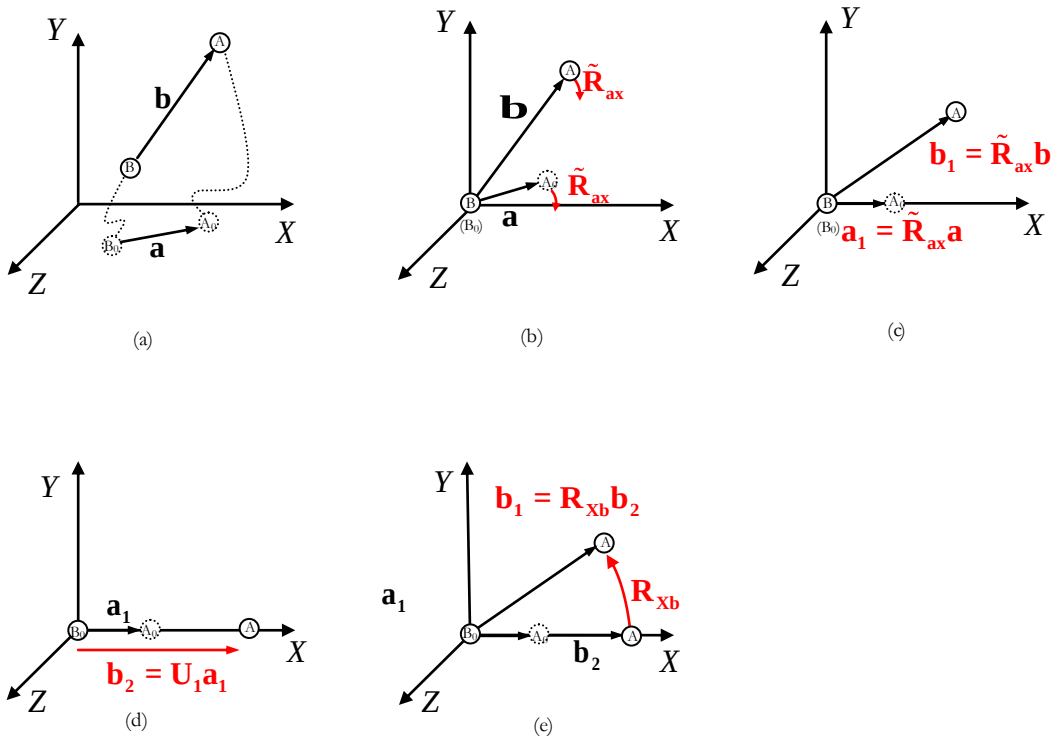

Figure 3-4 Deformation of two atoms: Atomistic Lagrangian strain

A. Lagrangian Strain in General 3-D case

Assume atom A and atom B moving from their original positions $\mathbf{X}^{A_0}$ and $\mathbf{X}^{B_0}$ to their current positions $\mathbf{X}^{A}$ and $\mathbf{X}^{B}$, respectively, as shown in figure 4a. Without losing any generality let the origin of the coordinate system be fixed at atom B. Define the relative original and current positions between atom A and atom B as (cf. figure 4b).

$$\mathbf{a} \equiv \mathbf{r}^{A_0B_0} = \mathbf{X}^{A_0} - \mathbf{X}^{B_0} \tag{3.105}$$

$$\mathbf{b} \equiv \mathbf{r}^{AB} = \mathbf{X}^{A} - \mathbf{X}^{B} \tag{3.106}$$

There always exists a special rotation matrix $\tilde{\mathbf{R}}_{aX}$ that rotates $\mathbf{a}$ to $\mathbf{a}_1$, which is aligned with $X-axis$ (cf. figure 4c), i.e.

$$\mathbf{a}_1 = \tilde{\mathbf{R}}_{aX}\mathbf{a} \tag{3.107}$$

Accordingly, $\mathbf{b}$ is rotated to $\mathbf{b}_1$, i.e.

$$\mathbf{b}_1 = \tilde{\mathbf{R}}_{aX}\mathbf{b} \tag{3.108}$$

Now we consider that vector $\mathbf{a}_1$ is deformed into $\mathbf{b}_1$

$$\mathbf{b}_1 = \mathbf{F}_1\mathbf{a}_1 \tag{3.109}$$

where $\mathbf{F}_1$ is the deformation gradient. Let polar decomposition of $\mathbf{F}_1$ be represented as:

$$\mathbf{F}_1 = \mathbf{R}_{Xb}\mathbf{U}_1 \tag{3.110}$$

which means $\mathbf{F}_1$ can be decomposed into to a pure deformation $\mathbf{U}_1$ (cf. figure 4d) followed by a pure rotation $\mathbf{R}_{Xb}$ which rotates vector $\mathbf{b}_2$ that aligned with $X-axis$ to its final position $\mathbf{b}_1$ (cf. figure 4e). It leads to

$$\mathbf{b}_1 = \mathbf{F}_1\mathbf{a}_1 = \mathbf{R}_{Xb}\mathbf{U}_1\mathbf{a}_1 \equiv \mathbf{R}_{Xb}\mathbf{b}_2 \tag{3.111}$$

This means that $\mathbf{R}_{Xb}$ rotates $\mathbf{b}_2$ to $\mathbf{b}_1$; Notice that $\mathbf{b}_2$ and $\mathbf{a}_1$ are both aligned with X-axis. The calculation of $\mathbf{U}_1$ is identical to that in simple-tension case between two atoms. Recall Green deformation tensor

$$\mathbf{C}_1 = \mathbf{F}_1^{\mathrm{T}}\mathbf{F}_1 = \left(\mathbf{R}_{Xb}\mathbf{U}_1\right)^{\mathrm{T}}\mathbf{R}_{Xb}\mathbf{U}_1 = \mathbf{U}_1^{\mathrm{T}}\mathbf{R}_{Xb}^{\mathrm{T}}\mathbf{R}_{Xb}\mathbf{U}_1 = \mathbf{U}_1^{\mathrm{T}}\mathbf{U}_1 \tag{3.112}$$

Notice that $\mathbf{C}_1$ is independent of $\mathbf{R}_{Xb}$. Thus Lagrangian strain

$$\mathbf{E}_1 = \frac{\mathbf{1}}{\mathbf{2}}\left(\mathbf{C}_1 - \mathbf{I}\right) = \frac{\mathbf{1}}{\mathbf{2}}\left(\mathbf{U}_1^{\mathrm{T}}\mathbf{U}_1 - \mathbf{I}\right) \tag{3.113}$$

is independent of $\mathbf{R}_{Xb}$ as well. In other words, Green deformation tensor and Lagrangian strain calculated from simple tension case are identical to those in general 3D case of which $\mathbf{a}$ is aligned with X-axis. Now rotation $\tilde{\mathbf{R}}_{aX}$ is preformed to transfer $\mathbf{E}_1$ (cf. Figure 4.c) back to $\mathbf{E}$ (cf. eq. (3.115)) in its original configuration (cf. Figure 4.b). Notice that this transformation is due to coordinate rotation, not deformation, which means

$$\begin{aligned}\mathbf{C} = \mathbf{F}^{\mathrm{T}}\mathbf{F} &= \left(\tilde{\mathbf{R}}_{aX}^{-1}\mathbf{F}_1\tilde{\mathbf{R}}_{aX}\right)^{\mathrm{T}}\tilde{\mathbf{R}}_{aX}^{-1}\mathbf{F}_1\tilde{\mathbf{R}}_{aX} \\ &= \tilde{\mathbf{R}}_{aX}^{\mathrm{T}}\mathbf{F}_1^{\mathrm{T}}\tilde{\mathbf{R}}_{aX}\tilde{\mathbf{R}}_{aX}^{-1}\mathbf{F}_1\tilde{\mathbf{R}}_{aX} \\ &= \tilde{\mathbf{R}}_{aX}^{\mathrm{T}}\mathbf{F}_1^{\mathrm{T}}\mathbf{F}_1\tilde{\mathbf{R}}_{aX} = \tilde{\mathbf{R}}_{aX}^{\mathrm{T}}\mathbf{C}_1\tilde{\mathbf{R}}_{aX}\end{aligned} \tag{3.114}$$

$$\begin{aligned}\mathbf{E} &= \tilde{\mathbf{R}}_{aX}^{-1}\mathbf{E}_1\tilde{\mathbf{R}}_{aX} = \tilde{\mathbf{R}}_{aX}^{\mathrm{T}}\mathbf{E}_1\tilde{\mathbf{R}}_{aX} \\ &= \frac{1}{2}\tilde{\mathbf{R}}_{aX}^{\mathrm{T}}\begin{bmatrix}\left(r/r_0\right)^2 - 1 & 0 & 0 \\ 0 & m^2 - 1 & 0 \\ 0 & 0 & n^2 - 1\end{bmatrix}\tilde{\mathbf{R}}_{aX}\end{aligned} \tag{3.115}$$

It is straight forward to verify that

$$\tilde{\mathbf{R}}_{\mathbf{aX}} = \begin{bmatrix} a_x / a & a_y / a & a_z / a \\ -a_y / a & \dfrac{1}{a_y^{\,2} + a_z^{\,2}}\left(a_z^{\,2} + \dfrac{a_x a_y^{\,2}}{a}\right) & \dfrac{a_y a_z}{a_y^{\,2} + a_z^{\,2}}\left(\dfrac{a_x}{a} - 1\right) \\ -a_z / a & \dfrac{a_y a_z}{a_y^{\,2} + a_z^{\,2}}\left(\dfrac{a_x}{a} - 1\right) & \dfrac{1}{a_y^{\,2} + a_z^{\,2}}\left(a_y^{\,2} + \dfrac{a_x a_z^{\,2}}{a}\right) \end{bmatrix} \tag{3.116}$$

Again m and n are to be determined by Poisson's ratio and compressibility.

B. Atomistic Second Order Piola-Kirchhoff Stress

Virial Stress of atom B between atom A and atom B at zero temperature can be expressed as

$$\mathbf{s} = -\frac{1}{2V_0}\mathbf{b} \otimes \mathbf{f} \tag{3.117}$$

In Section 7, virial stress $\mathbf{S}$ is proved to be Kirchhoff Stress $\boldsymbol{\tau}$. Since Second Order Piola-Kirchhoff stress $\mathbf{T}$ is related to Kirchhoff stress as

$$\begin{aligned} \mathbf{T}_1 &= \mathbf{F}_1^{-1}\boldsymbol{\tau}_1\mathbf{F}_1^{-T} = \mathbf{F}_1^{-1}\mathbf{s}_1\mathbf{F}_1^{-T} = \left(\mathbf{R}_{\mathbf{Xb}}\mathbf{U}_1\right)^{-1}\mathbf{s}_1\left(\mathbf{R}_{\mathbf{Xb}}\mathbf{U}_1\right)^{-T} \\ &= \mathbf{U}_1^{-1}\mathbf{R}_{\mathbf{Xb}}^{-1}\mathbf{s}_1\mathbf{R}_{\mathbf{Xb}}\mathbf{U}_1^{-T} = \mathbf{U}_1^{-1}\left(\mathbf{R}_{\mathbf{Xb}}^{-1}\mathbf{s}_1\mathbf{R}_{\mathbf{Xb}}\right)\mathbf{U}_1^{-T} \\ &= \mathbf{U}_1^{-1}\left(\mathbf{s}_2\right)\mathbf{U}_1^{-T} = \mathbf{F}_2^{-1}\mathbf{s}_2\mathbf{F}_2^{-T} = \mathbf{T}_2 \end{aligned} \tag{3.118}$$

where $\mathbf{S}_1$ is the virial stress due to deformation from $\mathbf{a}_1$ to $\mathbf{b}_1$; $\mathbf{s}_2$ is the virial stress due to deformation from $\mathbf{a}_1$ to $\mathbf{b}_2$; $\mathbf{F}_1 = \mathbf{R}_{\mathbf{Xb}}\mathbf{U}_1$ is the deformation gradient between $\mathbf{a}_1$ and $\mathbf{b}_1$;

$\mathbf{F}_2 = \mathbf{U}_1$ is deformation gradient between $\mathbf{a}_1$ and $\mathbf{b}_2$ (cf. figure 4d) ; $\mathbf{T}_1$ is the 2nd order Piola-Kirchhoff stress due to deformation between $\mathbf{a}_1$ and $\mathbf{b}_1$ (cf. figure 4c); $\mathbf{T}_2$ is the 2nd order Piola-Kirchhoff stress due to deformation between $\mathbf{a}_1$ and $\mathbf{b}_2$ (cf. figure 4d). Notice that $\mathbf{a}_1$ and $\mathbf{b}_2$ are both aligned with X-axis; the deformation from $\mathbf{a}_1$ to $\mathbf{b}_2$ is previously discussed simple tension case. Thus we have proved that the 2nd order Piola-Kirchhoff stress of general 3D case (cf. figure 4.c) is identical to that of simple tension case (cf. figure 4.d) in which vector $\mathbf{a}$ is aligned with X-axis. Now $\mathbf{T}_1$ is rotated to $\mathbf{T}$ in its original position by $\tilde{\mathbf{R}}_{\mathbf{aX}}^{-1}$

$$\mathbf{T} = \tilde{\mathbf{R}}_{\mathbf{aX}}^{-1}\mathbf{T}_1\tilde{\mathbf{R}}_{\mathbf{aX}} = \tilde{\mathbf{R}}_{\mathbf{aX}}^{-1}\mathbf{T}_2\tilde{\mathbf{R}}_{\mathbf{aX}} \tag{3.119}$$

where

$$\mathbf{T}_2 = \begin{bmatrix} -k^{-2}\tau_{11} & 0 & 0 \\ 0 & 0 & 0 \\ 0 & 0 & 0 \end{bmatrix} = -\frac{1}{2V_o}\begin{bmatrix} (r_0/r)^2 rf & 0 & 0 \\ 0 & 0 & 0 \\ 0 & 0 & 0 \end{bmatrix} \tag{3.120}$$

C. Work Conjugacy between Lagrangian Strain and Atomistic 2nd order Piola-Kirchhoff Stress in discrete system

Now we want to prove that $\mathbf{E}$ and $\mathbf{T}$ commute and $\mathbf{ET}$ is symmetric. Recall

$$\mathbf{T} = \tilde{\mathbf{R}}_{aX}^{-1}\mathbf{T}_2\tilde{\mathbf{R}}_{aX} \tag{3.121}$$

It is straightforward to arrive at (cf. eqs. (3.115)(3.121))

$$\mathbf{ET} = \tilde{\mathbf{R}}_{aX}^{-1}\mathbf{E}_1\tilde{\mathbf{R}}_{aX}\tilde{\mathbf{R}}_{aX}^{-1}\mathbf{T}_2\tilde{\mathbf{R}}_{aX} = \tilde{\mathbf{R}}_{aX}^{-1}\mathbf{E}_1\mathbf{T}_2\tilde{\mathbf{R}}_{aX} \tag{3.122}$$

$$\mathbf{TE} = \tilde{\mathbf{R}}_{aX}^{-1}\mathbf{T}_2\tilde{\mathbf{R}}_{aX}\tilde{\mathbf{R}}_{aX}^{-1}\mathbf{E}_1\tilde{\mathbf{R}}_{aX} = \tilde{\mathbf{R}}_{aX}^{-1}\mathbf{T}_2\mathbf{E}_1\tilde{\mathbf{R}}_{aX} \tag{3.123}$$

$$\mathbf{E}_1\mathbf{T}_2 = \mathbf{T}_2\mathbf{E}_1 = \frac{1}{2}\begin{bmatrix} -rf/2V_o + \left(r_0/r\right)^2 rf/2V_o & 0 & 0 \\ 0 & 0 & 0 \\ 0 & 0 & 0 \end{bmatrix} \tag{3.124}$$

It simply says $\mathbf{E}_1\mathbf{T}_2 = \mathbf{T}_2\mathbf{E}_1$, which leads to $\mathbf{ET} = \mathbf{TE}$, i.e. $\mathbf{E}$ and $\mathbf{T}$ commute. Since $\mathbf{E}$ and $\mathbf{T}$ commute and both are symmetric, their product $\mathbf{ET}$ is symmetric. Now we prove the conjugacy between $\mathbf{E}$ and $\mathbf{T}$ following Fitzgerald's procedure (Fitzgerald 1980).

$$\begin{aligned}
&\mathbf{T}:\dot{\mathbf{E}} = tr\left(\mathbf{T}^{\mathrm{T}}\dot{\mathbf{E}}\right) = tr\left[\tilde{\mathbf{R}}_{aX}^{-1}\mathbf{T}_2\tilde{\mathbf{R}}_{aX}\left(\dot{\overline{\tilde{\mathbf{R}}_{aX}^{-1}\mathbf{E}_1\tilde{\mathbf{R}}_{aX}}}\right)\right] \\
&= tr\left[\tilde{\mathbf{R}}_{aX}^{-1}\mathbf{T}_2\tilde{\mathbf{R}}_{aX}\tilde{\mathbf{R}}_{aX}^{-1}\dot{\mathbf{E}}_1\tilde{\mathbf{R}}_{aX} + \tilde{\mathbf{R}}_{aX}^{-1}\mathbf{T}_2\tilde{\mathbf{R}}_{aX}\dot{\tilde{\mathbf{R}}}_{aX}^{-1}\mathbf{E}_1\tilde{\mathbf{R}}_{aX} + \tilde{\mathbf{R}}_{aX}^{-1}\mathbf{T}_2\tilde{\mathbf{R}}_{aX}\tilde{\mathbf{R}}_{aX}^{-1}\mathbf{E}_1\dot{\tilde{\mathbf{R}}}_{aX}\right] \\
&= tr\left[\tilde{\mathbf{R}}_{aX}^{-1}\mathbf{T}_2\dot{\mathbf{E}}_1\tilde{\mathbf{R}}_{aX}\right] + tr\left[\tilde{\mathbf{R}}_{aX}^{-1}\mathbf{T}_2\tilde{\mathbf{R}}_{aX}\dot{\tilde{\mathbf{R}}}_{aX}^{-1}\mathbf{E}_1\tilde{\mathbf{R}}_{aX}\right] + tr\left[\tilde{\mathbf{R}}_{aX}^{-1}\mathbf{T}_2\tilde{\mathbf{R}}_{aX}\tilde{\mathbf{R}}_{aX}^{-1}\mathbf{E}_1\dot{\tilde{\mathbf{R}}}_{aX}\right] \\
&\equiv I + II + III
\end{aligned} \tag{3.125}$$

$$
\begin{aligned}
II &= tr\left[\tilde{\mathbf{R}}_{aX}^{-1}\mathbf{T}_2\tilde{\mathbf{R}}_{aX}\,\dot{\tilde{\mathbf{R}}}_{aX}^{-1}\mathbf{E}_1\tilde{\mathbf{R}}_{aX}\right] \\
&= tr\left[\tilde{\mathbf{R}}_{aX}^{-1}\tilde{\mathbf{R}}_{aX}\mathbf{T}\tilde{\mathbf{R}}_{aX}^{-1}\tilde{\mathbf{R}}_{aX}\,\dot{\tilde{\mathbf{R}}}_{aX}^{-1}\tilde{\mathbf{R}}_{aX}\mathbf{E}\tilde{\mathbf{R}}_{aX}^{-1}\tilde{\mathbf{R}}_{aX}\right] \\
&= tr\left[\mathbf{T}\dot{\tilde{\mathbf{R}}}_{aX}^{-1}\tilde{\mathbf{R}}_{aX}\mathbf{E}\right] \\
&= tr\left[\dot{\tilde{\mathbf{R}}}_{aX}^{-1}\tilde{\mathbf{R}}_{aX}\mathbf{E}\mathbf{T}\right]
\end{aligned}
\tag{3.126}
$$

Since $\dot{\tilde{\mathbf{R}}}_{aX}^{-1}\tilde{\mathbf{R}}_{aX}$ is anti-symmetric and $\mathbf{ET}$ is symmetric, $II = 0$. Similarly,

$$
\begin{aligned}
III &= tr\left[\tilde{\mathbf{R}}_{aX}^{-1}\mathbf{T}_2\tilde{\mathbf{R}}_{aX}\tilde{\mathbf{R}}_{aX}{}^{-1}\mathbf{E}_1\,\dot{\tilde{\mathbf{R}}}_{aX}\right] \\
&= tr\left[\tilde{\mathbf{R}}_{aX}^{-1}\tilde{\mathbf{R}}_{aX}\mathbf{T}\tilde{\mathbf{R}}_{aX}^{-1}\tilde{\mathbf{R}}_{aX}\tilde{\mathbf{R}}_{aX}^{-1}\tilde{\mathbf{R}}_{aX}\mathbf{E}\tilde{\mathbf{R}}_{ax}\,\dot{\tilde{\mathbf{R}}}_{aX}\right] \\
&= tr\left[\mathbf{TE}\tilde{\mathbf{R}}_{ax}\,\dot{\tilde{\mathbf{R}}}_{aX}\right] \\
&= tr\left[\tilde{\mathbf{R}}_{ax}\,\dot{\tilde{\mathbf{R}}}_{aX}\mathbf{TE}\right] \\
&= 0
\end{aligned}
\tag{3.127}
$$

Therefore, we obtain

$$
\mathbf{T}:\dot{\mathbf{E}} = tr\left[\tilde{\mathbf{R}}_{aX}^{-1}\left(\mathbf{T}_2\dot{\mathbf{E}}_1\right)\tilde{\mathbf{R}}_{aX}\right] = tr[\mathbf{T}_2\dot{\mathbf{E}}_1] = \mathbf{T}_2:\dot{\mathbf{E}}_1 \tag{3.128}
$$

which gives (cf. eqs. (108, 133))

$$
\begin{aligned}
&\mathbf{T}:\dot{\mathbf{E}} = \mathbf{T}_2:\dot{\mathbf{E}}_1 = tr\left(\mathbf{T}_2\dot{\mathbf{E}}_1\right) \\
&= tr\left\{\frac{1}{2}\begin{bmatrix} -\left(r_0/r\right)^2 rf/2V & 0 & 0 \\ 0 & 0 & 0 \\ 0 & 0 & 0 \end{bmatrix}\frac{d}{dt}\begin{bmatrix} \left(r/r_0\right)^2-1 & 0 & 0 \\ 0 & m^2-1 & 0 \\ 0 & 0 & n^2-1 \end{bmatrix}\right\} \\
&= tr\left\{\frac{1}{2}\begin{bmatrix} -\frac{r_0^{\,2}rf}{2r^2V_0} & 0 & 0 \\ 0 & 0 & 0 \\ 0 & 0 & 0 \end{bmatrix}\begin{bmatrix} \frac{2r\dot{r}}{r_0^{\,2}} & 0 & 0 \\ 0 & 2m\dot{m} & 0 \\ 0 & 0 & 2n\dot{n} \end{bmatrix}\right\} = tr\left\{\begin{bmatrix} -\frac{\dot{r}f}{2V_0} & 0 & 0 \\ 0 & 0 & 0 \\ 0 & 0 & 0 \end{bmatrix}\right\} \\
&= -\frac{\dot{r}f}{2V_0}
\end{aligned}
\tag{3.129}
$$

or equivalently $\mathbf{T}:d\mathbf{E} = -\dfrac{f}{2V_0}dr$. Now the strain energy density can be obtained as

$$
\Sigma = \int_{r_0}^{r}\mathbf{T}:d\mathbf{E} = -\int_{r_0}^{r}\frac{f}{2V_0}dr = -\frac{1}{2V_0}\int_{r_0}^{r}fdr = \frac{1}{2V_0}\int_{r_0}^{r}dU = \frac{1}{2V_0}\left(U\big|_r - U\big|_{r_0}\right) \tag{3.130}
$$

where $U_{atom}\big|_r$ and $U_{atom}\big|_{r_0}$ are the interatomic potential between atom A and B at distance r and r_0, respectively. From the view point of continuum mechanics, the total potential energy, or say the total strain energy, of system can be calculated as

$$
U^B = \int_{V_o}\Sigma dV = \Sigma\int_{V_o}dV = \Sigma V_0 = \frac{1}{2}\left(U\big|_r - U\big|_{r_0}\right) \tag{3.131}
$$

where the strain energy density Σ is considered as a constant throughout the entire virtual specimen and can be pulled out of integral sign. Thus we have proved that the energy calculated from the interatomic potential is identical to the energy calculated from strain

energy density when the stress and the strain are taken to be the atomistic 2nd order Piola-Kirchhoff stress and the atomistic Lagrangian strain, respectively.

3.8 Generalization of stress and strain to multi-atom system

In previous sections we have proved work conjugacy for stress/strain pair in two-atom case as follows (cf. eqs. (3.103),(3.130)):

$$s_{ij}^{\alpha} = \frac{\partial \Sigma^{\alpha}}{\partial h_{ij}^{\alpha}} = \frac{1}{V_0}\frac{\partial U^{\alpha}}{\partial h_{ij}^{\alpha}} \tag{3.132}$$

$$T_{ij}^{\alpha} = \frac{\partial \Sigma^{\alpha}}{\partial E_{ij}^{\alpha}} = \frac{1}{V_0}\frac{\partial U^{\alpha}}{\partial E_{ij}^{\alpha}} \tag{3.133}$$

where $U = \Sigma V_0$ is the interatomic potential U which equals to the strain energy density Σ times the original volume V_o. This section endeavors the generalization to the multi-atom system. Assume an atom occupies a volume V_o in the original configuration (cf. fig 5). Notice the entire volume can be divided into numerous Wigner-Seitz cells(Kittel 2005), one for each atom without gap or overlap.

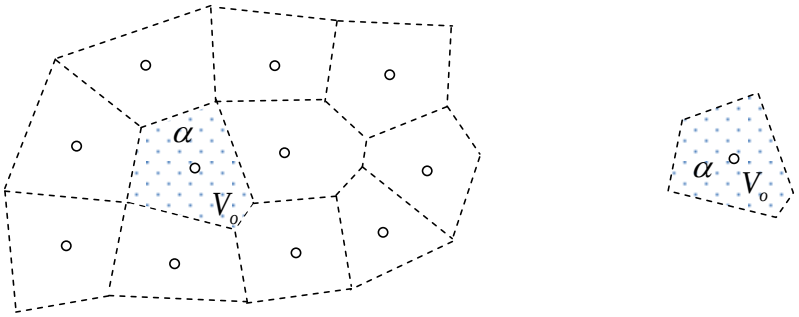

Figure 3-5 (a): Atomistic point of view and defined original volume. (b): Continuum point of view with the region seen as solid material with all quantities uniform within its boundary.

Because stress is additive, the stress of atom α, s_{ij}^{α}, equals to the summation of all $\mathbf{s}^{\alpha\beta}$ from possible $\alpha-\beta$ pairs with α being specified (cf. eq. (3.135)). Notice that the original definition of virial stress also implicitly implies the stress is additive (cf. eq. (3.63)). Now let us rewrite atomistic Kirchhoff stress (local virial stress) at zero temperature (cf. eq. (3.63)) as

$$s_{ij}^{\alpha}=\sum_{\beta\neq\alpha}s_{ij}^{\alpha\beta}=-\frac{1}{2V_0}\sum_{\beta\neq\alpha}r_i^{\alpha\beta}f_j^{\alpha\beta} \tag{3.134}$$

Stress being additive can also be expressed as

$$\begin{aligned} s_{ij}^{A}&=\overbrace{s_{ij}^{AB}+s_{ij}^{AC}+s_{ij}^{AD}+\ldots}^{N-1\text{ terms}}\\ or\quad s_{ij}^{A}&=\sum_{B=1}^{N-1}s_{ij}^{AB}\end{aligned} \tag{3.135}$$

Now we write stress/strain conjugacy as (cf. eq. (3.132))

$$N-1\text{ terms}\begin{cases} s_{ij}^{AB}=\dfrac{1}{V_0}\dfrac{\partial U^{AB}}{\partial h_{ij}^{AB}}\\ s_{ij}^{AC}=\dfrac{1}{V_0}\dfrac{\partial U^{AC}}{\partial h_{ij}^{AC}}\\ s_{ij}^{AD}=\dfrac{1}{V_0}\dfrac{\partial U^{AD}}{\partial h_{ij}^{AD}}\\ \ldots\end{cases} \tag{3.136}$$

Hencky strain $\mathbf{h}$ between two arbitrary atoms α and β is a function of their current relative position $\mathbf{r}^{kl}$ and original distance r_0^{kl} (cf. eqs.(3.89)(3.90))

$$\mathbf{h}^{\alpha\beta}=\mathbf{h}^{\alpha\beta}\left(\mathbf{r}^{\alpha\beta};r_0^{\alpha\beta}\right) \tag{3.137}$$

Since $\mathbf{h}$ monotonically changes with respect to $\mathbf{r}$ (cf. eq.(3.89)), one may rewrite

$$\begin{aligned}\mathbf{r}^{\alpha\beta} &= \mathbf{r}^{\alpha\beta}\left(\mathbf{h}^{\alpha\beta}; r_0^{\alpha\beta}\right) \\ r^{\alpha\beta} &\equiv \left\|\mathbf{r}^{\alpha\beta}\right\| = r^{\alpha\beta}\left(\mathbf{h}^{\alpha\beta}; r_0^{\alpha\beta}\right)\end{aligned} \tag{3.138}$$

Recall that interatomic potential is a function of the current distance between atoms

$$U^{\alpha\beta} = U^{\alpha\beta}\left(r^{\alpha\beta}\right) \tag{3.139}$$

It leads to

$$U^{\alpha\beta} = U^{\alpha\beta}\left(\mathbf{h}^{\alpha\beta}; r_0^{\alpha\beta}\right) \tag{3.140}$$

Since Hencky strains, $\mathbf{h}^{AB}, \mathbf{h}^{AC}, \mathbf{h}^{AD}, \ldots$ are independent of each other, now the total potential can be expressed as

$$\begin{aligned}U &= U^{AB}\left(\mathbf{h}^{AB}; r_0^{AB}\right) + U^{AC}\left(\mathbf{h}^{AC}; r_0^{AC}\right) + U^{AD}\left(\mathbf{h}^{AD}; r_0^{AD}\right)\ldots \\ &= U\left(\mathbf{h}^{AB}, \mathbf{h}^{AC}, \mathbf{h}^{AD}, \ldots; r_0^{AB}, r_0^{AC}, r_0^{AD}, \ldots\right)\end{aligned} \tag{3.141}$$

Therefore

$$\frac{\partial U}{\partial \mathbf{h}^{AB}} = \frac{\partial U^{AB}}{\partial \mathbf{h}^{AB}} \quad , \quad \frac{\partial U}{\partial \mathbf{h}^{AC}} = \frac{\partial U^{AC}}{\partial \mathbf{h}^{AC}} \quad , \quad \ldots \tag{3.142}$$

Now we define the Hencky strain of atom A as the arithmetic average of Hencky strain of all possible pairs with atom A

$$h_{ij}^{A} \equiv \frac{1}{N-1}\overbrace{\left[h_{ij}^{AB} + h_{ij}^{AC} + h_{ij}^{AD} + \ldots\right]}^{N-1 \text{ terms}} \tag{3.143}$$

$$\text{or} \quad h_{ij}^{A} \equiv \frac{1}{N-1}\sum_{B=1}^{N-1} h_{ij}^{AB}$$

Since

$$\frac{\partial h_{ij}^{A}}{\partial h_{kl}^{AB}} = \frac{1}{N-1}\delta_{ik}\delta_{jl} \quad , \quad \frac{\partial h_{ij}^{A}}{\partial h_{kl}^{AC}} = \frac{1}{N-1}\delta_{ik}\delta_{jl} \quad , \quad \frac{\partial h_{ij}^{A}}{\partial h_{kl}^{AD}} = \frac{1}{N-1}\delta_{ik}\delta_{jl} \quad ,.... \tag{3.144}$$

It is straightforward to show (cf. eqs. (3.142)(3.144))

$$\begin{aligned}
s_{ij}^{A} &= \left[s_{ij}^{AB} + s_{ij}^{AC} + s_{ij}^{AD} + \ldots\right] \\
&= \frac{1}{V_0}\left[\frac{\partial U^{AB}}{\partial h_{ij}^{AB}} + \frac{\partial U^{AC}}{\partial h_{ij}^{AC}} + \frac{\partial U^{AD}}{\partial h_{ij}^{AD}} + \ldots\right] \\
&= \frac{1}{V_0}\left[\frac{\partial U}{\partial h_{ij}^{AB}} + \frac{\partial U}{\partial h_{ij}^{AC}} + \frac{\partial U}{\partial h_{ij}^{AD}} + \ldots\right] \quad \Leftarrow \quad \frac{\partial U^{AB}}{\partial h_{ij}^{AC}} = 0, \ldots \\
&= \frac{1}{V_0}\left[\frac{\partial U}{\partial h_{kl}^{A}}\frac{\partial h_{kl}^{A}}{\partial h_{ij}^{AB}} + \frac{\partial U}{\partial h_{kl}^{A}}\frac{\partial h_{kl}^{A}}{\partial h_{ij}^{AC}} + \frac{\partial U}{\partial h_{kl}^{A}}\frac{\partial h_{kl}^{A}}{\partial h_{ij}^{AD}} \ldots\right] \\
&= \frac{1}{V_0}\overbrace{\left[\frac{\partial U}{\partial h_{kl}^{A}}\frac{1}{N-1}\delta_{ki}\delta_{lj} + \frac{\partial U}{\partial h_{kl}^{A}}\frac{1}{N-1}\delta_{ki}\delta_{lj} + \frac{\partial U}{\partial h_{kl}^{A}}\frac{1}{N-1}\delta_{ki}\delta_{lj} \ldots\right]}^{N-1 \text{ terms}} \\
&= \frac{1}{V_0}\overbrace{\left[\frac{\partial U}{\partial h_{ij}^{A}}\frac{1}{N-1} + \frac{\partial U}{\partial h_{ij}^{A}}\frac{1}{N-1} + \frac{\partial U}{\partial h_{ij}^{A}}\frac{1}{N-1} \ldots\right]}^{N-1} \\
&= \frac{1}{V_0}\left[\frac{\partial U}{\partial h_{ij}^{A}}\right]
\end{aligned} \tag{3.145}$$

Thus we have proved the conjugacy is valid in multi-atom system if atomistic Kirchhoff stress (local virial stress) takes summation (cf. eq. (3.134) and Hencky strain takes arithmetic average (cf. eq. (3.143).

Similar to the pair of Hencky strain and atomistic Kirchhoff stress (local virial stress), we are going to prove that the atomistic second order Piola-Kirchhoff stress and the atomistic Lagrangian strain also hold conjugacy in multi-atom case. The second order Piola-Kirchhoff stress tensor is additive (cf. eq. (126)), we write

$$T_{ij}^{A} = \overbrace{T_{ij}^{AB} + T_{ij}^{AC} + T_{ij}^{AD} + \ldots}^{N-1 \text{ terms}} \tag{3.146}$$

where $\mathbf{T}^{AB}$ is the stress tensor due to the pair of atoms A and B; $\mathbf{T}^{A}$ is the sum of stress tensors due to all pairs associated with atom A, i.e. $\mathbf{T}^{AB}$, $\mathbf{T}^{AC}$, $\mathbf{T}^{AD}$, ... Now the stress/strain conjugacy can be expressed as (cf. eq. (126))

$$N-1 \text{ terms} \begin{cases} T_{ij}^{AB} = \dfrac{1}{V_0}\dfrac{\partial U^{AB}}{\partial E_{ij}^{AB}} \\ T_{ij}^{AC} = \dfrac{1}{V_0}\dfrac{\partial U^{AC}}{\partial E_{ij}^{AC}} \\ T_{ij}^{AD} = \dfrac{1}{V_0}\dfrac{\partial U^{AD}}{\partial E_{ij}^{AD}} \\ \ldots \end{cases} \tag{3.147}$$

Lagrangian strain $\mathbf{E}^{\alpha\beta}$ between two arbitrary atoms α and β is a function of their original relative position $\mathbf{r}_o^{\alpha\beta}$ and current distance $r^{\alpha\beta}$ (cf. eqs. (3.115)(3.116))

$$\mathbf{E}^{\alpha\beta} = \mathbf{E}^{\alpha\beta}\left(r^{\alpha\beta}; \mathbf{r}_o^{\alpha\beta}\right) \tag{3.148}$$

Since **E** monotonically changes with respect to $r^{\alpha\beta}$ (cf. eqs. (3.115)(3.116)), one may rewrite

$$r^{\alpha\beta} = r^{\alpha\beta}\left(\mathbf{E}^{\alpha\beta};\mathbf{r}_o^{\alpha\beta}\right) \tag{3.149}$$

Recall that the interatomic potential is a function of the current distance between atoms

$$U^{\alpha\beta} = U^{\alpha\beta}\left(r^{\alpha\beta}\right) \tag{3.150}$$

It leads to

$$U^{\alpha\beta} = U^{\alpha\beta}\left(\mathbf{E}^{\alpha\beta};\mathbf{r}_o^{\alpha\beta}\right) \tag{3.151}$$

Since atomistic Lagrangian strains, $\mathbf{E}^{AB}$, $\mathbf{E}^{AC}$, $\mathbf{E}^{AD}$, ..., are independent of each other, now the total potential can be expressed as

$$\begin{aligned} U &= U^{AB}\left(\mathbf{E}^{AB};\mathbf{r}_o^{AB}\right) + U^{AC}\left(\mathbf{E}^{AC};\mathbf{r}_o^{AC}\right) + U^{AD}\left(\mathbf{E}^{AD};\mathbf{r}_o^{AD}\right)... \\ &= U\left(\mathbf{E}^{AB},\mathbf{E}^{AC},\mathbf{E}^{AD},...;\mathbf{r}_o^{AB},\mathbf{r}_o^{AC},\mathbf{r}_o^{AD},...\right) \end{aligned} \tag{3.152}$$

Therefore

$$\frac{\partial U}{\partial \mathbf{E}^{AB}} = \frac{\partial U^{AB}}{\partial \mathbf{E}^{AB}} \quad , \quad \frac{\partial U}{\partial \mathbf{E}^{AC}} = \frac{\partial U^{AC}}{\partial \mathbf{E}^{AC}} \quad , \quad ... \tag{3.153}$$

Now we define the Lagrangian strain of atom A as the arithmetic average of Lagrangian strains of all possible pairs associated with atom A

$$E_{ij}^{A} \equiv \frac{1}{N-1}\overbrace{\left[E_{ij}^{AB} + E_{ij}^{AC} + E_{ij}^{AD} + ...\right]}^{N-1 \text{ terms}} \tag{3.154}$$

Since

$$\frac{\partial E_{ij}^{A}}{\partial E_{kl}^{AB}} = \frac{1}{N-1}\delta_{ik}\delta_{jl} \quad , \quad \frac{\partial E_{ij}^{A}}{\partial E_{kl}^{AC}} = \frac{1}{N-1}\delta_{ik}\delta_{jl} \quad , \quad \frac{\partial E_{ij}^{A}}{\partial E_{kl}^{AD}} = \frac{1}{N-1}\delta_{ik}\delta_{jl} \quad ,.... \tag{3.155}$$

It is straightforward to show

$$\begin{aligned}
T_{ij}^{A} &= \left[T_{ij}^{AB} + T_{ij}^{AC} + T_{ij}^{AD} + ... \right] \\
&= \frac{1}{V_0}\left[\frac{\partial U^{AB}}{\partial E_{ij}^{AB}} + \frac{\partial U^{AC}}{\partial E_{ij}^{AC}} + \frac{\partial U^{AD}}{\partial E_{ij}^{AD}} + ... \right] \\
&= \frac{1}{V_0}\left[\frac{\partial U}{\partial E_{ij}^{AB}} + \frac{\partial U}{\partial E_{ij}^{AC}} + \frac{\partial U}{\partial E_{ij}^{AD}} + ... \right] \quad \Leftarrow \quad \frac{\partial U^{AB}}{\partial \mathbf{E}^{AC}} = 0, \; ... \\
&= \frac{1}{V_0}\left[\frac{\partial U}{\partial E_{kl}^{A}}\frac{\partial E_{kl}^{A}}{\partial E_{ij}^{AB}} + \frac{\partial U}{\partial E_{kl}^{A}}\frac{\partial E_{kl}^{A}}{\partial E_{ij}^{AC}} + \frac{\partial U}{\partial E_{kl}^{A}}\frac{\partial E_{kl}^{A}}{\partial E_{ij}^{AD}} ... \right] \\
&= \frac{1}{V_0}\left[\overbrace{\frac{\partial U}{\partial E_{kl}^{A}}\frac{1}{N-1}\delta_{ki}\delta_{lj} + \frac{\partial U}{\partial E_{kl}^{A}}\frac{1}{N-1}\delta_{ki}\delta_{lj} + \frac{\partial U}{\partial E_{kl}^{A}}\frac{1}{N-1}\delta_{ki}\delta_{lj} ...}^{N-1 \text{ terms}} \right] \\
&= \frac{1}{V_0}\left[\overbrace{\frac{\partial U}{\partial E_{ij}^{A}}\frac{1}{N-1} + \frac{\partial U}{\partial E_{ij}^{A}}\frac{1}{N-1} + \frac{\partial U}{\partial E_{ij}^{A}}\frac{1}{N-1} ...}^{N-1} \right] \\
&= \frac{1}{V_0}\left[\frac{\partial U}{\partial E_{ij}^{A}} \right]
\end{aligned} \tag{3.156}$$

Thus this conjugacy holds true in multi-atom system if the second order Piola-Kirchhoff stress takes summation and the Lagrangian strain takes arithmetic average.

3.9 Summary

Here we summarize the definitions of work conjugate stresses and strains in general case:

Atomistic Kirchhoff Stress (local virial stress evaluated at original volume of each atom):

$$s_{ij}^{\alpha} = -\frac{1}{2V_0}\sum_{\substack{\beta=1 \\ \beta\neq\alpha}}^{N} r_i^{\alpha\beta} f_j^{\alpha\beta} \tag{3.157}$$

where $\mathbf{s}^{\alpha}$ is the atomistic Kirchhoff stress of atom α; $\mathbf{r}^{\alpha\beta} \equiv \mathbf{r}^{\alpha} - \mathbf{r}^{\beta}$ denotes the relative position vector at the current configuration; $\mathbf{f}^{\alpha\beta}$ is force acting on atom α due to interaction with atom β at current configuration. Atom α occupies volume V_0 in its original configuration. There are total N atoms in system.

Atomistic Kirchhoff Stress (Equivalent definition of eq. (3.157)) defined at principle axis:

$$\mathbf{s}^{\alpha} = \sum_{\substack{\beta=1 \\ \beta\neq\alpha}}^{N} \mathbf{s}^{\alpha\beta} = \sum_{\substack{\beta=1 \\ \beta\neq\alpha}}^{N} \left(\mathbf{R}_{\mathbf{bx}}^{\alpha\beta}\right)^{\mathbf{T}} \hat{\mathbf{s}}_{\mathbf{I}}^{\alpha\beta} \mathbf{R}_{\mathbf{bx}}^{\alpha\beta} \tag{3.158}$$

$$\hat{\mathbf{s}}_{\mathbf{I}}^{\alpha\beta} = -\frac{1}{2V_0} \mathbf{r}_{\mathbf{I}}^{\boldsymbol{\alpha\beta}} \otimes \mathbf{f}_{\mathbf{I}}^{\boldsymbol{\alpha\beta}} \tag{3.159}$$

where $\mathbf{R}^{\alpha\beta}$ is the rotational matrix to rotate relative position vector $\mathbf{r} \equiv \mathbf{X^A} - \mathbf{X^B}$ at the deformed state to align with X-axis (cf. eq. (3.88)).

$$\mathbf{R}^{\alpha\beta}=\begin{bmatrix} r_x/r & r_y/r & r_z/r \\ -r_y/r & \dfrac{1}{r_y^{\,2}+r_z^{\,2}}\left(r_z^{\,2}+\dfrac{r_x r_y^{\,2}}{r}\right) & \dfrac{r_y r_z}{r_y^{\,2}+r_z^{\,2}}\left(\dfrac{r_x}{r}-1\right) \\ -r_z/r & \dfrac{r_y r_z}{r_y^{\,2}+r_z^{\,2}}\left(\dfrac{r_x}{r}-1\right) & \dfrac{1}{r_y^{\,2}+r_z^{\,2}}\left(r_y^{\,2}+\dfrac{r_x r_z^{\,2}}{r}\right) \end{bmatrix} \tag{3.160}$$

$$\mathbf{r}_{\mathbf{I}}^{\alpha\beta}=\mathbf{R}^{\alpha\beta}\mathbf{r}^{\alpha\beta}=\begin{bmatrix} r & 0 & 0 \end{bmatrix}^T \tag{3.161}$$

$$\mathbf{f}_{\mathbf{I}}^{\alpha\beta}=\mathbf{R}^{\alpha\beta}\mathbf{f}^{\alpha\beta}=\begin{bmatrix} f & 0 & 0 \end{bmatrix}^T \tag{3.162}$$

where r is the only non-zero component of $\mathbf{r}_{\mathbf{I}}^{\alpha\beta}$, f is the only non-zero component of $\mathbf{f}_{\mathbf{I}}^{\alpha\beta}$.

Atomistic Hencky Strain:

$$\mathbf{h}^{\alpha}\equiv\frac{1}{N-1}\sum_{\substack{\beta=1\\ \beta\neq\alpha}}^{N}\mathbf{h}^{\alpha\beta}=\frac{1}{N-1}\sum_{\substack{\beta=1\\ \beta\neq\alpha}}^{N}\left(\mathbf{R}_{\mathbf{bx}}^{\alpha\beta}\right)^T\hat{\mathbf{h}}_{\mathbf{I}}^{\alpha\beta}\mathbf{R}_{\mathbf{bx}}^{\alpha\beta} \tag{3.163}$$

$$\hat{\mathbf{h}}^{\alpha\beta}=\begin{bmatrix} \ln(r/r_0) & 0 & 0 \\ 0 & \ln m & 0 \\ 0 & 0 & \ln n \end{bmatrix} \tag{3.164}$$

$$\mathbf{r}_{\mathbf{oI}}^{\alpha\beta}=\mathbf{R}^{\alpha\beta}\mathbf{r}_{\mathbf{o}}^{\alpha\beta}=\begin{bmatrix} r_o & 0 & 0 \end{bmatrix}^T \tag{3.165}$$

where $\mathbf{h}^{\alpha}$ is the atomistic Hencky strain of atom α; $\mathbf{h}^{\alpha\beta}$ is the atomistic Hencky strain between atoms α and β; m and n are undetermined parameters related to Poisson's effect

and compressibility (cf. Section 7). Note that $\mathbf{R}^{\alpha\beta}$ in eqs. (149,151) rotates the relative position vector $\mathbf{r}^{\alpha\beta}$ in the deformed state to align with X-axis (cf. eq. (84)). r_o is the magnitude of $\mathbf{r}_\mathbf{o}^{\alpha\beta}$; $r_o = \left|\mathbf{r}_\mathbf{o}^{\alpha\beta}\right|$

Atomistic Second Order Piola-Kirchhoff Stress:

$$\mathbf{T}^{\alpha} = \sum_{\substack{\beta=1 \\ \beta\neq\alpha}}^{N} \mathbf{T}^{\alpha\beta} = \sum_{\substack{\beta=1 \\ \beta\neq\alpha}}^{N} \left(\tilde{\mathbf{R}}_{\mathbf{aX}}^{\alpha\beta}\right)^{\mathbf{T}} \hat{\mathbf{T}}_{\mathbf{I}}^{\alpha\beta} \tilde{\mathbf{R}}_{\mathbf{aX}}^{\alpha\beta} \tag{3.166}$$

$$\hat{\mathbf{T}}_{\mathbf{I}}^{\alpha\beta} = \begin{bmatrix} -\left(r_0 / r\right)^2 rf / V_0 & 0 & 0 \\ 0 & 0 & 0 \\ 0 & 0 & 0 \end{bmatrix} \tag{3.167}$$

where $\mathbf{T}^{\alpha}$ is the atomistic second order Piola-Kirchhoff stress of atom α, $\mathbf{T}^{\alpha\beta}$ is the atomistic second order Piola-Kirchhoff stress between atoms α and β, $\hat{\mathbf{T}}^{\alpha\beta}$ is the atomistic second order Piola-Kirchhoff stress calculated along its principle direction. $\tilde{\mathbf{R}}_{\mathbf{aX}}^{\alpha\beta}$ is the rotational matrix transforming $\mathbf{T}^{\alpha\beta}$ to $\hat{\mathbf{T}}^{\alpha\beta}$ and it is also the rotational matrix which rotates $\mathbf{r}_o^{\alpha\beta}$ to align with X-axis, where $\tilde{\mathbf{R}}_{\mathbf{aX}}^{\alpha\beta}$ is defined as

$$\tilde{\mathbf{R}}_{\mathbf{aX}}^{\alpha\beta}=\begin{bmatrix} r_{ox}/r_o & r_{oy}/r_o & r_{oz}/r_o \\ -r_{oy}/r_o & \dfrac{1}{r_{oy}^{\,2}+r_{oz}^{\,2}}\left(r_{oz}^{\,2}+\dfrac{r_{ox}r_{oy}^{\,2}}{r_o}\right) & \dfrac{r_{oy}r_{oz}}{r_{oy}^{\,2}+r_{oz}^{\,2}}\left(\dfrac{r_{ox}}{r_o}-1\right) \\ -r_{oz}/r_o & \dfrac{r_{oy}r_{oz}}{r_{oy}^{\,2}+r_{oz}^{\,2}}\left(\dfrac{r_{ox}}{r_o}-1\right) & \dfrac{1}{r_{oy}^{\,2}+r_{oz}^{\,2}}\left(r_{oy}^{\,2}+\dfrac{r_{ox}r_{oz}^{\,2}}{r_o}\right) \end{bmatrix} \tag{3.168}$$

$$\mathbf{r}_{\mathbf{oI}}^{\alpha}=\mathbf{R}^{\alpha\beta}\mathbf{r}_{o}^{\alpha\beta}=\begin{bmatrix} r_o & 0 & 0 \end{bmatrix}^T \tag{3.169}$$

Atomistic Lagrangian Strain:

$$\mathbf{E}^{\alpha}=\sum_{\substack{\beta=1\\ \beta\neq\alpha}}^{N}\frac{1}{N-1}\mathbf{E}^{\alpha\beta}=\frac{1}{N-1}\sum_{\substack{\beta=1\\ \beta\neq\alpha}}^{N}\left(\tilde{\mathbf{R}}_{\mathbf{aX}}^{\alpha\beta}\right)^{\mathbf{T}}\hat{\mathbf{E}}_{\mathbf{I}}^{\alpha\beta}\tilde{\mathbf{R}}_{\mathbf{aX}}^{\alpha\beta} \tag{3.170}$$

$$\hat{\mathbf{E}}_{\mathbf{I}}^{\alpha\beta}=\begin{bmatrix} \left(r/r_0\right)^2-1 & 0 & 0 \\ 0 & m^2-1 & 0 \\ 0 & 0 & n^2-1 \end{bmatrix} \tag{3.171}$$

where $\mathbf{E}^{\alpha}$ is the atomistic Lagrangian strain of atom α, $\mathbf{E}^{\alpha\beta}$ is the atomistic Lagrangian strain between atoms α and β, $\hat{\mathbf{E}}_{\mathbf{I}}^{\alpha\beta}$ is the atomistic Lagrangian strain calculated along its principle direction. Note that $\tilde{\mathbf{R}}_{\mathbf{aX}}^{\alpha\beta}$ in eqs. (3.166)(3.170) rotates the original relative position vector $\mathbf{r}_{\mathbf{o}}$ to align with X-axis (cf. eq. (3.116)).

Atomistic Cauchy Stress (virial stress evaluated at deformed volume):

Virial stress is Cauchy stress if it is calculated in the deformed configuration. It is seen that Cauchy stress of an atomic pair (atoms α and β) can be further derived as:

$$\sigma_{ij}^{\alpha\beta} = j^{-1}\tau_{ij}^{\alpha\beta} = j^{-1}s_{ij}^{\alpha\beta} = \frac{V_0}{V}s_{ij}^{\alpha\beta} = -\frac{V_0}{V}\frac{1}{2V_0}r_i^{\alpha\beta}f_j^{\alpha\beta} = -\frac{1}{2V}r_i^{\alpha\beta}f_j^{\alpha\beta} \quad (3.172)$$

where V is the volume of the deformed state.

Cauchy stress of atom α :

$$\sigma_{ij}^{\alpha} = \sum_{\substack{\beta=1 \\ \beta\neq\alpha}}^{N}\sigma_{ij}^{\alpha\beta} = -\frac{1}{2V}\sum_{\substack{\beta=1 \\ \beta\neq\alpha}}^{N}r_i^{\alpha\beta}f_j^{\alpha\beta} \quad (3.173)$$

Note that for each α and β pair, deformed volume V is not determinable because the strain in transverse direction is not uniquely defined. However in a system of many atoms, deformed volume V can be calculated from the final configuration through Wigner-Seitz cells (Kittel 2005). It is worthwhile to mention that, for a general case with non-zero temperature, the kinetic part of viral stress needs to be added as thermal stress (Subramaniyan 2008, Li, Lee 2014).

Work Conjugacy between stress and strains

Thermodynamic conjugate stress and strain pair:

Atomistic Hencky Strain /Atomistic Kirchhoff Stress:

$$\mathbf{s}^{\alpha} = \frac{\partial \Sigma}{\partial \mathbf{H}^{\alpha}} = \frac{1}{V_0} \frac{\partial U}{\partial \mathbf{H}^{\alpha}} \tag{3.174}$$

Atomistic Lagrangian Strain / Atomistic Second Order Piola-Kirchhoff Stress:

$$\mathbf{T}^{\alpha} = \frac{\partial \Sigma}{\partial \mathbf{E}^{\alpha}} = \frac{1}{V_0} \frac{\partial U}{\partial \mathbf{E}^{\alpha}} \tag{3.175}$$

where Σ is the strain energy density. U is the interatomic potential.

3.10 Discussion

We have proved that the zero-temperature atomistic Kirchhoff stress (local virial stress) calculated at original volume is a work conjugate stress with respect to the atomistic Hencky strain. Recall that Kirchhoff stress and Hencky strain is a thermodynamic pair in continuum mechanics. Hence one may conclude that atomistic Kirchhoff stress (local virial stress) is the equivalence of Kirchhoff stress in MD. Following the relationship between Kirchhoff stress and Cauchy stress, it is demonstrated that the potential part of local virial stress calculated at current state is equivalent to Cauchy stress. We define the stress and the strain of an atom as the summation and the average, respectively, of those

calculated through all atomistic pairs originated from that atom. With these definitions, we have proved that atomistic-Hencky-strain/atomistic-Kirchhoff-stress is a thermodynamic pair in multi-atom system. Similarly, the atomistic-Lagrangian-strain forms a thermodynamic pair with the atomistic PK2 stress. Notice that our definitions of stress and strain are pined to a single atom with the consideration of all its neighbors. This point of view is different from the conventional concept of stress and strain being defined in a region The stresses and strains defined here have the discrete nature. The strain energy is considered uniform in the volume occupied by each atom. With these definitions, the strain energy is always equal to the interatomic potential energy.

Many simulation works already utilized the concept of defining stress (Jin, Yuan 2005b, Fenley 2014, Jin, Yuan 2005a) and strain (Jin, Yuan 2005a) at atom level and yield high resolution result.

We also found the formula to process simple tension test data (cf. eqs. (3.51)(3.52)), which leads to Kirchhoff-stress/Hencky-strain relation with no assumption of incompressibility or small-strain approximation. Eulerian strain and Cauchy stress can be readily obtained (cf. eqs. (3.53)(3.54)). Notice that $\ln(1+e_{eng})$ gives Hencky strain, not Eulerian strain (cf. eq. (50)); $\sigma_{eng}\left(1+e_{eng}\right)$ yields Kirchhoff stress, not Cauchy stress; in other words, the popular way of using simple tension test data to calculate Cauchy stress and Eulerian strain from engineering stress and strain (Caceres-Valencia 2004) is erroneous.

Chapter 4

Finite Element Study of Energy Release Rate Based Fracture Mechanics

4.1 Introduction

Previous chapters have concluded that the critical energy release rate is an adequate criterion in fracture mechanics. Following this idea, a simulation method has been developed in large strain finite element for elastic-plastic fracture. Such method requires only the critical energy release rate as the material constant, thus offers great flexibility to deal with dynamic crack propagation.

Some existing methods to simulate fracture are categorized as such:

Singular element method: This category including the extended finite element (XFEM)(Moës, Dolbow et al. 1999), Generalized Finite Element(GFEM)(Strouboulis 2000) and Symmetric Galerkin Boundary element Method(SGBEM-FEM)(Dong, Atluri 2013). The knowledge of asymptotic field around the crack tip is embedded within the element; this method allows the crack to propagate through the element (Freund 1990), which brings great flexibility when dealing with complex problems. However, such singular field is a direct conclusion from static LEFM with line crack assumption of an infinite specimen. As discussed in the first charter, LEFM overestimates the stress singularity. Freund predicted (Freund 1990) and we later on verified that the dynamic energy release rate is inversely proportional to the crack speed. Therefore the singular field will vary with respect to different crack speed. If a constant singular field is built into the specially treated element, the result will not represent a true dynamic crack. The

asymptotic field around crack tip is also influenced by the shape of the crack surface. An elliptical or notch void has different asymptotic field than the line crack around the crack tip, which is not suitable to model with the singular element tailored to treat only line crack. In general, singular element method suffers a loss of accuracy due to the crude assumption of constant singular field within the element.

Cohesive zone method (Ortiz 1999, Moës 2002, Xu 1994): This method allows the separation of nodes between elements to resemble crack opening. However, this method requires a clear knowledge of force vs. displacement relation between separated nodes (cohesive law) which does not have a clear physical meaning and is hard to obtain. To the least, this method requires several other material constants that need to be determined by material testing. In this chapter, it will be demonstrated that the cohesive law is a function of crack speed. Therefore assuming a constant cohesive relationship would limit the case to static fracture. The cohesive element will have a different stiffness comparing to the ordinary element. Even if the crack does not extend and all cohesive elements stay intact, cohesive zone model will predict different result comparing to the ordinary finite element due to the finite stiffness of the cohesive element. Without carefully calibrating these parameters, the cohesive zone method is more capable of reproducing test result than predicting test result.

Crack opening method: Also known as node release method. this method is one of the oldest method used to simulate crack(Kobayashi, Emery et al. 1976, F., W. 1980). The basic idea is to model the potential crack surface with double nodes that are rigidly connected together. As crack goes though, the nodal constraint force will be gradually released to mimic the crack propagation. This method is identical to cohesive zone

method if the force and displacement of the releasing process is explicitly specified. However in our approach, the force is scaled down monotonically with respect to the original connection force and the displacement is determined by satisfying the governing equation of FEM. We use a iterative scheme to adjust the crack speed to guarantee that the work done in the releasing process will always yields a constant energy release rate.

4.2. Methodology of crack opening method

A large strain dynamics finite element program as described in chapter 1 is developed. Firstly, a specimen is modeled with 3-D solid element. The pre-determined crack path was modeled with double nodes on each sides of the crack surface. Prior to the crack propagation, these paired nodes are constrained with forces that rigidly hold them together. The constraint force is of the same magnitude but opposite direction pointing toward each node. Symbolically, let it be nodes k and l. The displacement of which are U_i^k and U_i^l . Now we require these two nodes have same displacement vector

$$U_i^k = U_i^l \tag{4.1}$$

It is reasonable to assume that the accelerations of these two nodes are identical, i.e.

$$\ddot{U}_i^k = \ddot{U}_i^l \tag{4.2}$$

Recall that the final result of large strain FEM formulation gives

$$M_{i\beta}\ddot{U}_{k\beta} = F_{ki} \tag{4.3}$$

Now we add an additional term of spot-weld connection force f_i^k to the equation

$$M_{i\beta}\ddot{U}_{k\beta} = F_i^k + f_i^k \tag{4.4}$$

where f_i^k is the i-th component of nodal connection force on node k.

Similarly

$$M_{i\beta}\ddot{U}_{l\beta} = F_i^l + f_i^l \tag{4.5}$$

Now, we add these two equation

$$M_{i\beta}\ddot{U}_{k\beta} + M_{i\beta}\ddot{U}_{l\beta} = F_i^k + f_i^k + F_i^l + f_i^l \tag{4.6}$$

Recall that the connection force of node k and l are of the same magnitude but opposite direction

$$f_i^k = -f_i^l \tag{4.7}$$

and the nodal acceleration of k and l are identical. It leads to

$$\ddot{U}_{k\beta} = \ddot{U}_{l\beta} \tag{4.8}$$

$$\left(M_{i\beta} + M_{i\beta}\right)\ddot{U}_{k\beta} = F_i^k + F_i^l \tag{4.9}$$

$$\ddot{U}_{k\beta} = \frac{F_i^k + F_i^l}{M_{i\beta} + M_{i\beta}} \tag{4.10}$$

Now the connection force can be

$$f_i^l = M_{i\beta}\frac{F_i^k + F_i^l}{M_{i\beta} + M_{i\beta}} - F_i^l \tag{4.11}$$

and

$$f_i^k = -M_{i\beta}\frac{F_i^k + F_i^l}{M_{i\beta} + M_{i\beta}} + F_i^l \tag{4.12}$$

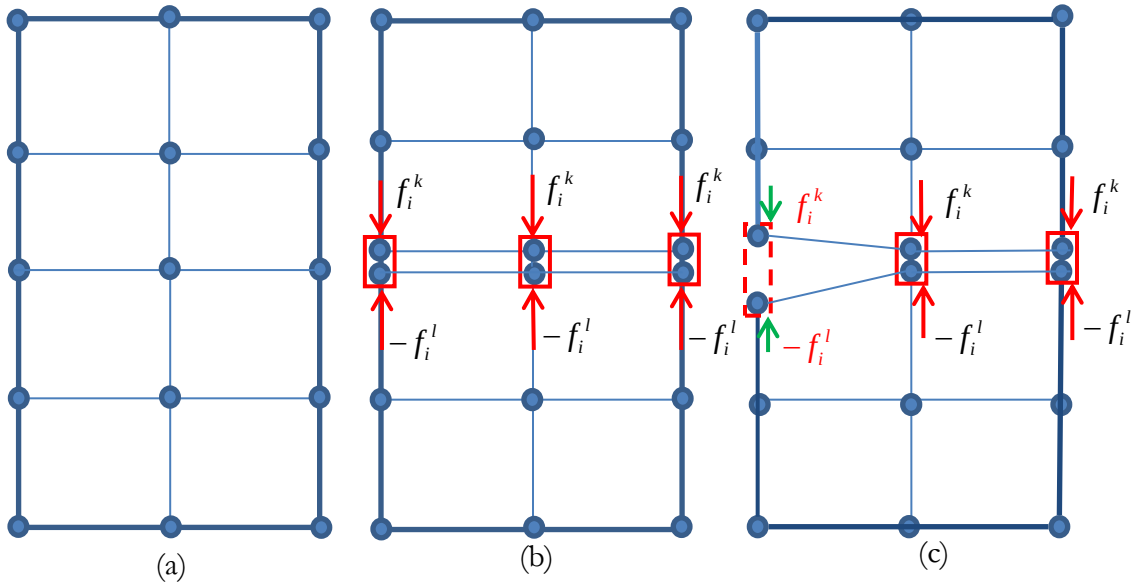

Figure 4-1 Nodal Force Releasing Method. (a) Ordinary Finite Element Mesh. (b) Rigid Body Connection with Double Nodes. (c) Releasing Connection Force

In example 1, a verification case is presented to verify that the model with rigid-connected paired nodes yields the same result as classical finite element.

As the crack propagates through the edge of the element, the connection force is gradually reduced to zero. A simple demonstrative example is given in Figure 4-2. Notice that the connection force is given by linear scaling but the relative displacement between paired nodes is solved by FEM. The relation of the displacement vs. force curve is not an input but an output . The shape of the releasing curve is verified to be independent of the number of releasing steps while keeping the crack speed constant (cf. example 2). This feature later allows a free choice of releasing steps N when calculating crack speed.

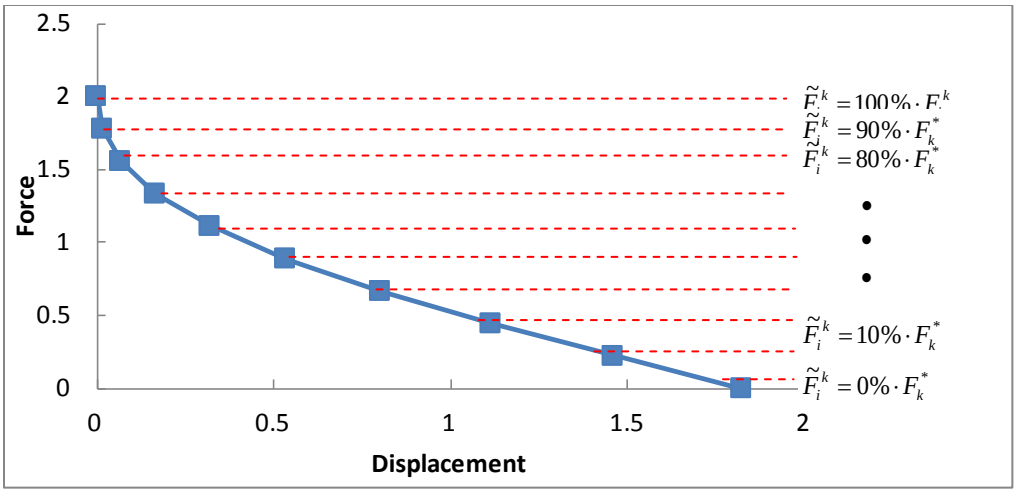

Figure 4-2 Force-displacement curve of a nodal point during releasing process.

In 3D, the connection force can be expressed as

$$\mathbf{f}_t^k = \frac{N-n}{N}\left|\mathbf{f}_{t_o}^k\right| \cdot \frac{\mathbf{f}_t^k}{\left|\mathbf{f}_t^k\right|} \tag{4.13}$$

$$\mathbf{f}_t^k = \left(1 - \frac{t-t_o}{N\Delta t}\right)\left|\mathbf{f}_{t_o}^k\right| \cdot \frac{\mathbf{f}_t^k}{\left|\mathbf{f}_t^k\right|} \tag{4.14}$$

Where t is the current time step, t_o is the crack opening time (the last moment of a rigid connection pair right before failure), Δt is the time step. N stands for the total time steps for the connection (spot-weld) force to be released to zero. $\mathbf{f}_t^k$ is the force vector acting on the k-th node at current time step t, $\mathbf{f}_{t_o}^k$ is the force vector acting on the k-th node at failure time. Notice that the magnitude of connection force at a particular time is scaled down with respect to the force at the crack opening time. But the direction of the connection force at a particular time is calculated from the connection force of current time. This

treatment allows the connection force always points toward the releasing node at any moment, as shown in Figure 4-3. A prescribed failing sequence determines the order of failure procedure. After one pair of node is fully released, the next pair starts to release.

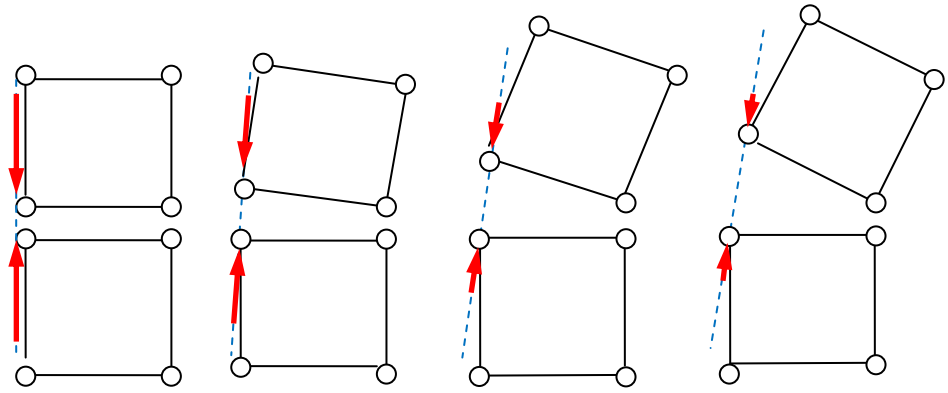

Figure 4-3 Node releasing procedure ensures the constraint force between the node pair is always point towards each other

4.3 Energy Release Rate Calculated by Virtual Crack Opening Method

Classical fracture mechanics define the energy release rate as the total mechanical energy decrease during unit crack advance [1][2]. This definition is easy to understand when the crack is actually extending. The total energy before crack extension subtract the total energy after crack extension is the energy difference, which can be divided by new crack surface to calculate energy release rate. As shown in Figure 4-4, the shaded area underneath the force-displacement curve divided by the extension of crack length yields the energy release rate.

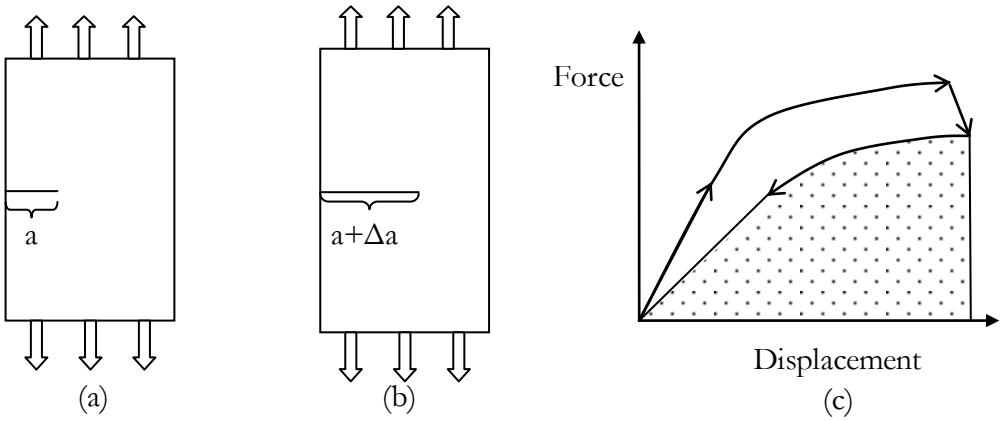

Figure 4-4 Conventional Energy Release Rate Calculation (a) Initial Fracture Specimen (b) Final Fracture Specimen (c) The Shaded Area of Force Displacement Curve is the Energy Reduced Due to Fracture.

When the specimen undergoes a loading that is smaller than the maximum loading the structure can withstand, the crack remains stationary and the energy release rate cannot be applied directly because no potential energy is actually decreased. Traditionally, J-integral is utilized to calculate energy release rate of such case. J-integral measures the flow of strain energy across a fixed border around the crack tip. It can be proved that the J-integral is path independent in LEFM (Rice 1968).

Recall that the traditional method of calculating energy release rate is J-integral

$$J = \int_{\Gamma} \left(W dy - T_i \frac{\partial u_i}{\partial x} d\Gamma \right) \tag{4.15}$$

For linear elastic fracture mechanics

$$J = G \tag{4.16}$$

Here we define energy release as such : The total energy would be released if the crack propagates at current stage. For example, a static crack undergoes a small loading under

which condition the crack is stationary. Now we use a scissors to artificially cut open that crack and measure the energy released during the process. The potential energy decrease over new crack surface area during cut-open process is equal to energy release rate. In finite element analysis, the energy release rate can be defined as the energy reduced during the node release process.

$$G = -\frac{dE}{dl} = -\frac{\Delta E}{\Delta L} \tag{4.17}$$

$$G = \frac{1}{\Delta a \cdot d} \sum_{n=1}^{n=N} \frac{1}{2} \left[f_j(n-1) + f_j(n) \right] \cdot \left[u_j(n-1) - u_j(n) \right] \tag{4.18}$$

$$f_j(n) = \frac{N-n}{N} F_j \tag{4.19}$$

where $f_j(n)$ is the connection force of the $n-th$ releasing steps; N is the total steps for the force released to zero. It has concluded by Sun (Sun 2002) that the choice of virtual crack advance distance ΔL does not influence the energy release rate calculation as long as the steps of releasing process $N \geq 50$. We presents a verification case in example 3. The energy release rate calculated with analytically LEFM solution is compared with energy release rate calculated from node releasing method (cf. eqs. (4.18)). The result shows less than 0.5% error. The example validates that the definition in eqs. (4.17) and (4.18) yields the same result as the energy release rate calculated with LEFM and J-integral in small strain static case.

4.4 Crack Speed Control

Crack speed is an essential part of energy release based fracture mechanics simulation.

Crack speed can be calculated as

$$v = \frac{\Delta a}{N \cdot \Delta t} \tag{4.20}$$

where Δt is the time step interval; Δa stands for crack advance distance for releasing a paired node; d is the specimen thickness. It simply means the crack takes N time steps to propagate through a distance of Δa, therefore the connection force is released to zero in N time steps.

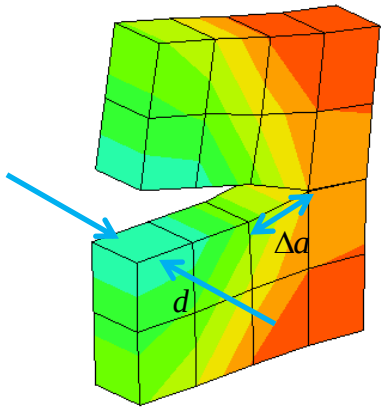

Figure 4-5 Finite Element Model for nodal releasing method

At the very beginning of fracture, crack speed is very slow. This can be achieved by setting N to a large number representing a very slow crack speed. During crack propagation, N is fixed for simplicity, Δt is modified to control the crack speed. Notice that Δt cannot be bigger than the critical time step required by central different method. Freund has introduce a simple relation predicting the dynamic energy release rate

$$G = G_o(1 - v / v_R) \tag{4.21}$$

where G is the dynamic energy release rate; G_o is the static energy release rate.

A constant crack speed simulation in example 5 also indicates that

$$G \propto 1/v_R \tag{4.22}$$

We verified eq. (4.21) numerically in example 5. It is noted that the relationship between static and dynamic energy release rates indeed obey the linear relationship suggested by Freund in the case of fixed grip boundary condition.

4.5 Energy Release Rate Fracture Criterion

Energy release rate fracture criterion is summarized as such: crack will extend if energy release rate equal to the critical energy release rate; crack will be stationary if energy release rate smaller than critical energy release rate. Energy release rate will never exceed critical energy release rate, i.e.

$$\begin{cases} G < G_{cr} & \text{Crack is Stationary} \\ G = G_{cr} & \text{Crack Extend} \\ G > G_{cr} & \text{Impossible} \end{cases}$$

Notice this criterion is different from classical definition: Crack will extend when the energy release rate is equal to or greater than the critical value, which can be expressed as

$$\begin{cases} G < G_{cr} & \text{Crack is Stationary} \\ G \geq G_{cr} & \text{Crack Extend} \end{cases}$$

The difference lays at whether energy release rate is able to exceed the critical value. In previous chapter, interatomic and strain energy are proved to be equivalent. It has been analyzed that the energy release rate is the decrease of interatomic potential divided by the

atomistic bond density. For crack advances one atom forward, critical energy release rate stands for the maximum interatomic potential energy stored at the bond, the interatomic potential energy of the bond during tensile loading cannot surplus the maximum interatomic potential at lattice constant. It is reasonable to assume that the energy release rate equals to critical energy release rate during crack extension procedure. Recall that

$$v = \frac{\Delta a}{N \cdot \Delta t} \tag{4.23}$$

One may adjust the time step Δt and release steps N to adjust crack speed v which influences the energy release rate

$$G = G(v) \tag{4.24}$$

Energy release rate G is monotonically decreasing with respect to crack speed v. One may adjust the crack speed such that the corresponding energy release rate of such speed always equals to the critical energy release rate. For crack initiation, it is suggested that the crack start to extend in a very slow speed. The time step Δt cannot be set to a very large number due to the stability of central different method. Therefore Δt is kept as a constant and N is set to be a large number. For example, in the numerical example 3, N=150 represents a crack speed of 3% of the shear wave speed.

A trial releasing process is utilized to determine whether the crack starts to extend at current load. The flow chart is shown in Figure 4-6. The program saves a copy of all variables at every time step. The crack is assumed to be initiating at current stage and the corresponding energy release rate is calculate. If the energy release rate calculated equals to critical value, the assumption is correct and the crack indeed opens. The program proceeds to next time step. If energy release rate is smaller than the critical energy release

rate, the assumption is wrong and the crack is stationary. All saved variables are retrieved and the current time step is run again with rigid connection.

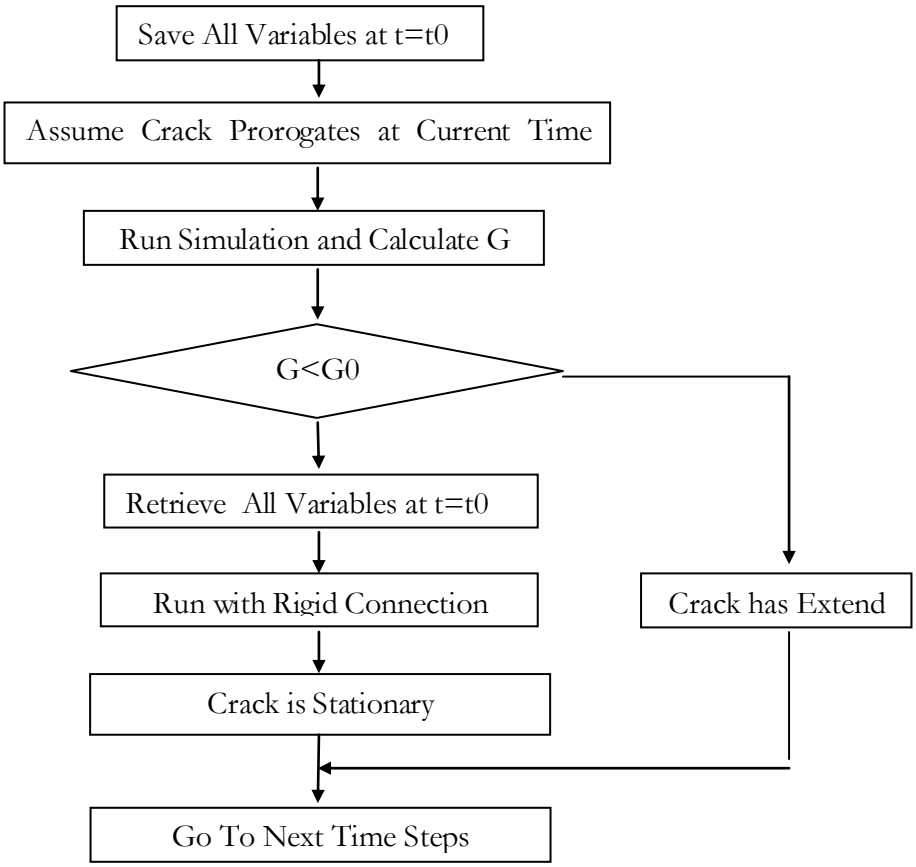

Figure 4-6 Flow Chart of Crack Initiation Judgment

During crack propagation, N is set to be a fixed number for simplicity. Therefore the effort lays at finding the right time step value enables the energy release rate equals to the critical value, i.e.

$$G_{cr} = G(\Delta t) \tag{4.25}$$

To facilitate this algorithm, an iterative process is performed to adjust the time step such that the energy release rate always equal to the critical value. At first guess, the time step T1 is set to a large enough value to represent a slow crack growth. The calculated energy release rate G1 is recorded. At second guess, the time step T2 is set to be a very small number to represents a very fast crack growth. The energy release rate G2 is recorded. Now if we assume the relationship between energy release rate and time step is linear, the candidate time step

$$T3 = T1 - (T1 - T2)(G1 - G0)/(G1 - G2) \tag{4.26}$$

where $G0$ stands for the critical energy release rate.

If the energy release rate of T3, G3>G0,then let T1=T3, otherwise let T2=T3. After less than 7 iterations, the time step value that enable G=G0 will be achieved with little error. The flow chart are presented in Figure 4-7

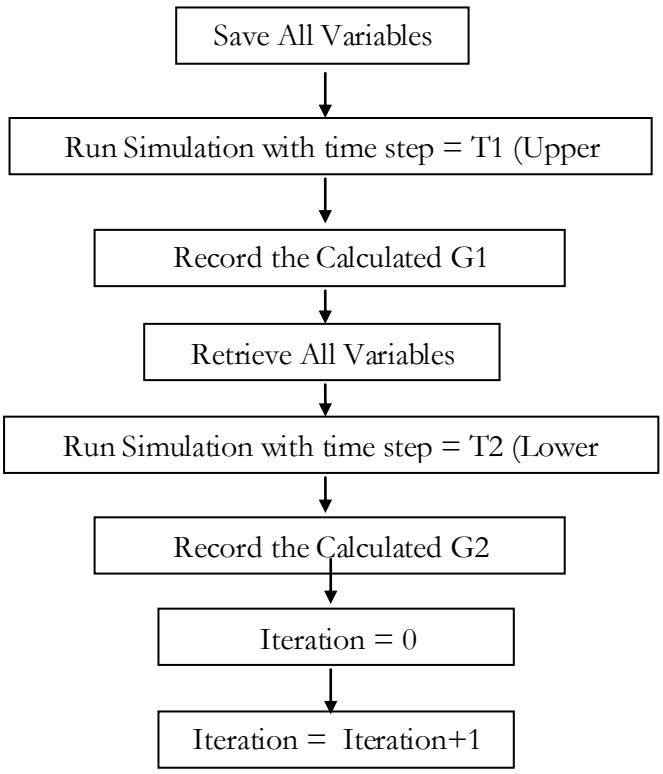

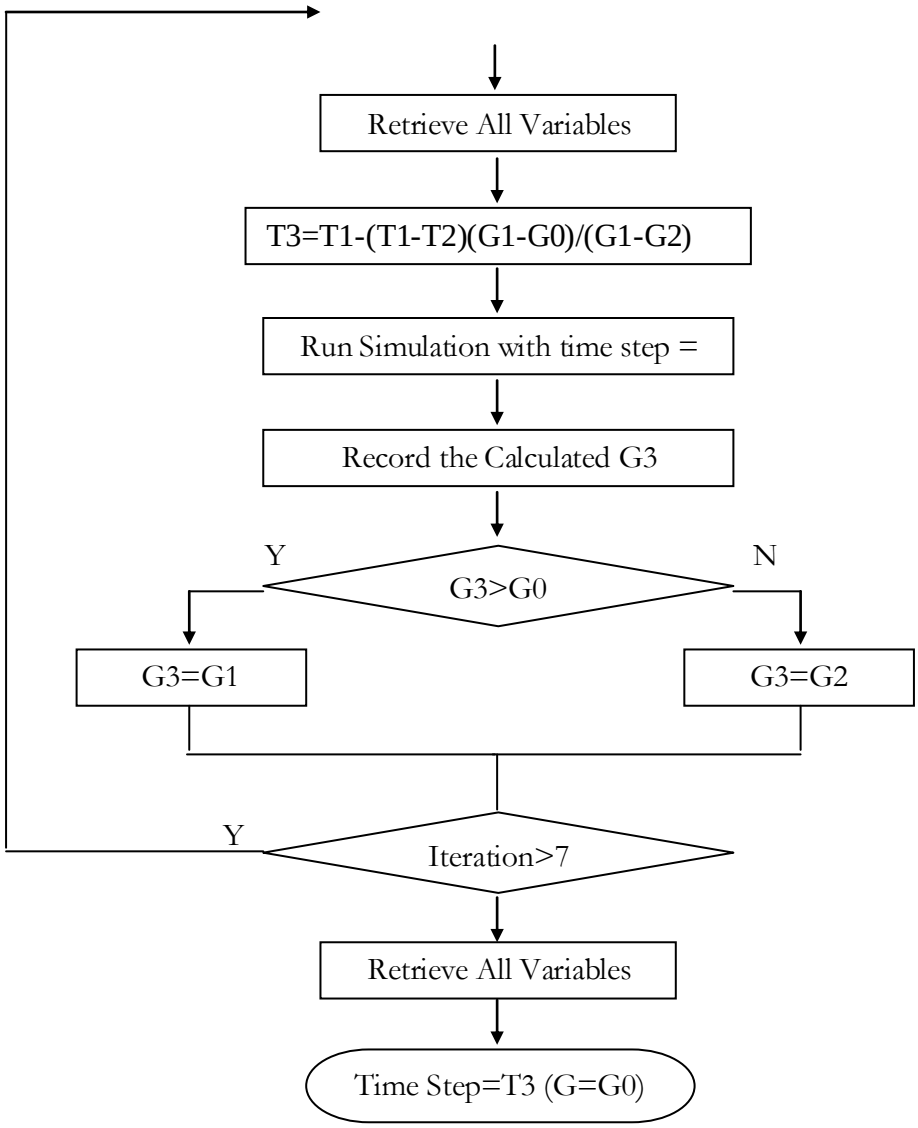

Figure 4-7 Flow Chart of Energy Release Rate Control

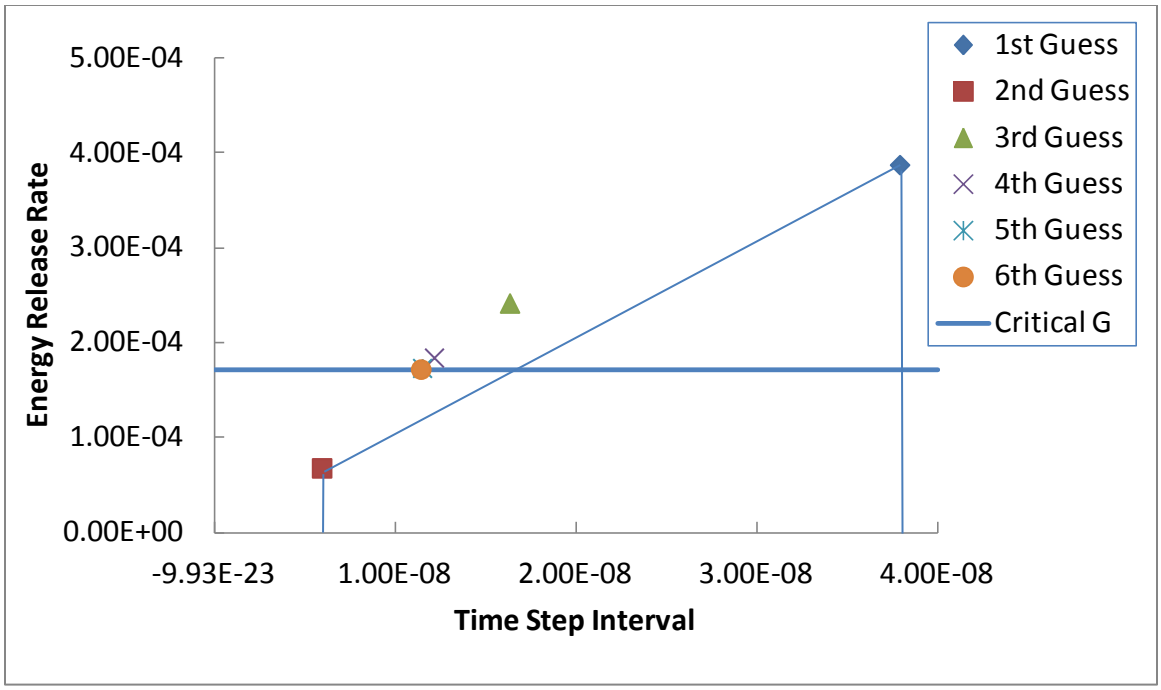

Figure 4-8 Iterative process to adjusts time step such that energy release rate reaches critical energy release rate.

This process utilized the observation in previous section: energy release rate is monotonically decreasing with respect to increasing crack speed.

4.6 Iterative meshing to determine the crack propagation direction

Crack propagation direction is critical to simulate mixed mode condition. Here a simple criterion is utilized. *Crack propagates at the direction perpendicular to the connection force*. This criterion is based on maximum force fracture criterion. The iterative meshing method is described as such. Connection force between the first paired node is calculated and the node of the second connection is moved to the perpendicular direction of the

connection force of the first pair. Then the simulation start all over again from t=0 and the second nodal pair position is adjusted again according to the new mesh. After several iteration, the second node position is close enough to the perpendicular direction of the nodal release force. Then the position of second node is considered final and the simulation move on to find the position of the third node pair. This process will continue until the positions of all paired nodes are adjusted. The final mesh will ensure that crack surface always lays at the perpendicular direction of the connection force of each pair. It can be seen from the simulation, plasticity effect plays a role in determine crack propagation direction. In another word, if plastic effect is neglected in the simulation, the crack propagation direction predicted will not be correct. The result is presented in example 8.

Examples for node releasing method

Example 1: Verification of rigid connection

If the rigid connection is indeed rigid, then the finite element model with the rigid connection will yields the same result as the model without such connection. Here a mode I tension case is modeled with finite element method with (Figure 4-9 right) and without (Figure 4-9 left) rigid connection. The model with rigid connection on the right figure prescribed double nodes to the left of the crack tip all the way through the specimen where the potential crack would be. Von-Misses stress contour is compared and the results shows no difference in both the contour shape and the sampling point (marked with a "+"

sign on the contour) value. This is an advantage compare to the cohesive zone element method, which would require the connection to be elastic and cause the structural to be weaker before the crack extends.

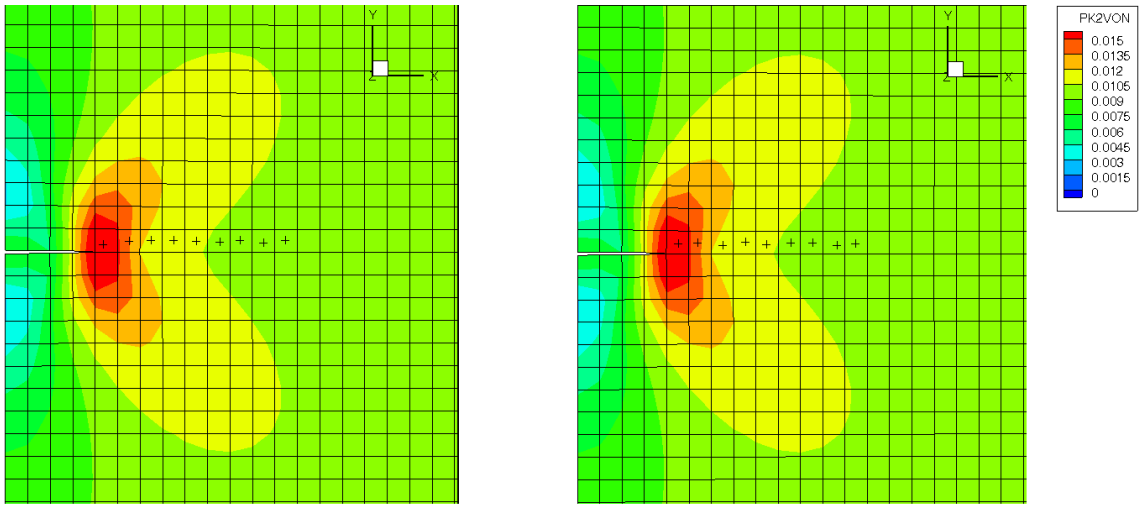

Figure 4-9 Left: Line crack specimen modeled with ordinary FEM Right: Line Crack Specimen modeled with Rigid Spot-weld Connection

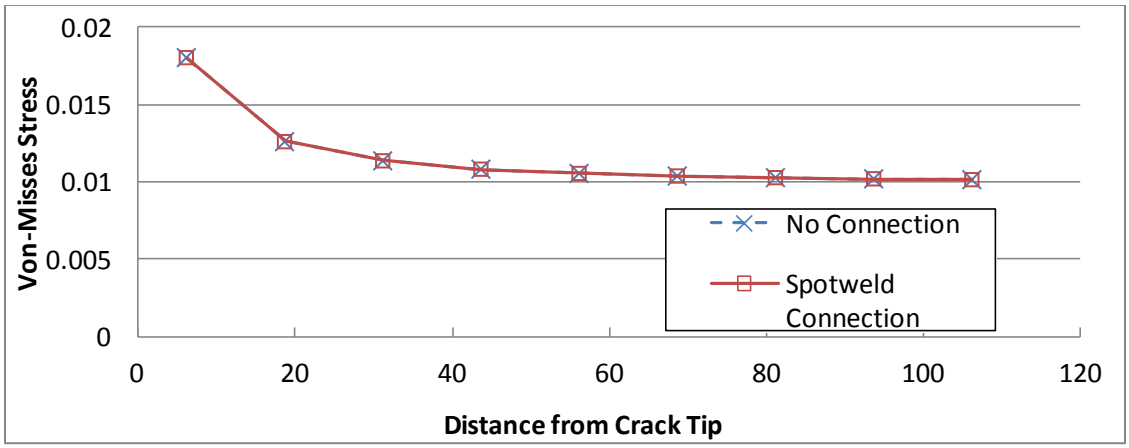

Figure 4-10 Displacement vs. Stress Comparisons with and without Spot-weld Connected

Example 2. Node Connection Force-Displacement Relation.

In this method, the connection force-displacement relation is an output rather than the input parameter. The force of releasing connection is linearly scaled down from rigid connection force. The displacement is calculated by considering force as a boundary condition and solve for the governing equation. If such method is valid, the force-displacement history should be independent of time step interval given the same crack speed. In other word, we have to verify that the N does not influence the shape of the force displacement curve given the same crack velocity.

The simulation with identical crack speed is compared in figure 1. The first simulation utilize a time step interval Δt and N steps. The second simulation utilize time step $\Delta t / 2$ and a 2N steps. The force-displacement curves are identical in these two cases, which indicates that releasing step N has no influence on the force-displacement curve given the same crack speed.

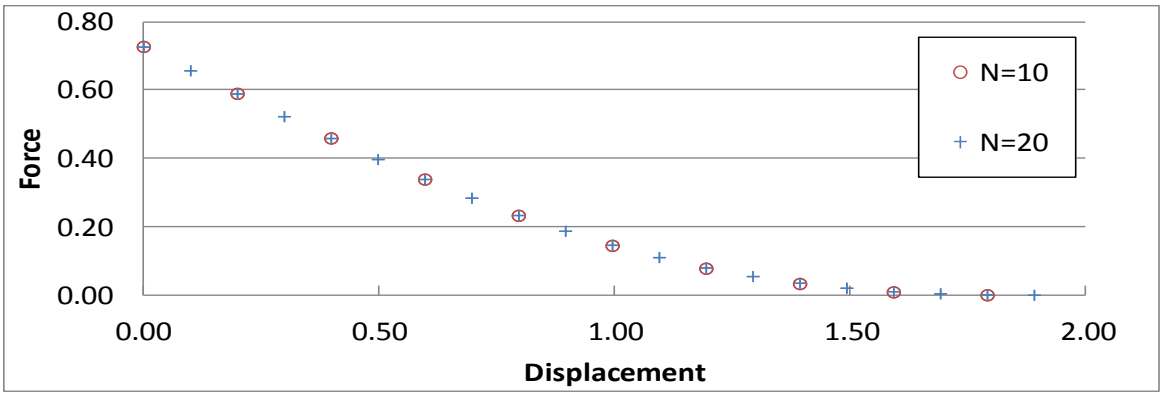

Figure 4-11 Force displacement curve of different time step of the same crack speed.

To discuss the influence of crack speed to the force-displacement curve. Identical numerical models with different crack speed is simulated. It can be seen from Figure 4-12 that the crack speed influence the force-displacement relationship greatly. It can be seen that the force-displacement holds a linear relationship when crack speed is very slow. As the crack speed goes higher, the force-displacement is no longer a linear relation. In many fracture mechanics methods, the connection force and nodal separation displacement relationship is a single function regardless of crack speed. This approximation will limit to the case in which crack speed is constant.

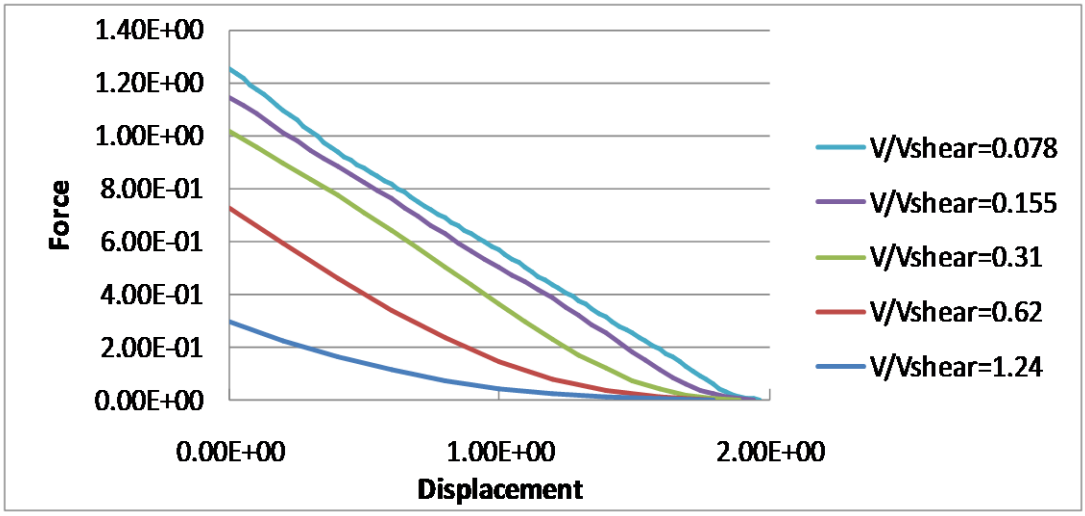

Figure 4-12 Force displacement relation of releasing nodes with respect to different crack speed. The relationship is linear only when crack speed is very low

Example 3 Verification of Energy Release Rate Calculation and Crack Initiation Speed.

This method calculates the energy release rate by an unconventional method. First, it assume that static energy release rate equals to dynamic energy release rate of a very low

velocity. Second, the energy release rate is calculated as the energy would be released per unit of new crack surface if the crack starts to propagates now at a certain speed.

Now the question is: Would this new method of calculating static energy release rate be identical to the energy release rate calculated by J-integral in LEFM? In principle, the answer is yes. Because J-integral calculates the amount of energy flow into a fixed boundary, while our method calculate energy acquired by the released nodes. From simulation point of view, these two quantities are the same thing. If the answer is yes, it is verified that

1. Energy release rate definition by virtual opening method is correct.
2. Node releasing method is correct.
3. Energy release rate calculated from node releasing method is correct.
4. Crack starts to extend in a very slow speed.

A numerical example is shown here to prove these points.

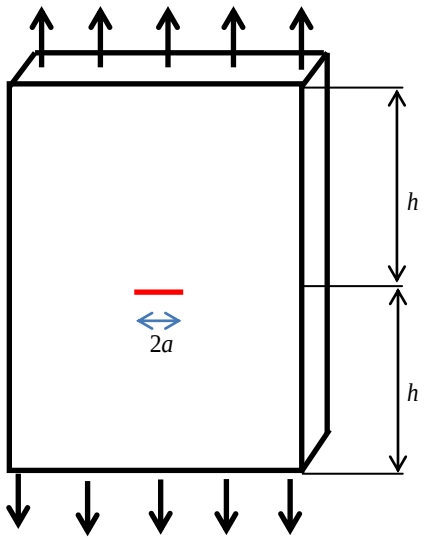

Figure 4-13 Specimen Configuration for verify the energy release rate defined by the virtual opening method.

A LEFM analytical solution with respect to a special dimension is acquired through handbook (Tada, Paris et al. 2000). With $a/b=0.1$ and $h/b=1.5$, $\frac{K_1}{\sigma\sqrt{\pi a}}=1.006$. If we adopt a dimension $a=50$, $b=500$, $h=500$, $E=1$, $\rho=4$, $\sigma=0.01$, $A=12500$. The analytical energy release rate from the handbook

$$G_{LEFM}=\frac{K_I^2}{E}=0.0159 \tag{4.27}$$

The analytical result is a static result, which can be interpreted as the test done under a very slow crack speed. In this simulation, it is assumed that the crack starts to prorogates at a very slow speed. N is set to 150 to represents the spot-weld connection is release to zero force in 150 time steps. This yields the crack speed about 4% of the shear wave speed.

$$v=\frac{\Delta a}{N\cdot\Delta t}=0.0413v_s \tag{4.28}$$

A mode I simple tension test of the exact dimension is simulated with large strain finite element code by using node releasing method. A uniform tensile stress of 0.01 is applied on the y direction(Figure 4-14 (a), (b)). After some time, damping is applied to damp out the remaining kinetic energy (Figure 4-14 (c)(d)). After the equilibrium is achieved, the damping is removed and the crack is manually triggered with the crack speed equals to 4% of the shear wave speed. The crack only advance for one element (Figure 4-14 (e)) and the energy release rate is calculated by the above described method. The force-displacement history of the first pair of spot-weld is given in Figure 4-15 Notice that the force-displacement curve is almost a linear relation. However this linear relation is a simulation

result, not an input. In general, crack speed influences the shape of force-displacement curve. This will be elaborated in the coming section.

$$G = \frac{1.2348089 + 1.2348089}{12.5 \times 12.5} = 0.0158 \tag{4.29}$$

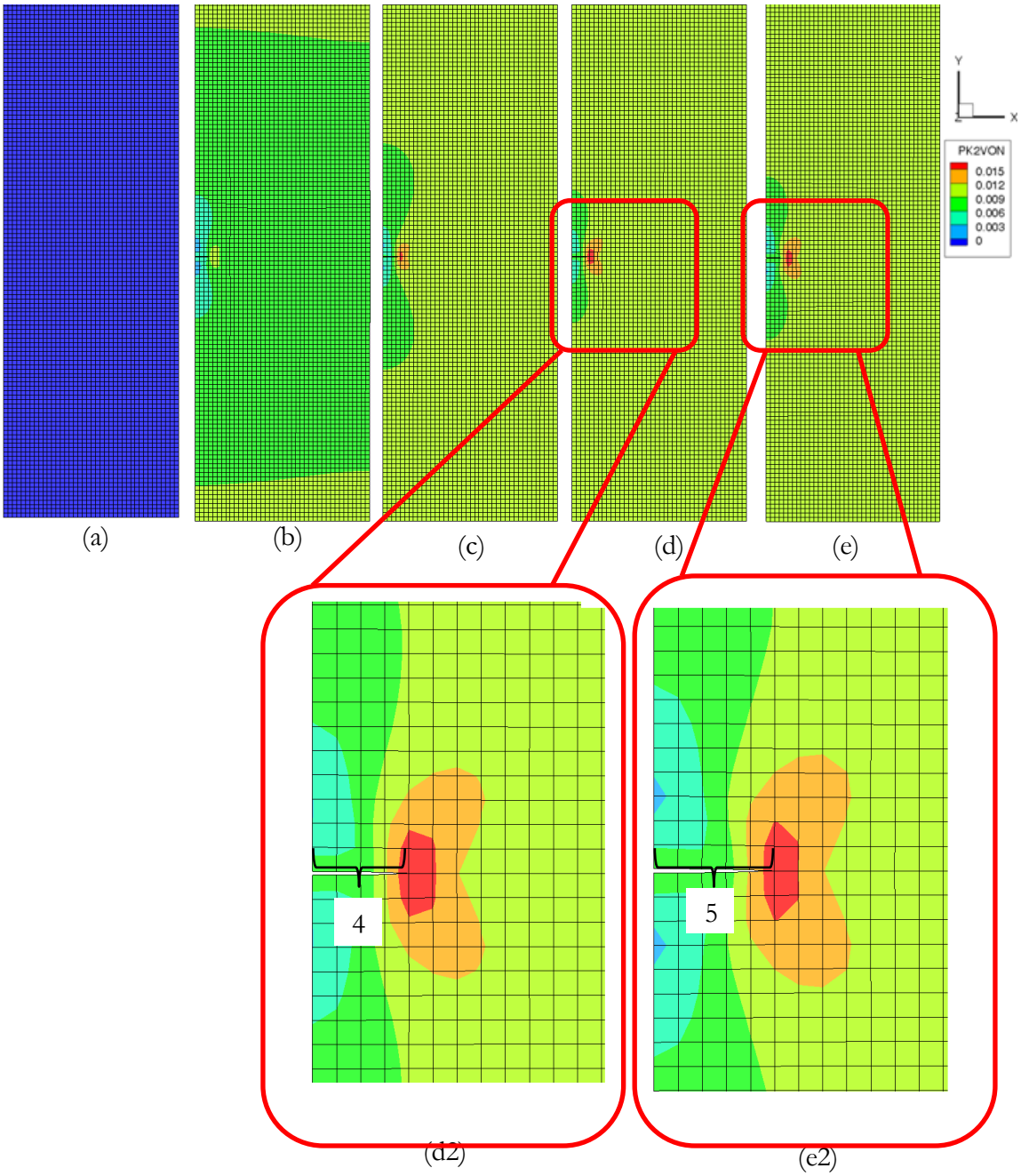

Figure 4-14 FEM Simulation with Node Releasing Method. (a) Initial Stress Free Stage (b) Tensile Loading Applied (c) Grip Fixed (d) Damping is applied until kinetic energy damped out then damping is removed (e) Crack advance one element forward with a very low crack speed.

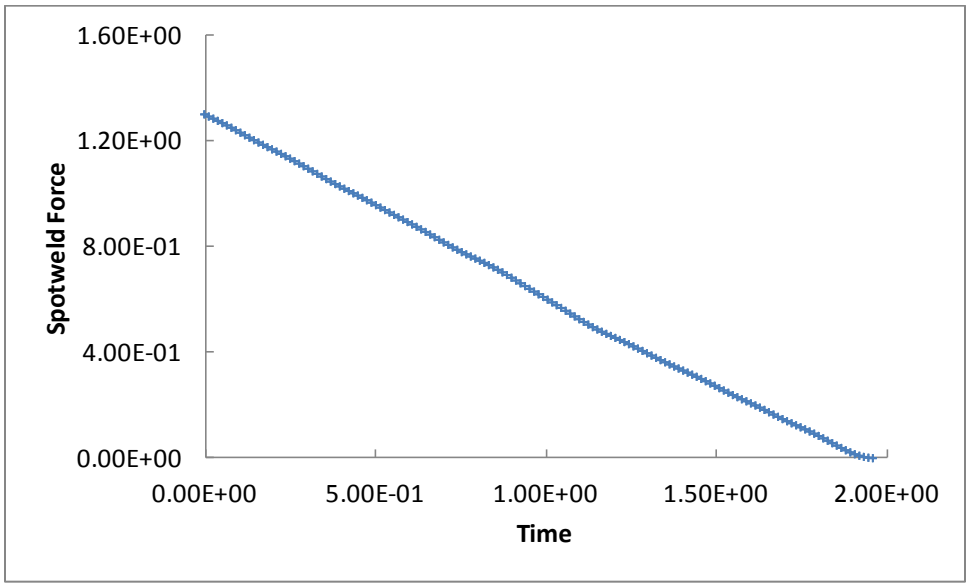

Figure 4-15 Force Displacement Curve of Connection Force Releasing History

The difference between the handbook-calculated value and our simulation result is less than 0.6%. This result verified that: The energy release rate definition in eq. (4.17) is correct. Crack begins to extend at a very low speed. Static energy release rate equals to dynamic energy release rate at low speed.

For the sake of discussion, let us assume the crack starts to extend at a high speed say 41.3% of shear wave speed and calculate energy release rate of such condition. The force-

displacement relation is shown in Figure 4-16. The energy release rate $G = \frac{0.44789037 + 0.44789037}{12.5 \times 12.5} = 0.005733$. The analytical formula of LEFM gives G=0.0158970243. We can see the error is 64%, which indicates the assumption that the crack starts to extend at a high speed is erroneous.

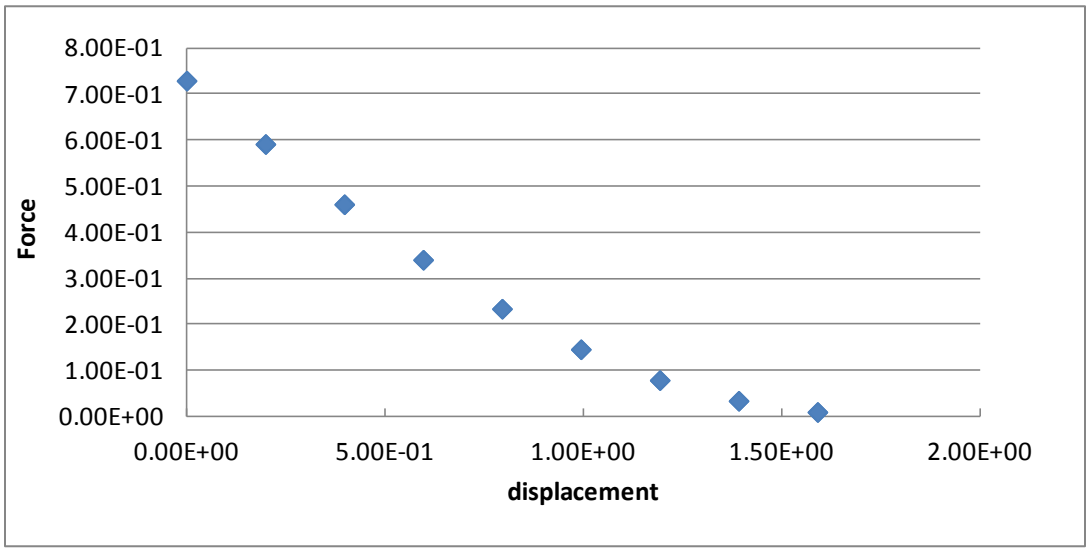

Figure 4-16 Force-Displacement curve of node releasing process at constant crack speed of 41.3% Rayleigh Wave Speed

Example 4 Calculating fracture toughness G from Simple Tension Test Data

Traditional fracture mechanics parameters, such as stress intensity factor, J-integral, Crack tip opening displacement, crack tip opening angle etc., have to be acquired by special fracture mechanics test. The question is: Is it possible, at least for some brittle material,

that the fracture toughness can be acquired from a stress-strain relation? In principle, the answer should be yes. Because the end point of stress-strain curve serves as a indicator of material failure, and the fracture mechanics parameter is also a indicator of material failure. One material could not have two independent failure parameters that both govern the failure. Therefore , a conversion between these two parameters must exist. Notice that the nodal force releasing method requires no initial crack to calculate energy release rate. A simulation of a simple tension test with this method will serve as a bridge to connect fracture parameters with failure criterion.

Cast iron is picked as the material for study, Because it is a brittle material with percentage of elongation $\leq 0.8\%$. The failure surface of the simple tension specimen indicates that the material indeed fails at brittle fracture (cf. Figure 4-17)(Davis 1996).

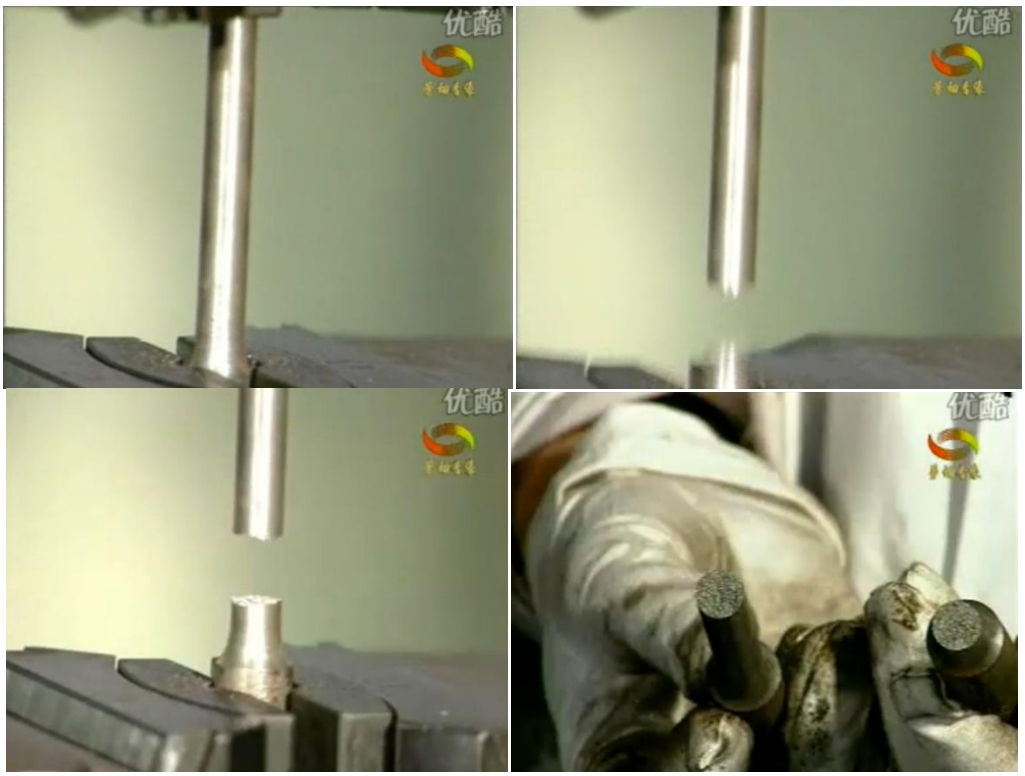

Figure 4-17 Cast Iron Simple Tension Specimen(Unknown)

The hand book gives the stress-strain relation for class 40 cast iron as shown in Figure 4-18. The elastic region is linearized to give a Young's module $E = 138GPa$ and Poisson's Ratio $\nu = 0.3$ and the strain of failure $\varepsilon_f = 0.07$ (cf. Figure 4-18 (a))

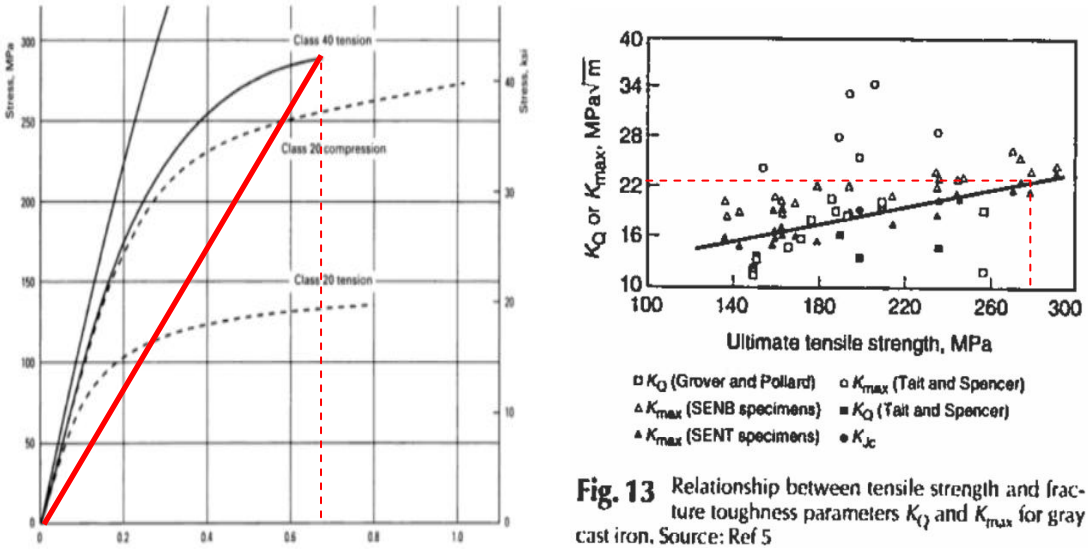

Fig. 13 Relationship between tensile strength and fracture toughness parameters K_Q and K_{max} for gray cast iron. Source: Ref 5

(a) (b)

Figure 4-18 (a) Class 40 Cast Iron Tensile Test Data. (b) Class 40 Cast Iron Fracture Toughness Test Data (Davis 1996)

With the similar procedure as mentioned in the previous example. The specimen is loaded to 0.007 strain and artificial damping is used to damp out the kinetic energy. After all dynamic motion is damped out, the damping is removed and crack opening is artificially triggered. The crack is allowed to advance for one element and the energy release rate G is calculated. By utilizing the LEFM relation $K = \sqrt{GE}$ (Sun, Jin et al. 2012), stress intensity factor can be calculated as $K_{IC} = 20.88MPa\sqrt{m}$. The handbook experimental value $K_{IC} \approx 22MPa\sqrt{m}$ as shown in Figure 4-18 (b). The error is within 5%. Therefore it

is possible to calculate fracture toughness parameter from simple tension test for brittle material. This result also verified that the node release method is adequate to model static crack problem by specifying a low crack speed.

Example 5 Constant Crack Speed Simulation

In reality, critical energy release rate is a material constant and crack speed changes over time. However the simulation of constant crack speed may better explain the relationship between crack speed and energy release rate. The simulation is conducted with a constant crack speed of approximately 60% of the Rayleigh wave speed (cf. Figure 4-19 (c)). Notice that the energy release rate increases with a fixed crack speed (cf. Figure 4-19 (b)). The connection force and the relative displacement between paired nodes is not a simple linear relations (cf. Figure 4-20).

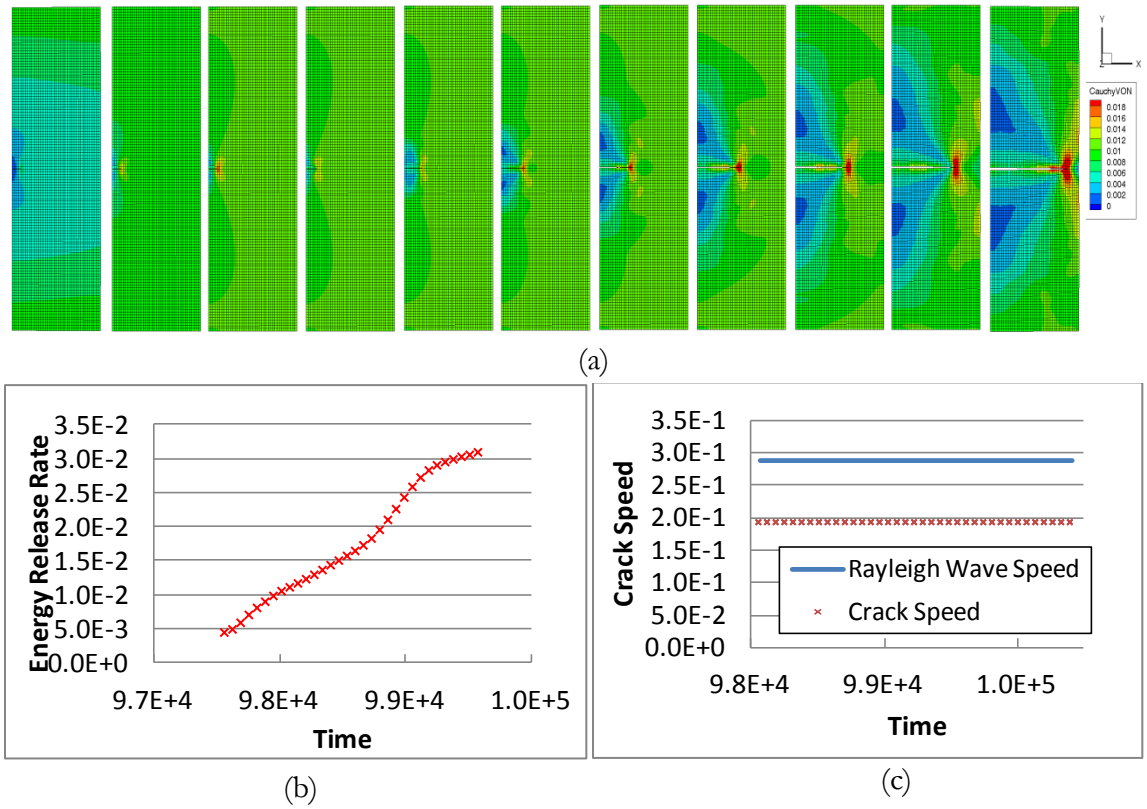

Figure 4-19 (a) Von-Mises Stress Contour of Crack Extension at Different Time (b)Energy Release Rate Time History. (c) Crack Speed Time history

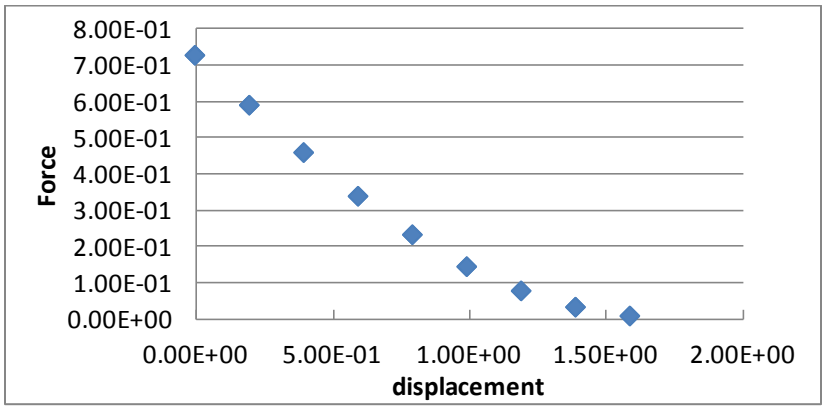

Figure 4-20 Connection Force and Relative Displacement between Paired Nodes During Node Releasing Process

Example 6 Crack Speed under Constant Energy Release Rate Criterion

We first provide a simple "back of the envelope" derivation from Freund's dynamic energy release rate formula $G = G_o(1 - v / v_R)$ and the constant energy release rate assumption. It is verified that these conditions leads to the conclusion that the crack speed goes monotonically to the Rayleigh wave speed. Freund (Freund 1990) derived energy release rate with respect to crack speed as

$$K\left(t,l,\dot{l}\right) = k\left(\dot{l}\right)K\left(t,l,0\right) \tag{4.30}$$

$$G = \frac{1-\upsilon^2}{E} A_I\left(\dot{l}\right)K_I\left(t,l,\dot{l}\right) \tag{4.31}$$

$$\frac{EG}{(1-\upsilon^2)K^2} = A_I\left(\dot{l}\right)k_I\left(t,l,\dot{l}\right) \approx 1 - \dot{l} / v_R \tag{4.32}$$

$$G\left(v\right) = G\big|_{v=0} \ \left(1 - \dot{l} / v_R\right) \tag{4.33}$$

where K is stress intensity factor, l is the crack length, G is energy release rate, v is the crack speed, v_R is the Rayleigh wave speed. Now, we derive the crack tip equation of motion based on his formula. If we adopt that $G = G_{cr} = constant$ at all times. We derive the equation of motion as such

$$G = \left(1 - \dot{a} / v_R\right)\frac{\sigma^2 \pi a}{E} \tag{4.34}$$

Because $G = G_{cr} = constant$ which means $\dot{G} = 0$

$$0 = \dot{G} = -\frac{\ddot{a}\sigma^2 \pi a}{v_R E} + \left(1 - \frac{\dot{a}}{v_R}\right)\left[\left(\frac{\sigma^2 \pi \dot{a}}{E}\right) + \frac{2\sigma\dot{\sigma}\pi a}{E}\right] \tag{4.35}$$

We assume fixed loading, i.e. $\dot{\sigma} = 0$

$$\frac{\ddot{a}\sigma^2\pi a}{v_R E} = \left(\frac{v_R - \dot{a}}{v_R}\right)\left(\frac{\sigma^2\pi\dot{a}}{E}\right) \tag{4.36}$$

$$\ddot{a} = \frac{(v_R - \dot{a})\dot{a}}{a} \tag{4.37}$$

Now we define

$$y_1 \equiv a, \quad y_2 \equiv \dot{a} \tag{4.38}$$

$$\begin{aligned} \dot{y}_1 &= y_2 \\ \dot{y}_2 &= \frac{(v_R - y_2)y_2}{y_1} \end{aligned} \tag{4.39}$$

We assume crack extend from a very low speed; let $y_2 = 10^{-2}$ as the initial condition. Numerical result of this equation is shown in Figure 4-21. We notice that the crack speed gradually picked up as the crack starts to extend. The crack speed asymptotically approaches the Rayleigh wave speed as crack propagates. The crack tip acceleration has a peak at around 0.4 times Rayleigh wave speed.

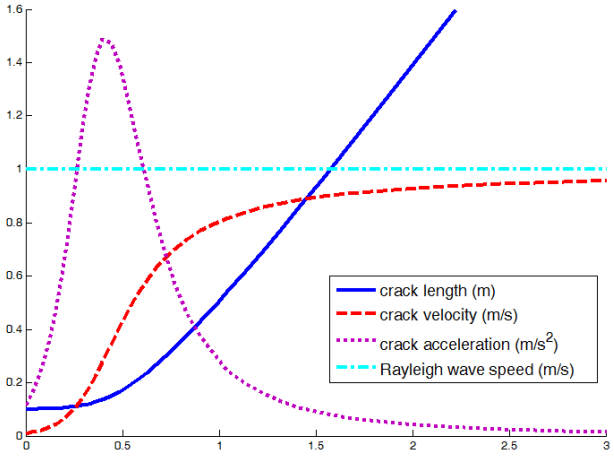

Figure 4-21 Crack tip displacement, velocity and acceleration according to $G = G_o(1 - v/v_R)$ and $G = const.$

This result graphically verified the crack speed will monotonically goes to Rayleigh wave speed as the crack propagates. To test this conclusion in a finite element simulation, a simple tension case with fixed grip boundary condition is simulated with node releasing method. Notice that Freund derived his dynamic fracture mechanics theory mostly based on steady state assumption, which means no external input of energy during fracture extension process. Therefore, fixed grip condition in the simulation is picked to satisfy this assumption. Unlike the analytical prediction, the simulation method only need constant energy release rate assumption. The relation between crack speed and energy release rate is an simulation output. The specimen is pulled to strain = 0.04 and then the boundary condition changed to a fixed grip boundary condition. The artificial damping is prescribed until all kinetic energy is damped out. After the model reaches steady state, the crack extension is triggered. Von Mises contour of this simulation is shown in Figure 4-23.

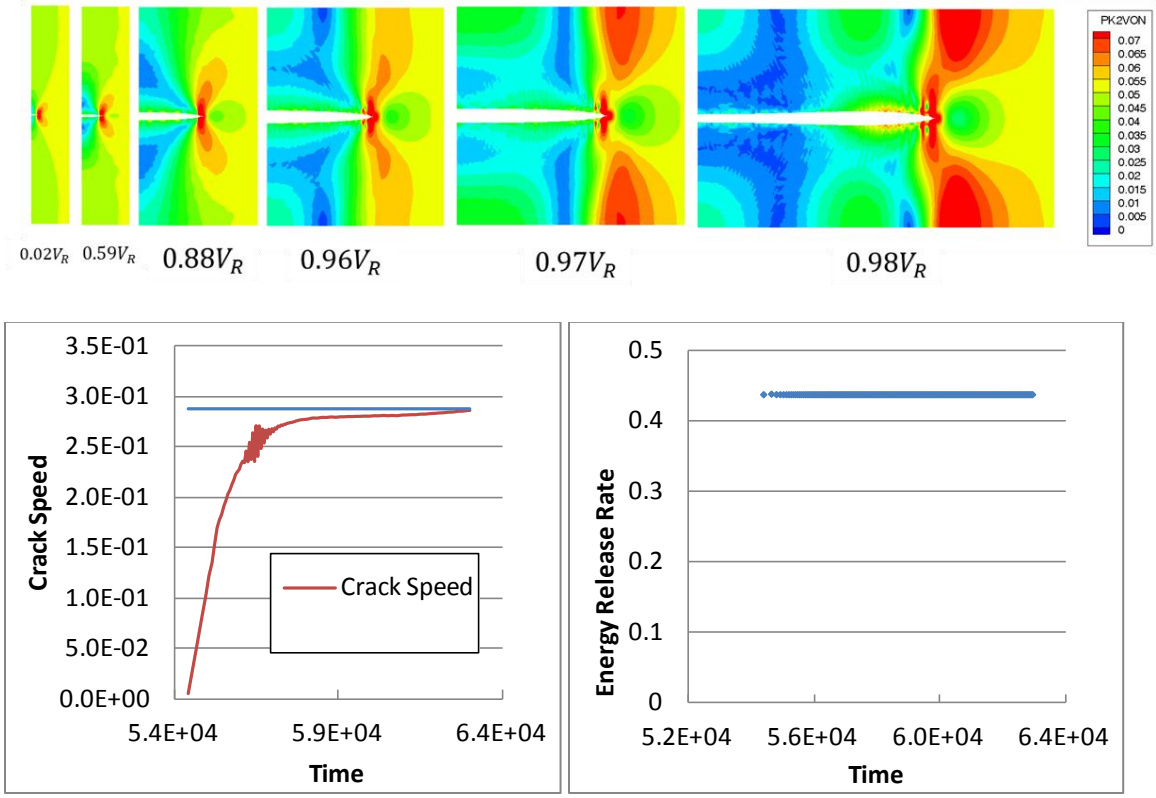

Figure 4-22 Top: Von-Mises Stress Contour and Crack Speed at Different Stage of Crack Extension Left: Crack Speed vs. Time Right: Energy Release Rate vs. Time.

It is observed that the crack speed asymptotically reaches Rayleigh wave speed in a constant grip condition. Let the static energy release rate G_o be calculated with LEFM formula, i.e.

$$G_o = \frac{\sigma^2 \pi a}{E} \tag{4.40}$$

with crack length a and applied loading σ. The crack speed can be normalized with Rayleigh wave speed and the energy release rate can be normalized with static energy

release rate. The result verified that the linear relationship $G = G_o(1 - v / v_R)$ predicted by Freund has a good agreement with simulation. Notice the prediction line at low crack speed deviates from the simulation. This is due to the pick of fixed grip boundary condition. To be precise, eq. (4.40) is only valid under fixed loading condition of infinite specimen.

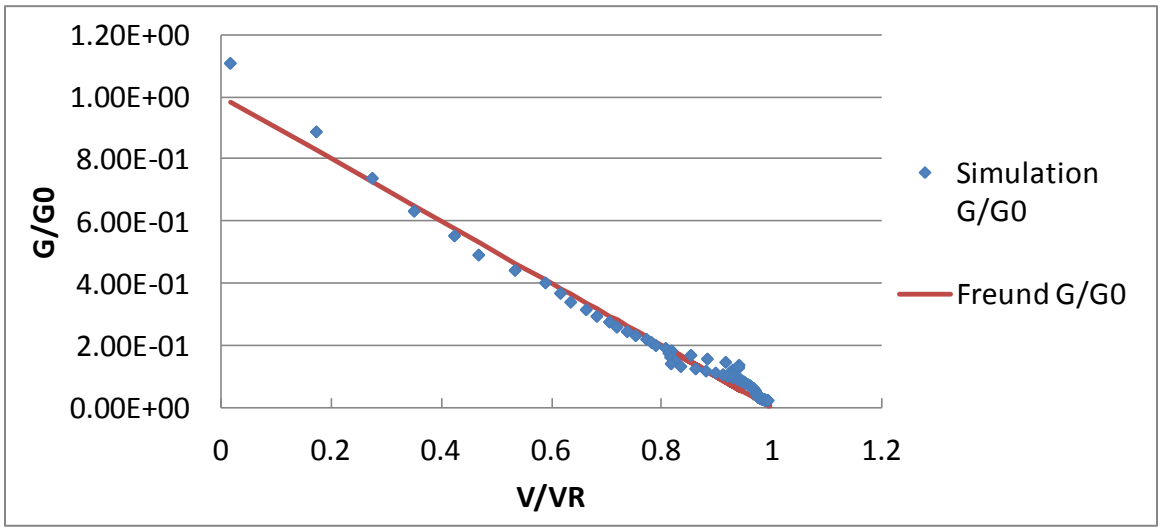

Figure 4-23 Normalized Energy Release Rate vs. Normalized Crack Speed

Example 7 Plasticity reduces crack speed.

Experimentally observed crack speed is much slower than the predicted speed limit, i.e., the Rayleigh wave speed. Here this phenomenon is reproduced when considering plasticity. Notice that most engineering materials have some plasticity. The influence of plasticity is discussed with FEM simulation with nodal force releasing method. The plasticity is modeled with return mapping algorithm, of which the parameters are shown in

Figure 4-24. It can be clearly seen that plasticity lowers the crack speed to 60% of the Rayleigh wave speed.

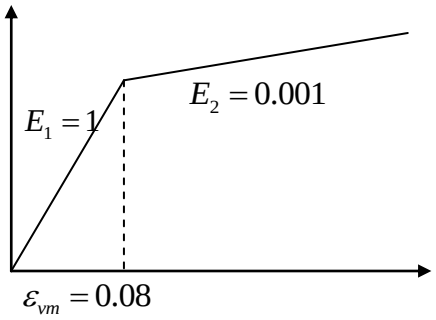

Figure 4-24 Elasto-Plastic Material Model

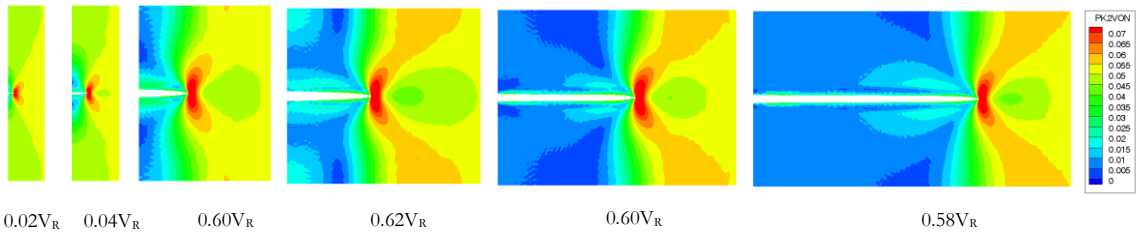

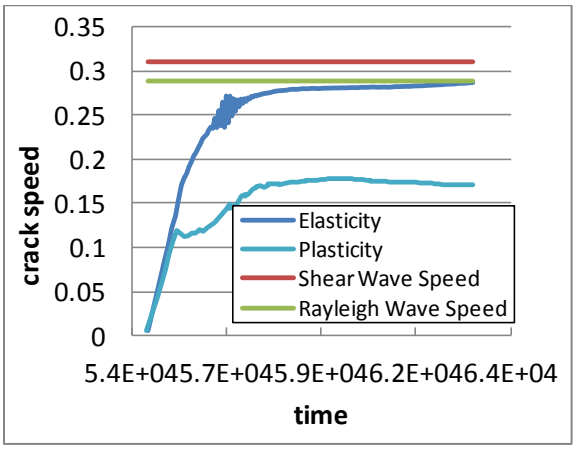

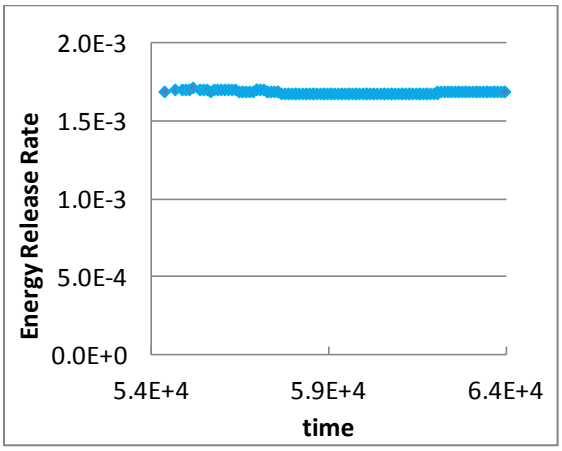

Figure 4-25 Top: Von-Mises Stress Contour and Crack Speed at Different Stage of Crack Extension. Left: Crack Speed vs. Time for Mode. Right: Energy Release Rate vs. Time (E=1, ε0=0.05, σvm=0.08, Fixed Grip Boundary Condition, Mode I Crack)

Example 8 Plasticity influenced crack propagation direction.

Mixed mode case is studied by crack opening method and iterative remeshing method. *The final mesh enables the crack surface to be perpendicular to the connection force.* A mixed mode case (Mode I /Mode II) is simulated with both elasticity and elasto-plasticity. The elastic material has a Young's modulus $E = 1$. The plastic material has a Young's modulus $E = 1$ and Von Mises Stress $\sigma_v = 0.0075$. The fixed grip boundary condition is applied on one end and the force boundary condition is applied on the other end with $\sigma_{ox} = 0.01,\ \sigma_{oy} = 0.01$. The force is of 45 degree to the horizontal direction.

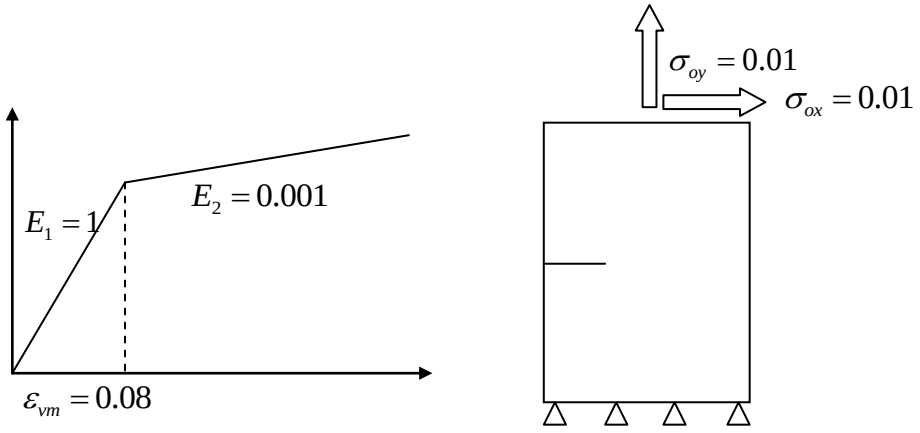

Figure 4-26 Left: Elasto-Plastic Material Model.

Right: Mixed Mode Loading Configuration

Notice that the elastic model and the elasto-plastic model predict different crack paths. Therefore plasticity is a factor must be considered in the simulation of mixed mode fracture.

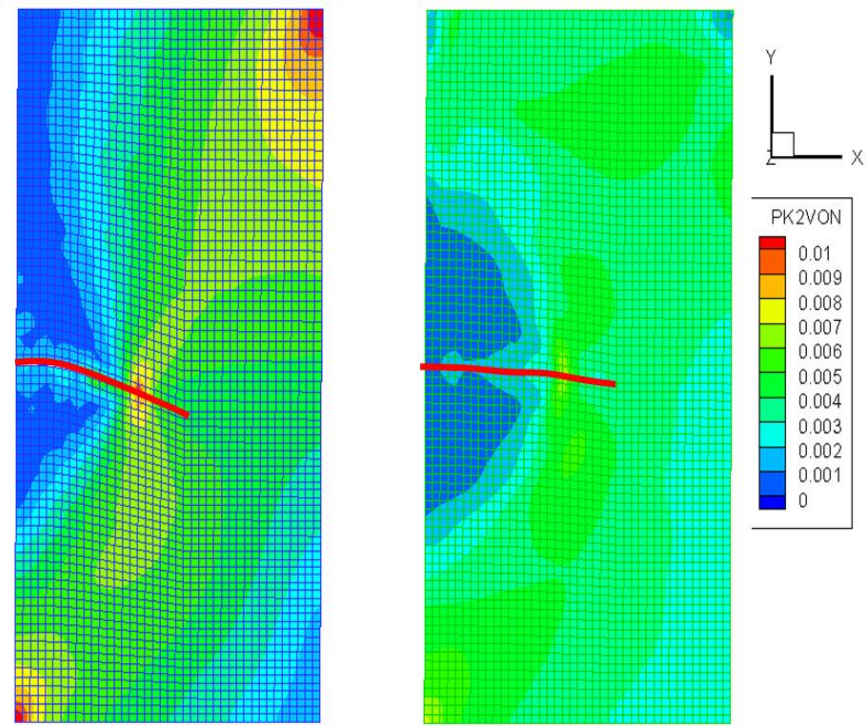

Figure 4-27 Left: Von-Mises Contour with Elastic Material Model. Right: Von-Mises Contour with Elasto-Plastic Material Model

Summary

In previous chapters, it is assumed that the critical energy release rate is a constant during the entire crack propagation process. It is noticed that *crack initiation is a special case of crack propagation with infinitesimal crack speed.* The direction of crack propagation is determined by an iterative routine that adjusts the mesh such that the crack path is

perpendicular to the connection force of the paired nodes. The constitutive theory of the material is formulated based on large-strain plasticity with return mapping algorithm. The small-strain elasticity is a special case of large-strain plasticity. Hence the numerical results can be verified with the result in linear elastic fracture mechanics. It is found that (1) the magnitude of crack tip stress decreases when large strain, instead of small strain, is considered; (2) node releasing method is adequate to determine the energy release rate of a specific geometry and loading configuration with high accuracy; (3) node releasing method enables one to simulate the fracture phenomenon with no initial crack—therefore ideally *a simple tension test is sufficient to determine the critical energy release rate of a material*; (4) crack speed asymptotically approaches to Rayleigh wave speed in case of elasticity, mode I, plain stress, and fixed grip; (5) crack speed asymptotically approaches to approximately half of Rayleigh wave speed if plasticity is considered; (6) plasticity affects the direction of crack propagation. node release method is introduced to model fracture mechanics with critical energy release rate as the sole criterion to determine the failure.

Examples are given to show such method is able to:

- Calculate force-displacement relation of connection force under different scenarios
- Calculate static energy release rate with great accuracy.
- Calculate critical energy release rate parameter from stress-strain relation
- Prove the crack speed monotonically approaches to Rayleigh wave speed.
- Demonstrate the plasticity effect reduces the ultimate crack speed to half

of the Rayleigh wave speed.

Chapter 5

Contribution and Future Work

This work consists the following contributions:

In chapter 1, we have proved that the deformed shape of a mode-I line crack is an ellipse. the deformed shape of an elliptical void is also an ellipse. The deformed shape of mixed mode line crack is not an ellipse. The small strain formulation overestimates the stress level at the crack tip. Stress intensity factor K or similar singular field method derived from LEFM is not appropriate to study fracture mechanics in large deformation or in close neighborhood of crack tip. Line crack solution contributes to the overestimation of crack tip stress.

In chapter 2. We modified the energy release rate failure criterion. It is proved by theory and simulation in molecular dynamics that the energy release rate does not equal to surface energy. The energy release rate is the decrease of potential energy of unit crack advance, the surface energy is the increase of potential energy of unit crack advance. It is also proved that the potential energy release rate is the kinetic and/or thermo energy generation rate in fixed grip condition; therefore the fracture problem is a dynamic problem in nature. Pure elastic fracture doesn't exist in nature, the brittle fracture in nature is still an irreversible process associated with plasticity in the form of lattice reorientation on the crack surface. It is first suggested that the energy release rate should be calculated in a proper region in order to represent a true fracture property. It is also suggested J-integral is path dependent. A general MD simulation method is introduced to calculate energy release rate in molecular dynamics.

In chapter 3, work conjugate stress and strain in molecular dynamics are derived. Such stress and strain are defined at each atom with stress taking summation and strain taking average of the influence from all other atoms. The conjugacy is proved to be valid for multi-atom, three-dimensional case of arbitrary atomic configuration at zero degree Kelvin. Therefore the strain energy of such stress-strain pairs are equivalent to the interatomic potential energy at all time. This work is the first to prove the conjugacy between stresses and strains in molecular dynamics.

In chapter 4 We systematically developed and verified the node release method in energy-release-rate based fracture simulation. We developed and verified the node releasing method, energy release rate calculation, crack speed control, energy release rate control, crack path prediction, etc. We also verified the updated energy-release-rate failure criterion as shown in chapter 2. There are new discoveries :

1) Cohesive law is crack speed dependent;
2) Static energy release rate equals to dynamic energy release rate in low crack speed;
3) Fracture toughness can be obtained by stress-strain curve
4) The linear relationship between static and dynamic energy release rate is numerically proved;
5) Crack speed monotonically approaches Rayleigh wave speed in elastic material. Crack speed only reaches to 60% of shear wave speed in elasto-plastic material;
6) Plasticity influences crack path.

Future works following this dissertation are listed as:

In chapter 2, the molecule dynamic simulation needs to be used to answer these question: Is energy release rate really a material constant? What is the mechanism for the strain energy to decrease with extending crack?

In chapter 3, work conjugate stress and strain with non-zero temperature needs to be studied.

In chapter 4, Node release method is limited to a single crack. Future research needs to generalize this method to multiple cracks with consideration of crack branching and merging.

Bibliography of Reference

BARVE, S., 1997. Are naked singularities forbidden by the second law of thermodynamics? *Modern physics letters A,* **12**(32), pp. 2415-2419.

BASINSKI, Z., 1971. Influence of shear stress on screw dislocations in a model sodium lattice. *Canadian Journal of Physics,* **49**(16), pp. 2160.

BOUCHBINDER, E., GOLDMAN, T. and FINEBERG, J., 2014. The dynamics of rapid fracture: instabilities, nonlinearities and length scales. *Reports on progress in physics. Physical Society (Great Britain),* **77**(4), pp. 046501-4885/77/4/046501. Epub 2014 Mar 19.

BOUCHBINDER, E., LIVNE, A. and FINEBERG, J., 2009. The 1/r singularity in weakly nonlinear fracture mechanics. *Journal of the Mechanics and Physics of Solids,* **57**(9), pp. 1568-1577.

BROWN, D.K., 1977. A computer program to calculate the elastic stress and displacement fields around an elliptical hole under any applied plane state of stress. *Computers & Structures,* **7**(4), pp. 571-580.

BUEHLER, M.J., 2006. Cracking and adhesion at small scales: atomistic and continuum studies of flaw tolerant nanostructures. *Modelling and Simulation in Materials Science and Engineering,* **14**(5), pp. 799-816.

C. E. INGLIS, 1913. Stresses in a Plate due to the Presence of Cracks and Sharp Corners. *Trans.Institute of Naval Architecture,* **55**, pp. 219-241.

CACERES-VALENCIA, G., 2004-last update, Engineering Materials for Electrical. Available: http://academic.uprm.edu/pcaceres/Courses/MatEng3045/EME8-2.pdf.

CHEN, Y., LEE, J.D. and ESKANDARIAN, A., 2006. *Meshless methods in solid mechanics.* New York, NY: Springer.

CHENG, S., 2014. Convergence of local atomistic stress based on periodic lattice. *International Journal of Solids and Structures,* **51**(10), pp. 2027-2035.

CHEUNG, K.S., 1991. Atomic-level stress in an inhomogeneous system. *Journal of Applied Physics,* **70**(10; 1), pp. 5688-5690.

CIMA, M.J., 2012-last update, 3.091x Introduction to Solid State Chemistry. Available: https://www.youtube.com/watch?v=9zm8G0_W_v8 [12, 2012].

CLAUSIUS, R., 1870. XVI. On a mechanical theorem applicable to heat. *Philosophical Magazine Series 4,* **40**(265), pp. 122-127.

CORMIER, J., 2001. Stress calculation in atomistic simulations of perfect and imperfect solids. *Journal of Applied Physics,* **89**(1), pp. 99-104.

DAVIES, P.I., 2003. A Schur-Parlett Algorithm for Computing Matrix Functions. *SIAM journal on matrix analysis and applications,* **25**(2), pp. 464-485.

DAVIS, J.R., 1996. *ASM specialty handbook: cast irons.* ASM international.

DONG, L. and ATLURI, S.N., 2013. Fracture & Fatigue Analyses: SGBEM-FEM or XFEM? Part 1: 2D Structures. *Computer modeling in engineering & sciences,* **90**(2), pp. 91-146.

DUFLOT, M., 2004. A meshless method with enriched weight functions for fatigue crack growth. *International Journal for Numerical Methods in Engineering,* **59**(14), pp. 1945-1961.

DUNN, M., 1994. The effects of crack face boundary conditions on the fracture mechanics of piezoelectric solids. *Engineering Fracture Mechanics,* **48**(1), pp. 25-39.

ERINGEN, A.C., 1989. *Mechanics of continua.* Malabar, Fla.: R.E. Krieger Pub. Co.

F., M. and W., K., 1980. *Fast fracture simulated by conventional finite elements: A comparison of two energy-release algorithms.* Philadelphia, PA, ETATS-UNIS: American Society for Testing and Materials.

FENLEY, A.T., 2014. Calculation and Visualization of Atomistic Mechanical Stresses in Nanomaterials and Biomolecules. *PloS one,* **9**(12), pp. 1-18.

FITZGERALD, J., 1980. A tensorial Hencky measure of strain and strain rate for finite deformations. *Journal of Applied Physics,* **51**(10), pp. 5111-5115.

FREUND, L.B., 1990. *Dynamic Fracture Mechanics.* Cambridge University Press.

GRIFFITH, A.A., 1921. The Phenomena of Rupture and Flow in Solids. *Philosophical Transactions of the Royal Society of London A: Mathematical, Physical and Engineering Sciences,* **221**(582-593), pp. 163-198.

H. M. WESTERGAARD, 1939. Bearing Pressures and Cracks. *Journal of Applied Mechanics,* **6**, pp. A49-A53.

HASHIGUCHI, K., 2013. *Elastoplasticity theory.* Ebooks Corporation; edn. Berlin Heidelberg: Springer Berlin Heidelberg.

HILL, R., 1970. Constitutive Inequalities for Isotropic Elastic Solids Under Finite Strain. *Proceedings of the Royal Society of London A: Mathematical, Physical and Engineering Sciences,* **314**(1519), pp. 457-472.

HOGER, A., 1987. The stress conjugate to logarithmic strain. *International Journal of Solids and Structures,* **23**(12), pp. 1645-1656.

HUI, C.Y. and RUINA, A., 1985. Why K? High order singularities and small scale yielding. *International Journal of Fracture,* **72**(2), pp. 97-120.

INGLIS, C.E., 1913. Stresses in Plates Due to the Presence of Cracks and Sharp Corners. *Transactions of the Institute of Naval Architects,* **55**, pp. 219-241.

JIN, Y. and YUAN, F.G., 2005a. Atomistic simulations of J-integral in 2D graphene nanosystems. *Journal of nanoscience and nanotechnology,* **5**(12), pp. 2099-2107.

JIN, Y. and YUAN, F.G., 2005b. Nanoscopic modeling of fracture of 2D graphene systems. *Journal of nanoscience and nanotechnology,* **5**(4), pp. 601-608.

JUN, S., 2008. Density-functional study of edge stress in graphene. *Physical Review B,* **78**(7), pp. 073405.

KITTEL, C., 2005. *Introduction to solid state physics*. United States of America: Wiley.

KOBAYASHI, A.S., EMERY, A.F. and MALL, S., 1976. Dynamic-finite-element and dynamic-photoelastic analyses of two fracturing homalite-100 plates. *Experimental Mechanics,* **16**(9), pp. 321-328.

KRISHNAN, V.R., HUI, C.Y. and LONG, R., 2008. Finite strain crack tip fields in soft incompressible elastic solids. *Langmuir : the ACS journal of surfaces and colloids,* **24**(24), pp. 14245-14253.

KY, M., 2014. Mode I fracture toughness analysis of a single-layer grapheme sheet. *Journal of mechanical science and technology,* **28**(9), pp. 3645-3652.

LI, J. and LEE, J.D., 2014. Reformulation of the Nosé–Hoover thermostat for heat conduction simulation at nanoscale. *Acta Mechanica,* **225**(4-5), pp. 1223-1233.

LUDWIK, P., 1909. *Elemente der technologischen*. Berlin: Springer Verlag.

MA, G.W., 2009. Modeling complex crack problems using the numerical manifold method. *International Journal of Fracture,* **156**(1), pp. 21-35.

MA, J., 2006. Multiscale simulation using generalized interpolation material point (GIMP) method and molecular dynamics (MD). *Computer modeling in engineering & sciences,* **14**(2), pp. 101-117.

MAXWELL, J.C., 1870. On Reciprocal Figures, Frames, and Diagrams of Forces. *Earth and Environmental Science Transactions of the Royal Society of Edinburgh,* **26**(01), pp. 1-40.

MECHOLSKY, J.J.,Jr, 1995. Fracture mechanics principles. *Dental materials : official publication of the Academy of Dental Materials,* **11**(2), pp. 111-112.

MIAO, Y., 2010. Multi-domain hybrid boundary node method for evaluating top-down crack in Asphalt pavements. *Engineering Analysis with Boundary Elements,* **34**(9), pp. 755-760.

MILLER, R. and TADMOR, E.B., 2002. The Quasicontinuum Method: Overview, applications and current directions. *Journal of Computer-Aided Materials Design,* **9**(3), pp. 203-239.

MOËS, N., 2002. Extended finite element method for cohesive crack growth. *Engineering Fracture Mechanics,* **69**(7), pp. 813-833.

MOËS, N., DOLBOW, J. and BELYTSCHKO, T., 1999. A finite element method for crack growth without remeshing. *International Journal for Numerical Methods in Engineering,* **46**(1), pp. 131-150.

MUBASHAR, A., 2014. Modelling Damage and Failure in Adhesive Joints Using A Combined XFEM-Cohesive Element Methodology. *The Journal of adhesion,* **90**(8), pp. 682-697.

MURDOCH, A.I., 2007. A Critique of Atomistic Definitions of the Stress Tensor. *Journal of Elasticity,* **88**(2), pp. 113-140.

NI, Z.H., WANG, H.M., KASIM, J., FAN, H.M., YU, T., WU, Y.H., FENG, Y.P. and SHEN, Z.X., 2007. Graphene thickness determination using reflection and contrast spectroscopy. *Nano letters,* **7**(9), pp. 2758-2763.

NORRIS, A., 2008. Eulerian conjugate stress and strain. *Journal of mechanics of materials and structures,* **3**(2), pp. 243-260.

ORTIZ, M., 1999. Finite-deformation irreversible cohesive elements for three-dimensional crack-propagation analysis. *International Journal for Numerical Methods in Engineering,* **44**(9), pp. 1267-1282.

RICE, J.R., 1968. A Path Independent Integral and the Approximate Analysis of Strain Concentration by Notches and Cracks. *Journal of Applied Mechanics,* **35**(2), pp. 379-386.

RÖSNER, H., 2009. In situ transmission electron microscopic observations of deformation and fracture processes in nanocrystalline palladium and Pd90Au10. *Materials science & engineering,properties, microstructure and processing,* **525**(1-2), pp. 102-106.

ROZPŁOCH, F., 2007. Graphenes bonding forces in graphite. *Acta physica Polonica, A,* **112**(3), pp. 557-562.

SADD, M., H., 2009. *Elasticity, Theory, Applications, and Numerics*. Boston: Elsiver.

SHENOY, V.B., 1999. An adaptive finite element approach to atomic-scale mechanics—the quasicontinuum method. *Journal of the Mechanics and Physics of Solids,* **47**(3), pp. 611-642.

SIH, G.C., 1966. On the westergaard method of crack analysis. *International journal of fracture mechanics,* **2**(4), pp. 628-631.

STANKOVICH, S., DIKIN, D.A., DOMMETT, G.H., KOHLHAAS, K.M., ZIMNEY, E.J., STACH, E.A., PINER, R.D., NGUYEN, S.T. and RUOFF, R.S., 2006. Graphene-based composite materials. *Nature,* **442**(7100), pp. 282-286.

STROUBOULIS, T., 2000. The design and analysis of the Generalized Finite Element Method. *Computer Methods in Applied Mechanics and Engineering,* **181**(1-3), pp. 43-69.

SUBRAMANIYAN, A.K., 2008. Continuum interpretation of virial stress in molecular simulations. *International Journal of Solids and Structures,* **45**(14-15), pp. 4340-4346.

SUN, C.T., 2002. A new look at energy release rate in fracture mechanics. *International Journal of Fracture,* **113**(4), pp. 295-307.

SUN, C.T., JIN, Z.-. and SCIENCEDIRECT, 2012. *Fracture mechanics*. Waltham, MA: Academic Press.

SUN, Z.H., 2006. On stress calculations in atomistic simulations. *Modelling and Simulation in Materials Science and Engineering,* **14**(3), pp. 423-431.

SUO, Z., 1990. Singularities, Interfaces and Cracks in Dissimilar Anisotropic Media. *Proceedings of the Royal Society.A, Mathematical, physical, and engineering sciences,* **427**(1873), pp. 331; 331-358; 358.

SWADENER, J.G., 2002. Molecular Dynamics Simulation of Brittle Fracture in Silicon. *Physical Review Letters,* **89**(8), pp. 085503.

SYNGE, J.L., 1955. Review: N. I. Muskhelishvili, Some basic problems of the mathematical theory of elasticity. , pp. 445-447.

TADA, H., PARIS, P. and IRWIN, G., 2000. *The analysis of cracks handbook*. New York: ASME Press.

THEOCARIS, P.S., PAZIS, D. and KONSTANTELLOS, B.D., 1986. The exact shape of a deformed internal slant crack under biaxial loading. *International Journal of Fracture,* **30**(2), pp. 135-153.

TONG, P., 2001. *Classical and computational solid mechanics*. Singapore: World Scientific.

TRUESDELL, C. and NOLL, W., 2004. *Non-linear field theories of mechanics.* Berlin ; New York: Springer.

UNKNOWN, , Cast Iron Tensile Test. Available: http://www.tudou.com/programs/view/VSgqs4jb6yA/;.

VITEK, V., 1987. Atomic Level Stresses in Solids and Liquids. *Physica status solidi.B, Basic research,* **144**(1), pp. 145-156.

XIAO, H., 1999. A natural generalization of hypoelasticity and Eulerian rate type formulation of hyperelasticity. *Journal of elasticity,* **56**(1), pp. 59-93.

XIAO,H., BRUHNS,O.T. AND MEYERS, M.,M., 1998. Objective corotational rates and unified work-conjugacy relation between Eulerian and Lagrangian strain and stress measures. *Archive of Mechanics,* **50**, pp. 1015-1045.

XU, M., 2012a. A constitutive equation for graphene based on density functional theory. *International Journal of Solids and Structures,* **49**(18), pp. 2582-2589.

XU, M., 2012b. A coupled quantum/continuum mechanics study of graphene fracture. *International Journal of Fracture,* **173**(2), pp. 163-173.

XU, X.-.X., 1994. Numerical simulations of fast crack growth in brittle solids. *Journal of the Mechanics and Physics of Solids,* **42**(9), pp. 1397-1434.

YANG, Q., 2005. Cohesive models for damage evolution in laminated composites. *International Journal of Fracture,* **133**(2), pp. 107-137.

ZHANG, Z., 2014. An atomistic methodology of energy release rate for graphene at nanoscale. *Journal of Applied Physics,* **115**(11), pp. 114314-114314.

ZHOU, M., 2003. A new look at the atomic level virial stress: on continuum-molecular system equivalence. *Proceedings of the Royal Society.A, Mathematical, physical, and engineering sciences,* **459**(2037), pp. 2347-2392.

ZI, G., 2003. New crack-tip elements for XFEM and applications to cohesive cracks. *International Journal for Numerical Methods in Engineering,* **57**(15), pp. 2221-2240.

ZIMMERMAN, J.A., BAMMANN, D.J. and GAO, H., 2009. Deformation gradients for continuum mechanical analysis of atomistic simulations. *International Journal of Solids and Structures,* **46**(2), pp. 238-253.

ZIMMERMAN, J.A., WEBBIII, E.B., HOYT, J., JONES, R.E., KLEIN, P. and BAMMANN, D.J., 2004. Calculation of stress in atomistic simulation. *Modelling and Simulation in Materials Science and Engineering,* **12**(4), pp. S319.

ZUMDAHL, S.S. and ZUMDAHL, S.A., 2007. *Chemistry*. 7 edn. Boston: Houghton Mifflin.